Exploring Quantum Computation Through the Lens of Classical Simulation

Author:

Padraic Calpin

Supervisor:

Prof. Dan Browne

Submitted in partial fulfilment for the degree of **Doctor of Philosophy**

August 8, 2019

I, PADRAIC CALPIN, confirm that the work presented in this thesis is my own. Where information has been derived from other sources, I confirm that this has been indicated in the thesis.

_____

Signature

                    August 8, 2019
_____

Date

Abstract

It is widely believed that quantum computation has the potential to offer an exponential speedup over classical devices. However, there is currently no definitive proof of this separation in computational power.

This separation would in turn imply that quantum circuits cannot be efficiently simulated classically. However, it is well known that certain classes of quantum computations nonetheless admit an efficient classical description. Recent work has also argued that accurate classical simulation of quantum circuits would imply the collapse of the Polynomial Hierarchy, something which is commonly invoked in classical complexity theory as a no-go theorem. This suggests a route for studying this 'quantum advantage' through classical simulations.

This project looks at the problem of classically simulating quantum circuits through decompositions into stabilizer circuits. These are a restricted class of quantum computation which can be efficiently simulated classically. In this picture, the rank of the decomposition determines the temporal and spatial complexity of simulating the computation.

We approach the problem by considering classical simulations of stabilizer circuits, introducing two new representations with novel features compared to previous methods. We then examine techniques for building these so-called 'stabilizer rank' decompositions, both exact and approximate. Finally, we combine these two ingredients to introduce an improved method for classically simulating broad classes of circuits using the stabilizer rank method.

Impact Statement

UCL theses now have to include an impact statement. *(I think for REF reasons?)* The following text is the description from the guide linked from the formatting and submission website of what that involves. (Link to the guide: `http://www.grad.ucl.ac.uk/essinfo/docs/Impact-Statement-Guidance-Notes-for-Research-Students-and-Supervisors.pdf`)

> The statement should describe, in no more than 500 words, how the expertise, knowledge, analysis, discovery or insight presented in your thesis could be put to a beneficial use. Consider benefits both inside and outside academia and the ways in which these benefits could be brought about.
>
> The benefits inside academia could be to the discipline and future scholarship, research methods or methodology, the curriculum; they might be within your research area and potentially within other research areas.
>
> The benefits outside academia could occur to commercial activity, social enterprise, professional practice, clinical use, public health, public policy design, public service delivery, laws, public discourse, culture, the quality of the environment or quality of life.
>
> The impact could occur locally, regionally, nationally or internationally, to individuals, communities or organisations and could be immediate or occur incrementally, in the context of a broader field of research, over many years, decades or longer.
>
> Impact could be brought about through disseminating outputs (either in scholarly journals or elsewhere such as specialist or mainstream media), education, public engagement, translational research, commercial and social enterprise activity, engaging with public policy makers and public service delivery practitioners, influencing ministers, collaborating with academics and non-academics etc.

Further information including a searchable list of hundreds of examples of UCL impact outside of academia please see `https://www.ucl.ac.uk/impact/`. For thousands more examples, please see `http://results.ref.ac.uk/Results/SelectUoa`.

Acknowledgements

Acknowledge all the things!

Contents

Chapter 1

Introduction

1.1 A section

1.1.1 A subsection

Hello

Chapter 2

Methods for Simulating Stabilizer Circuits

2.1 Introduction

In the previous chapter (INSERT SECTION REFERENCE LATER), we briefly introduced the notion of stabilizer circuits as a class of efficiently simulable quantum computations. In this chapter, we revisit stabilizer circuits in detail, with a focus on different classical data structures for encoding stabilizer states and the corresponding algorithms for simulations.

Several informal definitions of stabilizer circuits have been used in the quantum computing literature [1, 2, 3, 4]. However, what each definition has in common is that the operations $\mathcal{E}$ acting on an abelian subgroup $\mathcal{S} \subseteq \mathcal{P}_n$ generate a new subgroup $\mathcal{S}' \subseteq \mathcal{P}_n$. These groups $\mathcal{S}$ are also called a stabilizer groups.

In this thesis, we focus exclusively on stabilizer circuits acting on pure states $|\phi\rangle$ called stabilizer states. These can be entirely characterized by their associated stabilizer group as

$$s|\phi\rangle = |\phi\rangle \ \forall s \in \mathcal{S} \tag{2.1}$$

For an n-qubit state, the group $\mathcal{S}$ has 2^n elements [1]. As $\mathcal{S}$ is also abelian, this means it can be described by a generating set with n elements,

$$\mathcal{S} = \langle g_1, g_2, \ldots, g_n \rangle : g_i \in \mathcal{S}, \tag{2.2}$$

which are commonly referred to as the 'stabilizers' of the state $|\phi\rangle$. We also note

that this definition allows us to write

$$|\phi\rangle\langle\phi| = \frac{1}{2^n}\sum_{s\in\mathcal{S}}s = \frac{1}{2^n}\prod_{i=1}^{n}(\mathbb{I}+g_i) \tag{2.3}$$

Given that these circuits map stabilizer states to other stabilizer states, this means they must be built up of unitary operations U which map Pauli operators to other Pauli operators under conjugation. This set is commonly denoted as $\mathcal{C}_2$, or the 'second level of the Clifford hierarchy'

$$\mathcal{C}_2 \equiv \{U : UPU^\dagger \in \mathcal{P}_n \;\forall P \in \mathcal{P}_n\} \tag{2.4}$$

$$\mathcal{C}_j \equiv \{U : UPU^\dagger \in \mathcal{C}_{j-1} \;\forall P \in \mathcal{P}_n\} \tag{2.5}$$

where in Eq. 2.5 we have also introduced the (recursive) definition for level j of the Clifford hierarchy. From this definition

$$V\mathcal{S}V^\dagger = \langle Vg_iV^\dagger\rangle = \langle g_i'\rangle = \mathcal{S}' \tag{2.6}$$

We also allow stabilizer circuits to contain measurements in the Pauli basis [1].

Simulating stabilizer circuits

From the above definitions, we can see that simulating a stabilizer circuit on n qubits corresponds to updating the n stabilizer generators for each unitary and measurement we apply. As the number of generators grows linearly in the number of qubits, if these group updates can be computed in time $O(\mathrm{poly}(n))$ then it follows the circuits can be efficiently simulated clasically.

The first proof of this was given by Gottesman in [1], by showing through examples that stabilizer updates can be quickly computed for the CNOT, H and S gates, and for single qubit Pauli measurements. This is significant as the n qubit Clifford group can be entirely generated from these gates.

$$\mathcal{C}_2 = \langle CNOT_{i,j}, H_i, S_i : i,j \in \mathbb{Z}_n\rangle. \tag{2.7}$$

This result is typically referred to as the 'Gottesman-Knill' theorem.

A more formal proof follows from the work of Dehaene & de-Moor, who showed that the action of Clifford unitaries on Pauli operators corresponds to multiplication of $(2n+1) \times (2n+1)$ symplectic binary matrices with $(2n+1)$-bit binary vectors [5]. The dimension of these elements also grows just linearly in the number of qubits, and as matrix multiplication requires time $O(n^{2.37})$ it follows that we can update the stabilizers in $O(mn^{2.73})$ for m Clifford gates.

This work was then extended by Aaronson & Gottesman, who introduced an efficient data structure for stabilizer groups, and algorithms for their updates under Clifford gates and Pauli measurement [2]. This method avoids the need for matrix multiplications, instead providing direct update rules allowing stabilizer circuits to be simulated in $O(n^2)$.

Since 2004, there have been several papers looking at different data structures and algorithms for simulating stabilizer circuits of the type we consider here. For example, a method based on encoding stabilizer states as graphs [6], refinements of the Aaronson & Gottesman encoding [7], and an encoding using affine spaces and phase polynomials [3, 8].

In the rest of this section, we will discuss different aspects of simulating stabilizer circuits, focusing on updating stabilizer states under gates and measurements, computing stabilizer inner products, and the connections between stabilizer circuits and states.

2.1.1   Tableau Encodings of Stabilizer States

The method in [2] is based on a classical data structure they call the 'stabilizer tableau', a collection of Pauli matrices that define the stabilizer group, encoded using the binary symplectic representation of [5]

$$P = i^\delta - 1^\epsilon \bigotimes_{i=1}^{n} x_i z_i \tag{2.8}$$

where the Pauli matrix at qubit i is defined by two binary bits such that

$$x_i z_i = \begin{cases} I & x_i = z_i = 0 \\ X & x_i = 1, z_i = 0 \\ Z & x_i = 0, z_i = 1 \\ Y & x_i = z_i = 1 \end{cases} \tag{2.9}$$

Together with the δ and ϵ phases, a generic Pauli operator can be encoded in $2n + 2$ bits; two bits to encode the phase, and two n-bit binary strings $\tilde{x}, \tilde{z} \in \mathbb{Z}_2^n$ to encode the Pauli acting on each qubit, commonly referred to as 'x-bits' and 'z-bits' respectively. In this picture, multiplication of Pauli operators corresponds to addition of x and z bits modulo 2, with some additional, efficiently computable function for correcting the phase [5]

$$PQ = i^{\delta_{pq}} - 1^{\epsilon_{pq}} \bigotimes_{i=1}^{n} x_i' z_i' \tag{2.10}$$

$$x_i' = x_{pi} \oplus x_{qi} \tag{2.11}$$

$$z_i' = z_{pi} \oplus x_{qi} \tag{2.12}$$

where $\delta_{pq} = \delta_p \oplus \delta_q$, $\epsilon_{qr} = f(\tilde{x}_p, \tilde{z}_p, \tilde{x}_q, \tilde{z}_q)$.

In stabilizer groups, we can restrict ourselves to considering Pauli operators with only real phase. This is because if $iP \in \mathcal{S}$, then $(iP)^2 = -I \in \mathcal{S}$. But, this implies that $-I |\phi\rangle = |\phi\rangle$, which is a contradiction.

While only n generators S_i are needed to characterize the stabilizer group $\mathcal{S}$, the tableau also includes an additional $2n$ operators called 'destabilizers' $D_i \in \mathcal{P}_n$. Together, these $2n$ operators generate all 4^n elements of $\mathcal{P}_n$.

There are many possible choices of destabilizer, but the tableau chooses operators

such that [2]

$$[D_i, D_j] = 0 \; \forall i, j \in \{1, \ldots, n\}$$

$$[D_i, S_j] = 0 \iff i \neq j$$

$$\{D_i, S_i\} = 0$$

Altogether, the full tableau has spatial complexity $4n^2 + 2n$. These are sometimes referred to as 'Aaronson-Gottesman 'tableaux or 'CHP' tableaux, after the software implementation by Aaronson [9].

$$
\begin{array}{c}
\mathcal{D}_1 \\ \vdots \\ \mathcal{D}_n \\ \mathcal{S}_1 \\ \vdots \\ \mathcal{S}_n
\end{array}
\left[
\begin{array}{ccc|ccc|c}
x_{1,1} & \cdots & x_{1,n} & z_{1,n} & \cdots & z_{1,n} & r_1 \\
\vdots & \ddots & \vdots & \vdots & \ddots & \vdots & \vdots \\
x_{n,1} & \cdots & x_{n,n} & z_{n,1} & \cdots & z_{n,n} & r_n \\
\hline
x_{n+1,n} & \cdots & x_{n+1,n} & z_{n+1,1} & \cdots & z_{n+1,n} & r_{n+1} \\
\vdots & \ddots & \vdots & \vdots & \ddots & \vdots & \vdots \\
x_{2n,1} & \cdots & x_{2n,n} & z_{2n,1} & \cdots & z_{2n,n} & r_{2n}
\end{array}
\right]
\tag{2.13}
$$

Figure 2.1: Example of a 'CHP' tableau, where the first n rows are the Destabilizers and the next n rows are the stabilizers. The $2n+1$th column gives that phase -1^{r_i} for each operator.

Simulating Gates

Gate updates for each individual operator in the tableau can be computed constant time. For example, the Hadamard transforms single qubit Pauli matrices under conjugation as

$$
HPH^\dagger = \begin{cases}
I & P = I \\
Z & P = X \\
X & P = Z \\
-Y & P = Y
\end{cases}
\tag{2.14}
$$

In the symplectic form, we then have to update the ith Pauli operator as

$$x_i' z_i' = (x_i \oplus p)(z_i \oplus p) \; : \; p = x_i \oplus z_i \tag{2.15}$$

and the phase as

$$\delta' = \delta \oplus (x_i \wedge z_i) \tag{2.16}$$

Similar update rules exist for the CNOT and S gates, which together generate the n qubit Clifford group. As there are $O(n)$ operators in the tableau, and each update is constant time, gate updates overall take $O(2n)$ [2]. This is in contrast to the $O(n^{2.37})$ complexity of [5]

Simulating Measurements

The addition of the destabilizer information is used to speed up the simulation of Pauli measurements on Stabilizer states. Measuring some operator P on a stabilizer state will always produce either a deterministic outcome, or an equiprobable random outcome [1].

If the outcome is deterministic, then $\pm P$ is in the stabilizer group, and the outcome is $+1$ or -1 respectively. Using the stabilizer generators, this allows us to write

$$[P, S_i] = 0 \,\forall S_i \in \mathcal{S} \implies \prod_i c_i S_i = \pm P. \tag{2.17}$$

for binary coefficients c_i.

Checking if the outcome is deterministic takes $O(n^2)$ time in general, using the symplectic inner product to check the commutation relations [5]. However, checking which measurement outcome occurs involves computing the coefficients c_i. In the symplectic form, this can be rewritten as

$$Ac = P$$

where c is a binary vector, A is a matrix with each stabilizer as a column vector, P is the operator to measure, and we have dropped the phase. Solving this would require inverting the matrix A, and take time $O(n^3)$.

Aaronson & Gottesman show that for single qubit measurements, including destabilizer information instead allows us to compute the c_i and the resulting measurement outcome in $O(n^2)$. As this is a single qubit measurement, they also show that the commutivity relation requires checking only individual bits of the stabilizer vectors, also reducing that step to $O(n)$ time.

For random measurements, from Eq. 2.17, $\exists S_i : \{S_i, P\} = 0$, and it suffices to replace

this stabilizer with P, and update the other elements of the group as $S_j' = PS_j$ iff $\{S_j, P\} = 0$ [1, 2].

'Canonical' Tableaux

There are multiple possible choices of generators for each stabilizer group/state. For example, for the Bell state $\left|\phi^+\right\rangle = \frac{1}{2}(\left|00\right\rangle + \left|11\right\rangle)$

$$\mathcal{S} = \{II, XX, -YY, ZZ\} = \langle XX, -YY \rangle = \langle XX, ZZ \rangle = \langle -YY, ZZ \rangle. \qquad (2.18)$$

In simulation, tableau are fixed by choice of a convention. For example, it is possible to arrive at a 'canonical' set of stabilizer generators using an algorithm which strongly resembles Gaussian elimination [7]. This method rearranges the stabilizer rows of the tableau by multiplying and swapping generators, such that the overall stabilizer group is left unchanged. Computing this canonical form requires time $O(n^3)$ [7].
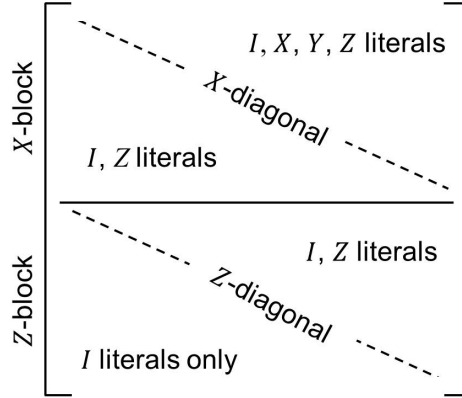
Figure 2.2: Representation of the canonical or 'row-reduced' set of stabilizer generators. Figure taken from [7].

These tableau can then be updated using the same methods as in [2], though this will in general not preserve the canonical form. Each Clifford gate will change one or two columns of the tableau, and thus an additional $O(n)$ row multiplications are required to restore it to canonical form, taking total time $O(n^2)$ per gate [10]. Importantly this canonical tableau can also be used to compute deterministic measurement outcomes in time $O(n)$, and so this method can simulate measurement outcomes more efficiently at the cost of more expensive gate updates [10].

In contrast, Aaronson & Gottesman fix the stabilizer tableau through an initial state, $|0\rangle^{\otimes n}$. The full tableau for this state looks like the identity matrix, with an additional zero-column for the phases. The tableau of a given state $|\phi\rangle$ is then built-up gate by gate using a stabilizer circuit $V : |\phi\rangle = V |0^{\otimes n}\rangle$.

2.1.2 Connecting Stabilizer States and Circuits

The convention for 'CHP' stabilizer tableaux mentioned above, and the definition of stabilizer circuits given in Section 2.1, show that stabilizer states can also be defined by a stabilizer circuit and an initial state.

In [2], the authors derive examples of these 'canonical circuits', and show that its possible for any stabilizer state to be synthesised by a unique circuit acting on the $|0^{\otimes n}\rangle$ state

$$|\phi\rangle = V |0\rangle = H\,C\,S\,C\,S\,C\,H\,S\,C\,S\,|0^{\otimes n}\rangle \tag{2.19}$$

where each letter denotes a layer made up of only Hadamard (H), CNOT (C) or S gates. The proof is based on a sequence of operations reducing an arbitrary tableau to the identity matrix, each step of which corresponds to applying layers of a given Clifford gate [2]. As a corollary, the total number of gates in the canonical circuit for an n-qubit stabilizer state scales as $O(n \log(n))$ [2], based on previous work on synthesising $CNOT$ circuits with the $O(n \log(n))$ gates [11], and that each H and P layer can act on at most n-qubits.

A slightly simpler canonical form was derived in 2008, which allows a stabilizer circuit to be written as

$$|\phi\rangle = S\,CZ\,X\,C\,H\,|0^{\otimes n}\rangle \tag{2.20}$$

where the CZ and X layers are made up of Controlled-Z gates and Pauli X gates, respectively [3]. This circuit follows from the work of [5], who showed that any stabilizer state can be written as

$$|\phi\rangle = \frac{1}{\sqrt{2^k}} \sum_{x \in \mathcal{K}} i^{f(x)} |x\rangle . \tag{2.21}$$

In this equation, $\mathcal{K} \subseteq \mathbb{Z}_2^n$ is an affine subspace of dimension k, and $f(x)$ is a binary function evaluated mod 4. Thus, a stabilizer state is always a uniform superposition

of computational basis strings, with individual phases $\pm i, \pm 1$. The affine space $\mathcal{K}$ has the form

$$\mathcal{K} = \{Gu + h\}$$

for k-bit binary vectors u, an $n \times k$ binary matrix G, and an n-bit binary 'shift-vector' h.

Van den Nest notes that this representation can be directly translated into a stabilizer circuit; we begin by applying H to the first k qubits to initialize the state $\sum_u |u\rangle \otimes \left|0^{\otimes n-k}\right\rangle$. We then apply CNOTs to prepare $\sum_u |Gu\rangle$, and finally Pauli Xs to prepare $\sum_u |Gu \oplus h\rangle$ [3].

The phases can be further decomposed into two linear and quadratic binary functions $l, q : \mathbb{Z}_2^n \to \mathbb{Z}_2$, such that $i^{q(x)} = i^{l(x)}(-1)^{q(x)}$. The linear terms correspond to single qubit phase gates, which can be generated by the S gate, and the quadratic terms to two-qubit phase gates, generated by the CZ [3]. Thus,

$$|\phi\rangle = \sum_{x \in \mathcal{K}} i^{l(x)}(-1)^{q(x)} |x\rangle = S \, CZ \, X \, C \, H \, |0\rangle \tag{2.22}$$

While [3] showed that these simpler canonical circuits exist, an algorithm to compute them first introduced in 2012 [7]. This method allowed such a circuit to be read off from the 'canonical' set of stabilizer generators introduced in Section 2.1.1.

2.1.3 Computing Inner Products

The final task we might consider in simulating stabilizer circuits is the problem of computing probability amplitudes $P(x) = |\langle x|\phi\rangle|^2$. As computational states are also stabilizer states, this corresponds more broadly to computing inner products between stabilizer states.

From the affine space form in Eq. 2.21, we can see that

$$\langle \varphi|\phi\rangle = \frac{1}{\sqrt{2^{k+k'}}} \sum_{x \in \mathcal{K} \cap \mathcal{K}'} i^{f(x)-f'(x)} \tag{2.23}$$

and the problem of computing the inner product corresponds to computing the magnitude of an 'exponential sum' of phase differences $(\pm i, \pm 1)$ for each string x in

the intersection of the two affine spaces [8]. From inspection, we can see that

$$
|\sum_x i^{f(x)-f'(x)}| = \begin{cases} 0 \\ 2^{s/2} : s \in \{0, 1, \ldots, n\} \end{cases}
$$

This sum can be solved in $O(n^3)$ time, using an algorithm developed by Sergey Bravyi [8, 12, 13]. An algorithm for computing this intersection was also described in [8], which we discuss further in Section 2.2.3.

Alternatively, the inner product can also be computed using the stabilizer generators directly. Consider two states $|\phi\rangle, |\varphi\rangle$ with respective generators G_i, H_i. If $\exists i, j : G_i = -H_j$, the states are orthogonal and the inner product is 0. Otherwise, the inner product is given by 2^{-s}, where s the number of generators $G_i \notin \{H_i\}$.

While there are multiple choices of stabilizer generators, we note that inner products are invariant under unitary operations U as

$$
\langle\varphi|\phi\rangle = \langle\varphi|U^\dagger U|\phi\rangle.
$$

Thus, given the canonical circuit $V : |\varphi\rangle = V|0^{\otimes n}\rangle$

$$
\langle\varphi|\phi\rangle = \langle\varphi|V^\dagger V|\phi\rangle = \langle 0^{\otimes n}|V|\phi\rangle.
$$

Each stabilizer G_i' of $|0^{\otimes n}\rangle$ has a single Pauli Z operator acting on qubit i. By simplifying the stabilizer H_i' of $V|\phi\rangle$ using Gaussian elimination, then we have

$$
|\langle 0^{\otimes n}|V|\phi\rangle| = \begin{cases} 0 & \exists H_i' = \bigotimes_i Z_i \\ 2^{-s} & \exists H_i' : \{H_i', G_i'\} = 0 \end{cases} \tag{2.24}
$$

where s is the number of stabilizers that anticommute with the corresponding stabilizer G_i' [2]. The second case arises as if $\{H_i', G_i'\} = 0$, then H_i' acts as either Pauli X or Y on qubit i. Thus, the qubit is in state $|\pm 1\rangle$ or $|\pm i\rangle$, and $\langle 0|\pm i, 1\rangle = \frac{1}{\sqrt{2}}$. Because this method involves computing the canonical circuit and then applying Gaussian elimination, it runs in time $O(n^3)$.

The first implementation of this algorithm was given in [7], where the authors first use their canonical form to construct a 'basis circuit' $B : |\varphi\rangle = B |b\rangle$ for some computational state $|b\rangle$, and then compute $\langle b|B|\phi\rangle$ using the same method outlined above [7].

2.2 Results

The main result of this chapter is to introduce two new classical representations of stabilizer states developed in collaboration with Sergey Bravyi [12]. We will discuss their algorithmic complexity, and implementation in software. We will also briefly discuss the implementation of a classical data-structure based on affine spaces, introduced in [8].

Finally, we present data evaluating the performance of all three methods. For the affine space representation, we benchmark against existing implementations in MAT-LAB [8]. For the two novel representations, we present data comparing their performance to two pieces of existing stabilizer circuit simulation software [2, 6].

2.2.1 Novel Representations of Stabilizer States

Existing classical simulators have two important limitations. One is that they focus only on implementations of single qubit Pauli measurements made in the Z basis. Multi-qubit measurements, or measurements in different bases, need to be built up in sequence, or involve applying additional basis changes gates like H and S, respectively.

These simulators also do not track global phase information. For the case of simulating individual stabilizer circuits, this is sufficient as global phase does not affect measurement outcomes. However, if we wish to extend our methods to simulating superpositions of stabilizer states, then phase differences between terms in the decomposition must also be recorded [10].

Here, we present two data structures, which we call the 'DCH' and 'CH' forms.

Definition 2.1. DCH Representation:

Any stabilizer state $|\phi\rangle$ can be written as

$$|\phi\rangle = \omega^e U_D U_{CNOT} U_H |s\rangle \tag{2.25}$$

where U_D is a diagonal Clifford unitary such that

$$U_D |x\rangle = i^{f(x)} |x\rangle ,$$

U_{CNOT} is a layer of $CNOT$ gates, U_H is a layer of Hadamard gates, acting on a computational state $|s\rangle$, and with a global phase factor w^e where $\omega = \sqrt{i}$ and $e \in \mathbb{Z}_8$.

Any diagonal Clifford matrix of the form U_D is described by its 'weighted polynomial' $f(x)$, evaluated mod 4, which can be expanded into linear and quadratic terms as

$$f(x) = \sum_i a_i x_i + 2 \sum_{c,t} x_j x_k \mod 4 = L(x) + 2Q(x)$$

where the coefficients $a_i \in \mathbb{X}_4$ [3, 14]. This was also the expansion used in the definition of the affine space representation in Eq. 2.22.

We observe that the linear terms can be entirely generated by the S, Z and $S^\dagger$ gates acting on single qubits, and the quadratic terms by CZ gates acting on pairs of qubits [14]. Thus, any unitary U_D can be built up of these gates. As a corollary, we note that these 'DCH' circuits can be obtained from the 7-stage circuits given in Eq. 2.20, by commuting the X layer through to the beginning of the circuit and acting it on the $|0^{\otimes n}\rangle$ initial state. [3].

The computational string s can be encoded as an n-bit binary row-vector. This is also true of the Hadamard layer, which can be expanded in terms of a binary vector h as

$$U_H = \bigotimes_{i=1}^{n} H^{h_i}. \tag{2.26}$$

A $CNOT$ gate controlled on qubit c and targeting qubit t transforms the computa-

tional basis states as

$$CNOT_{c,t} |x\rangle = CNOT_{c,t} \bigotimes_{i=1}^{n} |x_i\rangle = \bigotimes_{i=1}^{n} |x_i \oplus \delta_{i,t} x_c\rangle$$

i.e. it adds the value of bit c to bit t, modulo 2. Thus, we can encode the action of U_{CNOT} as an $n \times n$ binary matrix E which is equal to the identity matrix, with an additional one at $E_{c,t}$, such that

$$CNOT_{c,t} |x\rangle = |xE\rangle \ : \ E_{i,j} = \begin{cases} 1 & i = j \\ 1 & i = c, j = t \\ 0 & otherwise \end{cases} \tag{2.27}$$

We can then build up U_{CNOT} from successive CNOT gates as

$$U_{CNOT} |x\rangle = |xE_1 E2 E_3 \ldots E_m\rangle \equiv |xW\rangle \tag{2.28}$$

where $W = E_1 E_2 \cdots E_n$ is the matrix representing the full circuit, obtained by successive right multiplication of the matrices encoding a single CNOT.

Finally, we need to encode the action of U_D. The phase resulting from a single qubit diagonal Clifford is conditional on the qubits being in the $|1\rangle$ state. Thus, we can write the linear part of the weighted polynomial as Lx^T for some row-vector L of integers mod 4, which we call the linear phase vector. Each value in L can be stored using just 2 bits.

Each gate $CZ_{i,j}$ between qubits i and j also contributes a factor of 2 to the overall phase, conditioned on the ith and jth qubits being in the $|1\rangle$ state. For a given computational string x, the overall phase from the CZ gates is thus $2\sum_{i,j:CZ_{i,j}} x_i x_j$.

We can encode the action of the CZ gates using an $n \times n$ symmetric binary matrix Q where $Q_{i,j} = Q_{j,i} = 1$ if we apply $CZ_{i,j}$, and zero otherwise, which we call the

quadratic phase matrix. We can then compute the phase from the CZ gates as

$$
\begin{aligned}
xMx^t &= \sum_p x_p \left(Qx^T \right) \\
&= \sum_p x_p \left(\sum_q Q_{p,q} x_q \right) \\
&= \sum_{p,q} x_p x_q Q_{p,q} \\
&= 2 \sum_p \sum_{q>p} x_p x_q Q_{p,q} \\
&= 2 \sum_{i,j: CZ_{i,j} \in U_D} x_i x_j
\end{aligned}
$$

where the last line follows from the definition of the matrix Q. Altogether, this allows us to write [8]

$$
U_D \ket{x} = i^{f(x)} \ket{x} = i^{Lx^T + xQx^T} \ket{x} = i^{xBx^T} \ket{x} \tag{2.29}
$$

where B is a matrix such that $B_{ii} = L_i$, $B_{i,j} = Q_{i,j}$, as by definition Q has zero diagonal. We refer to B as simply the phase matrix, with diagonal elements stored mod 4 and off-diagonal elements stored mod 2.

Finally, we include the global phase factor, an integer modulo 8 and stored using just three bits, meaning overall the DCH representation is specified by the tuple (e, s, h, B, W). The spatial complexity is thus $\Theta(n^2)$. In order to optimize certain subroutines, which we discuss later in this section, we also store a copy of W^{-1}, the inverse of the CNOT matrix, and W^T, the transpose of the CNOT matrix. We further introduce two variables $p \in \{0, 1, \ldots, n\}$, $\epsilon = 0, 1$, which are used to ensure normalisation of the DCH state under certain operations. Together with the phase e, they define a coefficient we denote $c = 2^{-p/2} \epsilon \omega^e$. We store p as an unsigned integer, and ϵ as a single binary bit. Overall, then, the DCH form requires roughly $4n^2 + 4n + 36$ bits of memory.

Definition 2.2. CH Representation:

Any stabilizer state $\ket{\phi}$ can be written as

$$
\ket{\phi} = \omega^e U_C U_H \ket{s} \tag{2.30}
$$

where U_C is a Clifford operator such that

$$U_C \left|0^{\otimes n}\right\rangle = \left|0^{\otimes n}\right\rangle, \tag{2.31}$$

U_H is a layer of H gates, $|s\rangle$ is a computational basis state, and with global phase factor ω^e where $\omega = \sqrt{i}$ and $e \in \mathbb{Z}_8$.

The CH representation is based on a notion of a 'control-type' Clifford operator, which stabilizes the all zero computational basis state. Examples of control-type Clifford gates include the S, CZ and $CNOT$ gates. A control type operator U_C can be obtained from the DCH form, for example, by concatenating U_D and U_{CNOT} layers. Thus, we can see that any stabilizer state can be generated by a CH-type circuit.

Similarly to above, we encode the initial computational basis state s and the Hadamard layer U_H as n-bit binary row-vectors. The control-type layer we then encode using a stabilizer tableau, made up of $2n$ Pauli operators $U_C^\dagger X_i U_C$ and $U_C^\dagger Z_i U_C$. This tableau resembles a CHP-type tableau for the state $U_C \left|0^{\otimes n}\right\rangle$, where the Pauli X entries are the destabilizers and the Pauli Z entries are the stabilizers. Alternatively, we can see this as characterising the operator U_C by its action on the generators of the Pauli group.

Using a normal CHP-tableau, each Pauli would require $2n+1$ bits to encode. However, from the definition of the control-type operators, $U_C^\dagger Z_i U_C$ will never result in a Pauli X or Y operator, as otherwise $U_C \left|0^{\otimes n}\right\rangle \neq \left|0^{\otimes n}\right\rangle$. Thus, we can ignore the n 'x-bits' and phase-bits of each of the Pauli Z rows. Specifically, we write

$$U_C^\dagger Z_j U_C = \bigotimes_{k=1}^{n} Z^{G_{j,k}} \tag{2.32}$$

$$U_C^\dagger X_j U_C = i^{\gamma_j} \bigotimes_{k=1}^{n} X^{F_{j,k}} Z^{M_{j,k}} \tag{2.33}$$

for binary matrices G, F, M, and a phase vector $\gamma : \gamma_i \in \mathbb{Z}_4$, as $Y = -iXZ$. Note that this differs from the CHP method, where the string 11 encodes Pauli Y directly, without tracking a separate complex phase.

Finally, we again require three further bits to encode the global phase, and the CH representation is thus given by the tuple (e, s, h, G, M, F). Overall, the CH form also has spatial complexity $\theta(n^2)$. In order to optimize some subroutines, we additionally store copies of M^T and F^T, and again include the variables p and ϵ, requiring a total of $5n^2 + 4n + 36$ bits of memory.

2.2.2 Simulating circuits with the DCH and CH Representations

In this section, we will outline how to update the DCH and CH representations under different stabilizer circuit operations, and how to compute the inner product. For both methods, gate updates can be split into two types: control-type operators, and Hadamard gates. The technique for treating the Hadamard also shares some aspects with applying Pauli projectors to the states, and deciding measurement outcomes. Some of the techniques employed will be common to both representations, differing only in their implementation on the underlying data-strucutre.

Gate updates: The DCH Representation

In the DCH picture, the complexity of a gate depends on whether it is a $CNOT$, or a diagonal Clifford operator S, Z, $S^\dagger$ or CZ. Diagonal gates can be simulated in constant time $O(1)$ by simply updating the linear or quadratic part of the diagonal layer. Single qubit gates applied to qubit i update the ith element of the linear phase vector D, as they contribute only to the linear part of the weighted polynomial. Thus, we have

$$S_i \ket{\phi} \implies B_{i,i} \leftarrow B_{i,i} + 1 \mod 4 \tag{2.34}$$

$$Z_i \ket{\phi} = S^2 \ket{\phi} \implies B_{i,i} \leftarrow B_{i,i} + 2 \mod 4 \tag{2.35}$$

$$S_i^\dagger = s^3 \ket{\phi} \implies B_{i,i} \leftarrow B_{i,i} + 3 \mod 4. \tag{2.36}$$

Similarly, a CZ gate applied to qubits i and j will change entries $B_{i,j}$ and $B_{j,i}$ of the quadratic phase matrix as

$$B'_{i,j} \leftarrow B_{i,j} \oplus 1, \tag{2.37}$$

and equivalently for $B_{j,i}$.

For $CNOT$ gates, we first need to commute them past the diagonal layer before

updating U_{CNOT}. The overall effect on the DCH form is then

$$CNOT_{c,t}\ket{\phi} = i^e\, CNOT_{c,t}U_D U_{CNOT} U_H \ket{s}$$
$$= i^e\, CNOT_{c,t}U_D CNOT_{c,t}^\dagger U_{CNOT}' U_H \ket{s}$$
$$= i^e\, U_D' U_{CNOT}' U_H \ket{s} \tag{2.38}$$

updating U_{CNOT} using matrix multiplication as in Eq. 2.28, and where the last line relies on the following Lemma:

Lemma 1 *For any CNOT circuit U_{CNOT} and any diagonal Clifford circuit U_D, $U_{CNOT}^\dagger U_D U_{CNOT}$ is also a diagonal Clifford circuit U_D' with corresponding phase matrix $B' = WBW^T$.*

Proof of Lemma 1. Consider the case of a single CNOT gate on qubits c and t. We have

$$CNOT_{c,t}^\dagger U_D CNOT_{c,t}\ket{x} = CNOT_{c,t}U_D CNOT_{c,t}$$
$$= CNOT_{c,t}U_D\ket{x + x_j e_k \mod 2}$$
$$= i^{f(x+x_j e_k)}CNOT_{c,t}\ket{x + x_j e_k \mod 2}$$
$$= i^{f(x+x_j e_k)}\ket{x + 2x_j e_k \mod 2}$$
$$= i^{f(x+x_j e_k)}\ket{x} \tag{2.39}$$

where we have used the fact that a single CNOT gate is self-inverse. Thus, $CNOT_{c,t}^\dagger U_D CNOT_{c,t}$ acts as a diagonal Clifford gate. As any CNOT circuit is a sequence of individual CNOT gates, $U_C^\dagger U_D U_C$ is also a diagonal Clifford circuit.

Using the matrix representation of the action of U_C, it is easy to show that

$$U_C^\dagger U_D U_C = U_{C^\dagger}U_D\ket{xW}$$
$$= i^{(xW)B(xW)^T}U_C^\dagger\ket{xW}$$
$$= i^{(xW)B(xW)^T}\ket{xWW^{-1}}$$
$$= i^{xWBW^T x^t}\ket{x}, \tag{2.40}$$

completing the proof. $\qquad\square$

In general, computing the updated form of $U_{CNOT}^{\dagger} U_D U_{CNOT}$ would require time $O(n^2)$. However, for the case of a single gate $CNOT_{c,t}$, recall that the matrix E differs from the identity matrix at a single element, $E_{c,t} = 1$. This allows us to simplify the updates as

$$\left[E_{c,t} B E_{c,t}^T\right]_{i,j} = \sum_{k,l} E_{i,k} E_{j,l} B_{k,l} = \begin{cases} B_{i,j} & i,j \neq c \\ B_{c,j} + B_{t,j} & i = c, j \neq c \\ B_{i,c} + B_{i,t} & i \neq c, j = c \\ B_{c,c} + B_{t,t} + B_{c,t} + B_{t,c} & i = j = c \end{cases} \tag{2.41}$$

Additionally, we need to update W and W^{-1}. The inverse of U_C is the same sequence of CNOT gates, applied in reverse order. Thus, we have $W^{-1} = E_m E_{m-1} \cdots E_1$, and we update W^{-1} by left multiplication with the CNOT matrix. Using the definition of the CNOT matrix,

$$[WF]_{ij} = \sum_k W_{i,k} F_{k,j} = \begin{cases} W_{i,j} & j \neq t \\ W_{i,c} + W_{i,t} & j = t \end{cases}$$

$$[FW^{-1}]_{i,j} = \sum_k F_{i,k} W_{k,j}^{-1} = \begin{cases} W_{i,k}^{-1} & i \neq c \\ W_{c,j}^{-1} + W_{t,j}^{-1} & i = c \end{cases}$$

updating just the target column and the control row of W and W^{-1}, respectively.

Putting together these two pieces, we thus have

$$CNOT_{c,t} |\phi\rangle \implies \mathrm{row}_c(B) \leftarrow \mathrm{row}_c(B) + \mathrm{row}_t(B)$$
$$\mathrm{col}_c(B) \leftarrow \mathrm{col}_c(B) + \mathrm{col}_t(B)$$
$$\mathrm{col}_t(W) \leftarrow \mathrm{col}_t(W) + \mathrm{col}_c(W)$$
$$\mathrm{row}_c(W^{-1}) \leftarrow \mathrm{row}_c(W^{-1}) + \mathrm{row}_t(W^{-1}) \tag{2.42}$$

These updates take $O(n)$ time, as we update a constant number of rows and columns.

Gate Updates: The CH Representation

For the CH representation, whenever we apply a new control-type operator C we need to update the stabilizer tableau by conjugating each element $U_C^\dagger X_i, Z_i U_C$ with the matrix C. This can be implemented using the usual rules for updating Pauli operators under Clifford operations, with the additional note that we have to adjust the updates to correctly track the phases of the Pauli X terms, and that we are conjugating as $U_C^{-1} P U_C$, rather than $U_C P U_C^{-1}$.

The control-type circuit is built out of individual operations $U_C = C_m C_{m-1} \dots C_1$. We we update U_C with some new operator C_{m+1}, change the tableau as

$$(C_{m+1} U_C)^\dagger P C_{m+1} U_C = U_C^\dagger \left(C_{m+1}^\dagger P C_{m+1} \right) U_C. \qquad (2.43)$$

Because C_{m+1} is a Clifford operator, the term $C_{m+1}^\dagger P C_{m+1}$ is also a Pauli operator $P' = i^\alpha \prod_{i=1}^n X_i^{x_i} Z_i^{z_i}$ for some phase α and bit strings x and z. This allows us to write

$$\begin{aligned}
U_C^\dagger C_{m+1}^\dagger P C_{m+1} U_C &= i^\alpha U_C^\dagger \left(\prod_{i=1}^n X_i^{x_i} Z_i^{z_i} \right) U_C \\
&= i^\alpha \prod_{i=1}^n U_C^\dagger X_i^{x_i} Z_i^{z_i} U_C \\
&= i^\alpha \prod_{i=1}^n U_C^\dagger X_i^{x_i} U_C \, U_C^\dagger Z_i^{z_i} U_C \\
&= i^\alpha \prod_{i=1}^n \left(i^{\gamma_i} \prod_{j=1}^n X_i^{F_{i,j}} Z_i^{M_{i,j}} \right)^{x_i} \left(\prod_{i=1}^n Z_i^{G_{i,j}} \right)^{z_i} \qquad (2.44)
\end{aligned}$$

where the last line is a product of terms from the tableau of U_C.

As an example, consider the action of the S gate. For each term, we have

$$S^\dagger P S = \begin{cases} I & \rightarrow & I \\ X & \rightarrow & -\mathrm{i} X Z \\ Z & \rightarrow & Z \end{cases}$$

The Z stabilizers are unchanged, and the X/Y stabilizers flip from $\mathrm{i}^\alpha X^a Z^b$ to $\mathrm{i}^{\alpha+3} X^a Z^{b\oplus1}$. On the tableau, acting an S gate on qubit q will only act non-trivially

on the term $U_C^\dagger X_q U_C$, and thus

$$U_C^\dagger S^\dagger X_q S_q U_C = i^3 U_C^\dagger X_q U_C U_C^\dagger Z_q U_C \implies \begin{cases} \text{row}_q(M) & \leftarrow & \text{row}_q(M) + \text{row}_q(G) \\ \gamma_q & \leftarrow & \gamma_q + 3 \mod 4 \end{cases}$$

We can compute the updates for CZ and CX in the same way, giving overall gate update rules

$$\begin{aligned} S & \begin{cases} \text{row}_q(M) & \leftarrow & \text{row}_q(M) + \text{row}_q(G) \\ \gamma_q & \leftarrow & \gamma_q + 3 \mod 4 \end{cases} \\ CZ_{q,p} & \begin{cases} \text{row}_q(M) & \leftarrow & \text{row}_q(M) + \text{row}_p(G) \\ \text{row}_p(M) & \leftarrow & \text{row}_p(M) + \text{row}_q(G) \end{cases} \\ CNOT_{q,p} & \begin{cases} \text{row}_p(G) & \leftarrow & \text{row}_p(G) + \text{row}_q(G) \\ \text{row}_q(F) & \leftarrow & \text{row}_q(F) + \text{row}_p(G) \\ \text{row}_q(M) & \leftarrow & \text{row}_q(M) + \text{row}_p(M) \\ \gamma_q & \leftarrow & \gamma_q + \gamma_p + 2\sum_i M_{q,i} F_{p,i} \mod 4 \end{cases} \end{aligned} \qquad (2.45)$$

Where on the final line, we apply an extra phase correction that results from re-ordering the Pauli operators in the CNOT updates. This arises as, expanding out the action on the X stabilizers,

$$\begin{aligned} U_C^\dagger CNOT_{q,p} X_q CNOT_{q,p} U_C &= U_C^\dagger X_q X_p U_C \\ &= U_C^\dagger X_q U_C U_C^\dagger X_p U_C \\ &= i^{\gamma_q + \gamma_p} \prod_{i=1}^n X_i^{F_{q,i}} Z_i^{M_{q,i}} X_i^{F_{p,i}} Z_i^{M_{p,i}} \end{aligned}$$

and we pick up an extra phase of -1 each time $M_{q,i} = F_{p,i} = 1$ as $ZX = -XZ$. All of these updates take time $O(n)$, as we are updating the n-element rows of $n \times n$ matrices.

Hadamard gates and Pauli Measurements

Simulating Hadamard gates and arbitrary Pauli measurements is done using an algorithm with the same general structure in the DCH and CH representation. These routines employ an algorithm developed by Sergey Bravyi for application to the CH method, which can also be applied to the DCH case.

Hadamard gates and Pauli projectors can both be written as $\frac{1}{\sqrt{2}}\left(P_1 + P_2\right)$ for some Pauli operators P_1, P_2. In the Hadamard case, we have $P_1 = X_i, P_2 = Z_i$, and in the projector case $P_1 = I, P_2 = P$. Given this structure, we then commute these operators through to the computational basis state

$$\epsilon 2^{-p/2} i^e \frac{1}{\sqrt{2}}\left(P_1 + P_2\right) U_C U_H \left|s\right\rangle = \epsilon 2^{-(p+1)/2} i^e U_C U_H \left(P_1' + P_2'\right)\left|s\right\rangle$$

$$= \epsilon 2^{-(p+1)/2} i^{e'} U_C U_H \left(\left|t\right\rangle + i^\beta \left|u\right\rangle\right)$$

where $P_{1,2}'$ can be efficiently computed as the circuit $U_C U_H$ is Clifford, $\beta \in Z_4$, and t and u are two new computational basis states obtained from the action of $P_{1,2}$ on s. Note that we are writing U_C here as a shorthand, as the circuit $U_D U_{CNOT}$ in the DCH representation is also a control-type unitary.

Once in this form, we employ the following proposition, called Proposition 4 in [12]:

Proposition 1 *Given a stabilizer state* $U_H\left(\left|t\right\rangle + i^\beta \left|u\right\rangle\right)$*, we can construct a circuit* W_C *built out of CNOT, CZ and S gates, and a new Hadamard circuit* U_H'*, such that we can write*

$$U_H\left(\left|t\right\rangle + i^\beta \left|u\right\rangle\right) = i^{\beta'} W_C U_H' \left|s'\right\rangle.$$

As a means of proving this proposition, we will go through and construct W_C and U_H'.

Proof of Proposition 1. Firstly, consider the case $t = u$. Then we have $s' = t$, and the result depends on the phase β. If $\beta = 0$, then the state is unchanged. If $\beta = 1, 3$, then we have

$$\frac{1}{\sqrt{2}} U_H \left(1 + i^\beta\right)\left|s'\right\rangle = \frac{(1 \pm i)}{\sqrt{2}} U_H \left|s'\right\rangle$$

and it suffices to update the global phase term

$$\beta = 1 \quad \Longrightarrow \quad e \leftarrow e + 1 \mod 8$$
$$\beta = 3 \quad \Longrightarrow \quad e \leftarrow e + 7 \mod 8$$

Finally, if $\beta = 2$, we have $\left|s'\right\rangle - \left|s'\right\rangle$ and the state is canceled out. We denote this by setting $\epsilon \leftarrow 0$. This only arises in the case of applying a Pauli projector that is

orthogonal to the state.

If $t \neq u$, then we instead note that we can always define some sequence of $CNOT$ gates V_C such that

$$|t\rangle = V_C |y\rangle \quad |u\rangle = V_C |z\rangle$$

where y, z are two n-bit binary strings such that $y_i = z_i$ everywhere except bit q where $z_q = y_q + 1$. We can assume without loss of generality that $\exists q : t_q = 0, u_q = 1$, else we swap the two strings and update the phase accordingly. Then

$$V_C = \prod_{i : i \neq q, \, t_i \neq u_i} CNOT_{q,i}$$

and we can commute this circuit past U_H to obtain a new circuit V_C'. We can always freely pick $q : v_q = 0$, unless $v_i = 1 \forall i$, and thus V_C' is given by:

$$V_C' = \begin{cases} \prod_{i \neq q, v_i = 0} CNOT_{q,i} \prod_{i \neq q, v_i = 1} CZ_{q,i} & v_q = 0 \\ \prod_{i \neq q} CNOT_{i,q} & v_i = 1 \forall i \end{cases}$$

We complete the proof by considering the action of U_H on the new strings $|y\rangle + \mathrm{i}^\beta |z\rangle$. Again, fixing $y_q = 0, z_q = 1$, we can write

$$U_H \left(|y\rangle + i^\beta |z\rangle \right) = H^{v_q} S^\beta |+\rangle = \omega^a S_q^b H_q^c |d\rangle$$

for some bits $a, b, c, d \in \{0, 1\}$ that can be computed exactly from the values of β and v_q.

This completes the proof of Proposition 1, where $W_C = V_C' S_q^b$, $U_H' = U_H H_q^{v_q+c}$, and $s' = y \oplus d e_q$, where e_q is an indicator vector that is 1 at position q and zero elsewhere. $\qquad \square$

Computing the circuits W_C and U_H' given the two strings t, u takes time $O(n)$, as it involves inspecting the $n-bit$ strings t, u and v. Given this proposition, we now need to show how to commute a Pauli operator through the stabilizer circuit in both representations, and then how to update the layers $U_D U_{CNOT}$ and U_C by right multiplication with the circuit W_C. This can be rewritten in terms of binary

vector-matrix multiplication, and we introduce the following notation:

$$\prod_{i=1}^{n} X_i^{x_i} \equiv X(x) \quad \prod_i Z_i^{z_i} \equiv Z(z)$$

for binary strings x and z.

Applying Proposition 1 to DCH States

When commuting a Pauli operator P through a Clifford circuit, it is important to fix the ordering of the X and Z terms, as Pauli operators can be expanded out as $P = i^a X(x) Z(z) = i^a (-1)^{x \cdot z} Z(z) X(x)$, as $XZ = -ZX$, and where we use $x \cdot z$ to denote the binary inner product

$$x \cdot z = \sum_i x_i z_i \mod 2.$$

In the DCH case, we fix $P = i^a Z(z) X(z)$, as this simplifies the phase terms when commuting past the U_D layer.

Pauli Z terms are unchanged by the DCH layer as they commute with diagonal Clifford oeprtors. To commute the X terms past the U_D layer, we use $X(x) U_D = U_D \left(U_D^\dagger X(x) U_D \right)$, and compute the new Pauli $U_D^\dagger P' U_D = i^{a'} Z(z') X(x)$.

The diagonal entries of the phase matrix B contribute as

$$(S^{B_{ii}})^\dagger X_i^{x_i} S^{B_{ii}} = \begin{cases} S^\dagger X^{x-i} S & \to & i(ZX)^{x_i} \\ ZXZ & \to & -X^{x_i} \\ SXS^\dagger & \to & -i(ZX)^{x_i} \end{cases} = i^{B_{ii}} X^{x_i} Z^{x_i B_{ii}} \ (\text{mod } 2)$$

We also have that $CZ(X \otimes I)CZ = XZ$, $CZ(I \otimes X)CZ = ZX$, i.e. a CZ conjugated with a Pauli X on the control (target) qubit adds a Pauli Z on the target (control) qubit. Qubit i picks up a Z operator each time there is a CZ between qubits i and j, and an X acting on qubit j. Using the off-diagonal entries of the phase matrix, we can write

$$Z_i^{z_i'} : z' = \sum_{j \neq i} x_j B_{j,i} \mod 2$$

Combining this with the fact we also pick up a Pauli Z from the diagonal if $B_{ii} = 1, 3$, we can write $z_i = aB \mod 2$. Finally, we need to consider the extra -1 phase con-

tributions for each $i : x_i z'_i = 1$, as a result of preserving the ordering of P'. Together with the diagonal phases, this can be simplified to

$$\sum_i x_i B_{ii} + 2\sum_i x_i \sum_{j\neq i} x_j B_{j,i} = xBx^T \mod 4$$

Overall then, we have

$$U_D^\dagger X(x) U_D = i^{xMx^T} Z(xM) X(x) \tag{2.46}$$

A similar result applies to commuting a Pauli operator through the U_{CNOT} layer. $CNOT$ has the property that it maps $I_c Z_t \rightarrow Z_c Z_t$ and $X_c I_t \rightarrow X_c X_t$ under conjugation. Thus, we can compute the new strings x', z' by applying an appropriate CNOT matrix.

For the X bits, we can simply apply $x' = xW^{-1}$, where we use the inverse matrix as we are computing $U_{CNOT}^\dagger X U_{CNOT}$ and thus the binary string is subject to the inverse sequence of CNOT gates.

For the string z, we need to apply a CNOT matrix with the controls and targets swapped. From the definition given in Eq. 2.27, we can see that if the binary matrix E encodes $CNOT_{c,t}$, then $CNOT_{t,c}$ is encoded by E^T. We then update the string z under the sequence $E_m^t E_{m-1}^t \ldots E_1^t = W^T$. This gives

$$U_{CNOT}^\dagger i^a Z(z) X(x) U_{CNOT} = i^a Z(zW^T) X(xW^{-1}). \tag{2.47}$$

As mentioned, we store copies of W^{-1} and W^T with the DCH representation. This helps to avoid the $O(n^3)$ computational cost associated with inverting W, and the $O(n^2)$ cost of transposing W. We can thus compute this update in time $O(n^2)$.

Finally, to commute a Pauli operator past the U_H layer, we note that the Hadamard acts as

$$\begin{aligned} HXH &\rightarrow Z \\ HZH &\rightarrow X \\ HZXH &\rightarrow -ZX \end{aligned}$$

The x and z bits are only changed for those bits where $v_i = 1$, and so we can write

$$z_i' = z_i(1 - v_i) + x_i v_i$$

and vice-versa for the x bits. In terms of boolean operations, this can also be written as $z_i' = z_i \wedge \neg v_i \oplus x_i \wedge v_i$. Finally, we have the phase correction whenever $x_i = z_i = z_i = 1$. Thus, overall, we can write

$$U_H^\dagger i^a Z(z) X(z) U_H = i^{a + v \cdot (x \wedge z)} Z(z \wedge \neg v \oplus x \wedge v) X(x \wedge v) \tag{2.48}$$

and this update takes time $O(n)$ to compute.

To complete the application of Proposition 1, we also need to be able to update $U_D U_{CNOT}$ by right multiplication with W_C. We can split $W_C = W_{CNOT} W_D$, where W_D is made up of CZ gates and the single S gate.

The U_{CNOT} layer updates as $U'_{CNOT} = U_{CNOT} W_{CNOT}$. Because of the ordering of the circuits, we here update the matrix W by left multiplication, and update $W^\dagger$ by right multiplication. Thus, for each $CNOT$ gate in W_{CNOT}, we update the columns of W^{-1} and the rows of W using the rules given in Eq. 2.47.

We then need to commute the diagonal layer W_D past U'_{CNOT}. We can do this by adapting Eq. 2.40 to instead compute $U_{CNOT} W_D U_{CNOT}^\dagger$, giving a new phase matrix $C' = W^{-1} C W^{-1}$ where C encodes the action of W_D. This computation again benefits from storing W^{-1} in the DCH information, and can be further optimized by noting that many entries of C are zero. Finally, we can combine the two phase matrices by simply adding all the elements, keeping the diagonal entries $\mod 4$ and the off-diagonal entries $\mod 2$. All together, including the Pauli updates, applying Proposition 1 takes time $O(n^2)$.

Applying Proposition 1 to CH States

Commuting a Pauli operator through the layers of the CH circuit can be done using methods already introduced in previous sections. Distinctly from the DCH case, here we fix $P = i^a X(x) Z(z)$.

To commute a Pauli past the U_C layer, we need to compute $U_C^\dagger P U_C$, and this can

be expanded out in a similar manner to Eq. 2.44. This gives

$$U_C^\dagger X(x)U_C = \prod_{i:x_i=1} U_C^\dagger X_i U_C$$

$$U_C^\dagger Z(z)U_C \quad \prod_{i:z_i=1} U_C^\dagger Z_i U_C$$

We can thus build up P' term by term as

$$U_C^\dagger P U_C = \prod_{j=1}^n x_j \left(\mathrm{i}^{\gamma_j} X(\mathrm{row}_j(F)) Z(\mathrm{row}_j(M))\right) \prod_{j=1}^n z_i \left(Z(\mathrm{row}_j(G))\right)$$

$$= \mathrm{i}^{\sum_{j=1}^n x_j \gamma_j + 2\sum_{j=1}^n \sum_{k>j} x_j x_k (\mathrm{row}_j(F) \cdot \mathrm{row}_j(M))} X(xF) Z(xM + zG)$$

$$= \mathrm{i}^{xJx^T} X(xF) Z(xM + zG). \tag{2.49}$$

The extra factor of 2 in the phase arises from having to commute the Pauli Z terms in $U_C^\dagger X_j U_C$ past the following Pauli X terms. We can encode these commutation relations as a binary matrix

$$MF^T : \left[MF^T\right]_{i,j} = \mathrm{row}_i(M) \cdot \mathrm{row}_j(F),$$

which is additionally symmetric as

$$\left[U_C^\dagger X_j U_C, U_C^\dagger X_k U_C\right] = [X_j, X_k] = 0.$$

Similar to the way we encode the phase polynomial in the DCH form, we can then simplify the overall phase calculation as

$$aJa^T : [J]_{i,j} = \begin{cases} \gamma_i & i = j \\ MF_{i,j}^T & i \neq j \end{cases}$$

where we pick up the correct factor of 2 from the symmetric nature of MF^T. Computing each of the matrix-vector multiplications to commute past U_C takes $O(n^2)$ time. We can then use the same update rule as for the DCH form to commute the Pauli operator past the U_H layer.

Finally, to finish applying Proposition 1, we need to update the tableau of U_C to

$U_C W_C$. We have

$$(U_C W_C)^\dagger X_i, Z_i (U_C W_C) = W_C^\dagger \left(U_C^\dagger X_i, Z_i U_C \right) W_C$$

an thus we need to update the Paulis in the tableau by conjugation with $CNOT$, CZ and S gates. These rules for updating U_C by right-multiplication with a control type unitary are the same as for the CHP tableau, with some additional corrections for phase.

$$
S \begin{cases}
\operatorname{col}_q(M) &\leftarrow& \operatorname{col}_q(M) + \operatorname{col}_q(G) \\
\gamma &\leftarrow& \gamma - \operatorname{col}_q(F) \bmod 4
\end{cases}
$$

$$
CZ_{q,p} \begin{cases}
\operatorname{col}_q(M) &\leftarrow& \operatorname{col}_q(M) + \operatorname{col}_p(F) \\
\operatorname{col}_p(M) &\leftarrow& \operatorname{col}_p(M) + \operatorname{col}_q(F) \\
\gamma &\leftarrow& \gamma + \operatorname{col}_p(F) \cdot \operatorname{col}_q(F)
\end{cases}
$$

$$
CNOT_{q,p} \begin{cases}
\operatorname{col}_q(G) &\leftarrow& \operatorname{col}_q(G) + \operatorname{col}_p(G) \\
\operatorname{col}_p(F) &\leftarrow& \operatorname{col}_p(F) + \operatorname{col}_q(F) \\
\operatorname{col}_q(M) &\leftarrow& \operatorname{col}_q(M) + \operatorname{col}_p(M)
\end{cases}
\qquad (2.50)
$$

There are $O(n)$ row and column updates to perform, and thus this final step runs in time $O(n^2)$. Overall, then, the complexity of applying Proposition 1 to the CH form is $O(n^2)$, arising from computing $U_C^\dagger P U_C$ and then updating the tableau under W_C.

Sampling Pauli Measurements with Proposition 1

Proposition 1 can also be extended to apply to sampling measurements of arbitrary Pauli operators. Measuring a Pauli operator P is closely related to applying a projector $\Pi_{\pm P} = \frac{1}{\sqrt{2}}(I \pm P)$. As mentioned previously, there are three possible outcomes for a Pauli measurement

$$
\begin{aligned}
\Pi_{+P} |\phi\rangle = |\phi\rangle \quad & P |\phi\rangle = |\phi\rangle \quad && \text{Deterministic Outcome } +1 \\
\Pi_{+P} |\phi\rangle = 0 \quad & P |\phi\rangle = -|\phi\rangle \quad && \text{Deterministic Outcome } -1 \\
\Pi{+P} |\phi\rangle = |\phi\rangle + |\varphi\rangle \quad & P |\phi\rangle = |\varphi\rangle \quad && \text{Random Outcome}
\end{aligned}
$$

In terms of measuring an operator P, then we can begin by commuting the projector $I + P$ through the Clifford circuit as described in the previous sections. Dropping

the normalisation, we have

$$(I + P)V|s\rangle = V\left(I + V^\dagger P V\right)|s\rangle$$
$$= V\left(|s\rangle + P'|s\rangle\right) = V\left(|s\rangle + i^\beta|s'\rangle\right)$$

which is the equivalent to the statement of Proposition 1, with $t = s$ and $u = s'$.

If $s = s'$, then the measurement outcome is deterministic. As we have used the projector Π_{+P}, the measurement outcome is $+1$ unless $\beta = 2$, in which case the outcome is -1. Otherwise, if $s \neq s'$, the measurement outcome is random and equiprobable. We can sample the ± 1 outcome using random number generation techniques, and then apply the corresponding projector $(I \pm P)$. As computing P' takes in general $O(n^2)$ time, deciding on the measurement outcome also takes $O(n^2)$ time. However, compare to other stabilizer simulators, we note that this algorithm works for arbitrary Pauli operators P as opposed to just single-qubit Pauli Z measurements.

Computational Amplitudes and Sampling Output Strings

Commuting Pauli operators through the layers of control type operators can also be used to compute the probability of a given computational basis state. Recall that a control-type Clifford circuit U_C is defined such that $U_C|0^{\otimes n}\rangle = |0^{\otimes n}\rangle$. Recall also that for the DCH representation, U_D and U_{CNOT} are also a control-type operators. Thus,

$$\langle 0^{\otimes n}|\phi\rangle = w^e\langle 0^{\otimes n}|U_C U_H|s\rangle$$
$$= w^e\left(\langle 0^{\otimes n}|U_C\right)U_H|s\rangle$$
$$= w^e\langle 0^{\otimes n}|U_H|s\rangle.$$

This trick, using the definition of a control-type operator to simplify the inner product, can be extended to any computational basis state. Writing $|t\rangle = X(t)|0^{\otimes n}\rangle$, we can then commute the X operators past the control-type layer (s) to obtain

$$\langle t|U_C U_H|s\rangle = \langle 0^{\otimes n}|P'U_H|s\rangle$$
$$= \langle 0^{\otimes n}|i^\mu Z(z')X(x')U_H|s\rangle = \langle x'|U_H|s\rangle \tag{2.51}$$

where we have used the 'ZX' convention in the definition of the Pauli operator. If instead we use the 'XZ' convention, then we pick up an additional phase factor of $-1^{x' \cdot z'}$.

The action of the Hadamard layer on a computational basis state can be expanded out as

$$U_H \ket{s} = 2^{-|v|/2} (-1)^{s \cdot v} \sum_{x \leq v} (-1)^{s \cdot x} \ket{s \oplus x} \tag{2.52}$$

where $x \leq v$ denotes the binary strings $x : x_i = v_i \iff v_i = 0$ and $|v|$ is the Hamming weight of the string v. Thus, we have overall that

$$\braket{t | \phi |} = 2^{-|v|/2} i^\mu \prod_{j : v_j = 1} (-1)^{x'_j s_j} \prod_{j : v_j = 0} \braket{x'_j | s}, \tag{2.53}$$

which equals 0 if any $u_j \neq s_j$ for $v_j = 0$, and is proportional to $2^{-|v|/2}$ otherwise. As this requires commuting a Pauli operator through the C/DC layer (s), computing these amplitudes takes time $O(n^2)$.

This result can also be extended to sample strings from the probability distribution $P(x) = |\braket{t | V | s}|^2$, where V_C is a Clifford circuit such that $V_C = U_C U_H \equiv U_D U_{CNOT} U_H$. From the above, we know that any string with a non-zero amplitude occurs with equal probability. This, it is sufficient to start with a binary string

$$w : w_j = \begin{cases} s_j & v_j = 0 \\ 0 & \text{otherwise} \end{cases}$$

and then pick each of the remaining $|v|$ bits at random with equal probability.

Computing Inner Products

The computational basis are a special case of stabilizer state inner products. Here, we present a general method for computing inner products $\braket{\varphi | \phi}$ using the DCH and CH forms. Both methods proceed by combining the two control-type layers, and then breaking down the computation into a sum of different computational basis

state amplitudes

$$\langle \varphi | \phi \rangle = \langle t | V_H V_C^\dagger U_C U_H | s \rangle$$
$$= \langle t | V_H | \Phi \rangle : | \Phi \rangle = V_C^\dagger | \phi \rangle \,.$$

Proposition 2 *Given a stabilizer inner product of the form*

$$\langle t | V_H | \Phi \rangle$$

where $|\Phi\rangle$ is encoded in DCH or CH form, we can compute the inner product by computing the computational state ampliude $\langle t | \Phi' \rangle$ where $|\Phi'\rangle = V_H |\Phi\rangle$, in time $O(n^3)$.

Proof of Proposition 2. In both the DCH and CH form, we can simulate the action of a single Hadamard gate in time $O(n^2)$. The Hadamard circuit V_H contains at most n Hadamard gates, and so we can compute $V_H |\Phi\rangle$ in time $O(n^3)$. The amplitude then reduces to computing the amplitude $\langle t | \Phi' \rangle$, which takes time $O(n^2)$. The overall worst-case complexity is thus $O(n^3)$. □

This method bares a strong resemblance to the 'basis circuit' method described in [7], with the advantage that the 'basis circuit' is explicitly stored in the DCH and CH data-structures, rather than needing to be computed froma tableau. In the following sections, we will show how to compute $|\Phi\rangle$ from the DCH/CH data of $|\varphi\rangle$ and $|\phi\rangle$.

The DCH Case

In this representation, we need to compute $U'_D U'_{CNOT} = V^\dagger_{CNOT} V^\dagger_D U_D U_{CNOT}$. We begin by combining the two phase layers, noting that

$$U_D^\dagger |x\rangle = \mathrm{i}^{-xBx^t} |x\rangle$$

and thus given the two phase matrices A, B, the phase matrix encoding the combined circuit is

$$V_D^\dagger U_D |x\rangle = \mathrm{i}^{x(A-B)x^T} |x\rangle$$

where, as per the definition, the subtraction is $\bmod 2$ on the off-diagonal entries and $\bmod 4$ on the diagonal entries.

We then need to commute $V_{CNOT}^{\dagger}$ past the new U_D' layer, and combine it with U_{CNOT}. As this circuit is an inverse, it is characterised by the binary matrix Q^{-1}, and its inverse is Q. Thus

$$
\begin{aligned}
B' &\leftarrow Q^{-1}B'Q \\
W &\leftarrow WQ^{-1} \\
W^{-1} &\leftarrow QW^{-1}
\end{aligned}
\tag{2.54}
$$

Altogether then, the updated DCH information of $|\Phi\rangle$ can be computed in time $O(n^2)$.

The CH Case

Given two tableau describing control-type unitaries V_C and U_C, we can combine them using Eq. 2.49, as

$$
\begin{aligned}
(V_C U_C)^{\dagger} X_j V_C U_C &= U_C^{\dagger}\left(V_C^{\dagger} X_j V_C\right) U_C \\
&= \mathrm{i}^{\gamma_j'} U_C^{\dagger} P U_C \\
&= \mathrm{i}^{\gamma_j' + \mathrm{row}_j(F')J\mathrm{row}_j(F')^T} X(\mathrm{row}_j(F')F)Z(\mathrm{row}_j(M')M),
\end{aligned}
$$

and similarly for the Z_j entries. Combining two tableau in this way will require time $O(n^3)$, as there are $2n$ entries and each update takes time $O(n^2)$. However, to compute the tableau of $|\Phi\rangle$, we will require the following Lemma:

Lemma 2 *Given the tableau of a control type operator U_C, specified by the binary matrices F, M and G, then the inverse tableau has matrices G', F' and M' such that*

$$
\begin{aligned}
G' &\equiv G^{-1} \\
F' &\equiv G^T \\
M' &\equiv M^T.
\end{aligned}
\tag{2.55}
$$

Proof of Lemma 2. The entries of the tableau for $U_C^\dagger$ have the property

$$U_C \left(U_C^\dagger X_j, Z_j U_C \right) U_C^\dagger = U_C^\dagger \left(U_C X_j, Z_j U_C^\dagger \right) U_C = X_j, Z_j$$

Consider first the Pauli Z terms. Using Eq. 2.49, can see that

$$U_C \left(U_C^\dagger Z_j U_C \right) U_C^\dagger = Z(\text{row}_j(G)G') = Z_j$$

for all $j \in \{1, 2, \dots, n\}$. Expanding out this requirement, we can see that $\text{row}_j(G) \cdot \text{col}_k(G') = \delta_{jk} \forall\, j, k$. If we change the order of the multiplications, we obtain the additional constraint $\text{row}_j(G') \cdot \text{col}_k(G) = \delta_{jk}$. We thus require that

$$GG' = G'G = I \qquad\qquad (2.56)$$

and thus, $G' = G^{-1}$.

A feature of CHP tableaux is that the jth stabilizer and destabilizer anti-commute. Here, similarly

$$U_C^\dagger X_j U_C \, U_C^\dagger Z_k U_C = (-1)^{\delta_{jk}} U_C^\dagger Z_k U_C \, U_C^\dagger X_j U_C$$

where the extra phase arises from the commutation relations of Pauli operators. In terms of the entries of the tableau, this tells us that

$$\text{row}_j(F) \cdot \text{row}_k(G) = \delta_{jk} \forall\, j, k \implies FG^T = I.$$

This also holds for the tableau of $U_C^\dagger$. From this, we can conclude that $F = \left(G^{-1} \right)^T$, and similarly $F' = G^T$.

Finally, consider the X_j entries. Again applying Eq. 2.49, we have

$$U_C \left(U_C^\dagger X_j U_C \right) U_C^\dagger = X(\text{row}_j(F)F')Z(\text{row}_j(F)M' + \text{row}_j(M)G') = X_j.$$

As the Pauli Z terms cancel, we have

$$\text{row}_j(F)\cdot\text{col}_k(M') + \text{row}_j(M)\cdot\text{col}_k(G') = 0 \ \forall j,k$$

$$\implies \text{row}_j(F)\cdot\text{col}_k(M') = \text{row}_j(M)\cdot\text{col}_k(G') \ \forall j,k.$$

Using $F^T = (G^{-1})$, and Eq. 2.56, we thus have

$$\text{row}_j(F)\cdot\text{col}_k(M') = \text{row}_j(M)\cdot\text{row}_k(F) \ \forall j,k \implies M_{j,k} = M'_{k,j} \qquad (2.57)$$

completing the proof. $\qquad\qquad\qquad\qquad\qquad\qquad\qquad\qquad\qquad\qquad\qquad\square$

Specialization for 'Equatorial' Stabilizer States

A specialisation exists for computing the inner product when the state $|\varphi\rangle$ is of the form

$$|\varphi\rangle = \sum_{x\in\mathbb{Z}_2^n} i^{xAx^T} |x\rangle$$

a superposition of all 2^n computational basis states with relative phases. We call these 'equatorial' stabilizer states, as they are like n-qubit generalisations of single qubit states $|0\rangle + e^{i\theta}|1\rangle$ which lie on the equator of the Bloch sphere.

Claim 1 *If $|\varphi\rangle$ is an equatorial state, we can write the inner product as*

$$\langle\phi|\varphi\rangle = 2^{-(n+|v|)/2}\mathrm{i}^{sKs^T+2s\cdot v} \sum_{x\in\mathbb{Z}_2^{|v|}} \mathrm{i}^{xK(1,1)x^T+2x[s+sK](1)^T} \qquad (2.58)$$

where $s(1)$ denotes the elements of a vector $s_j : v_j = 1$, and $K(1,1)$ is the sub-matrix with rows i and columns j such that $v_i, v_j = 1$.

Proof of Claim 1. Let us assume that, given a control-type unitary $U_C \equiv U_D U_{CNOT}$, we can write $U_C^\dagger |\varphi\rangle = \sum_{x\in\mathbb{Z}_2^n} i^{xKx^T} |x\rangle$ for an appropriate phase matrix K. We will show in the following section how to construct this matrix K given the CH and DCH representation of a state $|\phi\rangle$. Given this form then,

we have

$$\langle\varphi|\phi\rangle = (\langle\phi|\varphi\rangle)^*$$
$$= 2^{-n/2}\left(\sum_{x\in\mathbb{Z}_2^n} \mathrm{i}^{xKx^T}\langle s|U_H|x\rangle\right)^*$$

Using Eq. 2.52 to expand out the left hand side of this expression, we obtain a sum over terms

$$\sum_{x\in\mathbb{Z}_2^n} \mathrm{i}^{xKx^T}\langle s|U_H|x\rangle = 2^{-|v|/2}(-1)^{s\cdot v}\sum_{y<v}(-1)^{s\cdot y}\sum_{x\in\mathbb{Z}_2^n}\mathrm{i}^{xKx^T}\langle s\oplus y|x\rangle$$

From the orthogonality of computational basis states, we can set $x = s\oplus y$ and drop all other terms in the sum. Doing so changes the phase calculation to

$$(s\oplus y)K(s\oplus y)^T = sKs^T + yKy^T + yKs^T + sKy^T = sKs^T + yKy^T + 2yKs^T$$

where the final equality follows from the symmetric nature of K. From the the definition of $y \leq v$, $y_j = 0 \iff v_j = 0$. Thus, we can take the global phase of sKs^T out and reduce the sum to the sum over strings $y \in \mathbb{Z}_2^{|v|}$, as in Claim 1.

To complete the proof, we need to show how to obtain K in both cases. In the DCH form, we have

$$\langle\phi|\varphi\rangle = \langle s|U_H U_{CNOT}^{-1} U_D^{-1}|\varphi\rangle.$$

Using the definition of an equatorial stabilizer state, we can write $|\varphi\rangle = V_D\left|+^{\otimes n}\right\rangle$, and simply compute $|\varphi'\rangle = U_D^{-1}V_D\left|+^{\otimes n}\right\rangle$ by combining the two phase layers to obtain a new phase matrix $(A-B)$.

Another feature of the state $\left|+^{\otimes n}\right\rangle$ is that it is invariant under $CNOT$ circuits, as it is a superposition of all computational basis states and subsequently invariant under their permutation. Applying Lemma 1, we can commute the circuit U_{CNOT}^{-1} past $U_D' = U_D^{-1}V_D$ and eliminate it. This gives a new phase

Property	CH	DCH	CHP	Canonical	Graph States [6]
Memory	$O(n^2)$	$O(n^2)$	$O(n^2)$	$O(n^2)$	$O(nd)$
Z	$O(n)$	$O(1)$	$O(n)$	$O(n^2)$	$O(1)$
X	$O(n)$	$O(n)$	$O(n)$	$O(n^2)$	$O(1)$
S	$O(n)$	$O(1)$	$O(n)$	$O(n^2)$	$O(1)$
H	$O(n^2)$	$O(n^2)$	$O(n)$	$O(n^2)$	$O(1)$
CZ	$O(n)$	$O(1)$	$O(n)$	$O(n^2)$	$O(d^2)$
CX	$O(n)$	$O(n)$	$O(n)$	$O(n^2)$	$O(d^2)$
Measurement	$O(n^2)$	$O(n^2)$	$O(n^2)$	$O(n^2)$	$O(d^2)$
Inner Product	$O(n^3)$	$O(n^3)$	$O(n^3)$	$O(n^3)$	N/A

Table 2.1: Comparison of the asymptotic complexity of different stabilizer circuit simulators, including common operations and their memory footprint. We include the graph based representation of Anders & Briegel, discussed later in this section, and omit the 'Affine Space' simulator as it has no current implementation for gate updates.

Here, d is the degree of the graph used as an internal representation, which varies from $\log n$ to n [6]. We further note that, while all algorithms for measurement are in principle extensible beyond single qubit measurements, only the DCH and CH simulators currently implement arbitrary Pauli measurements.

matrix $K = G(A - B)G^T$.

In the CH case, using Eq. 2.49, we can write

$$U_C^{-1} |x\rangle = U_C^{-1} X(x) U_C \left|0^{\otimes n}\right\rangle = \mathrm{i}^{xJx^T} |xF\rangle$$

Applying this to $|\varphi\rangle$ thus gives

$$U_C^{-1} \sum_{x \in \mathbb{Z}_2^n} \mathrm{i}^{xAx^T} |x\rangle = \sum_{x \in \mathbb{Z}_2^n} \mathrm{i}^{x(A+J)x^T} |xF\rangle .$$

Using $FG^T = I$, as introduced in the previous section, and setting $x = yG^T$, we have

$$\sum_{y \in \mathbb{Z}_2^n} \mathrm{i}^{yG^T(A+J)Gy^T} |y\rangle = \sum_{y \in \mathbb{Z}_2^n} \mathrm{i}^{yKy^T} |y\rangle$$

as required where $K = G^T(A + J)G$.   □

Once the calculation is in this form, we can compute the inner product in time $O(|v|^3)$ using the algorithm for exponential sums developed by Sergey Bravyi [12]. Computing the phase matrix K takes time $O(n^2)$ in both cases, and thus as $|v| \leq n$ we have a general performance $O(n^3)$.

2.2.3 Implementations in Software

The DCH and CH data structures and most routines were implemented in `C++`, to produce a stabilizer circuit simulator. The one exception was the arbitrary stabilizer state inner product, which was derived but left unimplemented due to time constraints. In this section, we will review some of the optimizations employed, and present data comparing their performance with existing software implementations.

The resulting simulators were also validated through the use of testing random circuits. The CH representation was validated by comparison to a `MATLAB` version of the simulator developed independently by David Gosset. The DCH representation was then validated against this successfully tested CH representation, using random circuits and conversion to state-vectors through 2^n calls of the computational amplitude routine.

Efficient Binary Operations

The data-structures and subroutines underpinning the CH and DCH representations are built out of arithmetic performed modulo 2 and 4, depending on the context. This allows us to efficiently store the representations using binary bits as opposed to integers, and then use boolean operations as part of the simulation routines.

Addition and subtraction modulo 2, such as is required in the U_C updates of the CH representation and the U_D updates in the DCH representation, is equivalent to the boolean 'XOR' operation, defined as

a	b	$a \oplus b$	$a + b \,(\mathrm{mod}\,2)$	$a - b \,(\mathrm{mod}\,2)$
0	0	0	0	0
0	1	1	1	1
1	0	1	1	1
1	1	0	0	0

For addition modulo 4, we encode each number using two binary bits a and b as $2 * a + b$. In this context, a is typically referred to as the '2s' bit and b as

the '1s' bit. Addition can be done for the 1s and 2s terms separately, with an additional carry correction

$$x + y \pmod 4 = 2 * (a_x \oplus a_y \oplus (b_x \wedge b_y)) + (b_x \oplus b_y).$$

In the case of subtraction modulo 4, we note that adding and subtracting 2 can be achieved using just the *xor* operation, as only the two bit is changed. Otherwise, we note that

a	$a-3 \pmod 4$	$a-1 \pmod 4$
0	1	3
1	2	0
2	3	1
3	0	2

i.e. $a-3 = a+1$, and $a-1 = a+3$, where the addition is again modulo 4. This trick allows us to simplify $a-b \pmod 4$ by setting $b_2 \leftarrow b_2 \oplus b_1$, and then using addition.

Vector and matrix multiplications modulo 2 can also be reduced to a set of binary operations. Each element $[aM]_i$, $[LM]_{i,j}$ can be written as a binary inner product, respectively $a \cdot \mathrm{col}_i(M)$ and $\mathrm{row}_i(KL) \cdot \mathrm{col}_j(M)$. Computing the binary inner product can then be expanded out in terms of boolean operations as

$$x \cdot y = (x_1 \wedge y_1) \oplus (x_2 \wedge y_2) \cdots \oplus (x_n \wedge y_n).$$

Typically, we are applying the same operation to entire vectors, rows or columns of a binary matrix. Thus, we can employ a technique called 'bit-packing' to efficiently store and update these binary values. In `C++`, integers can by stored using 8, 16, 32 or 64 binary bits (1, 2, 3 and 4 bytes, respectively). The built-in in `bool` data-type is also typically stored using 1 byte, as this is the smallest unit of memory addressable by a processor [15].

Bitpacking instead stores up to 64 binary bits in a single variable, manipulating

them through the use of 'bitwise' operators [16]. Bitpacking typically achieves an 8-fold reduction in the memory footprint. Additionally, a bitwise operation between two variables acts on all bits simultaneously in a single time-step. For example, considering the XOR between two binary vectors, we can write

$$x \oplus y = [x_1 \oplus y_1, \cdots x_n \oplus y_n] \iff \texttt{uint64\_t z = x \textasciicircum y //bitwise XOR}$$

We can also make use of so called 'intrinsic' functions to optimise computing the binary inner product, and sums of terms modulo 4. Intrinsic functions allow certain special processor instructions to be called directly. Specifically, we use two intrinsics for calculating the hamming weight and the parity of a binary string, each of which are computed in a single time step. Using these operations, we can write the binary inner product as

$$\sum_i x_i y_i = |x \wedge y| \bmod 2 \iff \texttt{parity(x \& y)}$$

and a sum of integers modulo 4 as

$$2 * \sum_i a_i + \sum_i b_i \iff \texttt{(2*parity(2bits)+hamming\_weight(1bits))\%4}$$

where `%` is the `C++` modulo operator.

Using these operations allows us to reduce the effective complexity of many common subroutines by a factor of n, as long as the number of variables n is less than 64. For example, instead of $O(n)$ time, computing the binary inner product now requires just two operations: a bitwise logical AND, and the parity intrinsic. However, above 64 bits, we need to pack the bits across multiple variables, and so the number of calls to intrinsic functions will again asymptotically as $O(n)$. Specifically, the number of operations required will go as $n/64$.

Case study: Stabilizer simulations with Affine Spaces

As an example of the use of bitpacking to optimize stabilizer simulators, we

developed a `C++` implementation of the stabilizer state simulator introduced in Appendices B, C and E of [8]. While not a full simulator, they provide explicit algorithms for performing Pauli measurements and computing stabilizer inner products. These methods were implemented by the authors in `MATLAB`, using matrices of integers and repeated calls to the `mod` function in MATLAB.

In particular, in their encoding a stabilizer state is based on Eq. 2.21, described by a tuple

$$|\phi\rangle = \left(n, k, h, G, G^{-1}, Q, D, J\right)$$

where n is the number of qubits, k is dimension of the the affine space $\mathcal{K}$, generated by the first k columns of the $n \times n$ binary matrix G and an n-bit binary vector h. The inverse matrix G^{-1} is also stored. The phase terms are encoded in a quadratic form using a constant offset $Q \in \mathbb{Z}_4$, a vector D of elements $\bmod\, 4$, and a symmetric $n \times n$ binary matrix J.

The `C++` simulator makes use of bitpacking to efficiently store h, G, G^{-1} and J. Additionally, we store the elements of D using two binary variables, separating the 1s and 2s bits. The routines were verified and benchmarked against the existing `MATLAB` implementation using the `MATLAB` EXternal languages (MEX) interface, which allows compiled code to be called from within `MATLAB` applications [17].

The results of the benchmark are shown in Figure 2.3. We include two core subroutines specific to the affine space simulator, called `Shrink` and `Extend`, which are called as part of computing stabilizer inner products and simulating Pauli measurements respectively, as well as results for arbitrary n qubit Pauli measurements and computing the inner product between stabilizer states.

The observed differences in runtime are relatively consistent across each routine. In general, the `C++` implementation has a significant advantage in the 5–15 qubit range, with a speedup of anywhere from 1.6 to 10 times. This advantage then drops off as the number of qubits increases, tending to a constant speedup of between 1.5 to 3 times. The notable exception to this is in the

Figure 2.3: Figures showing the performance of the `MATLAB` and `C++` implementations of a stabilize simulator based on Affine Spaces.
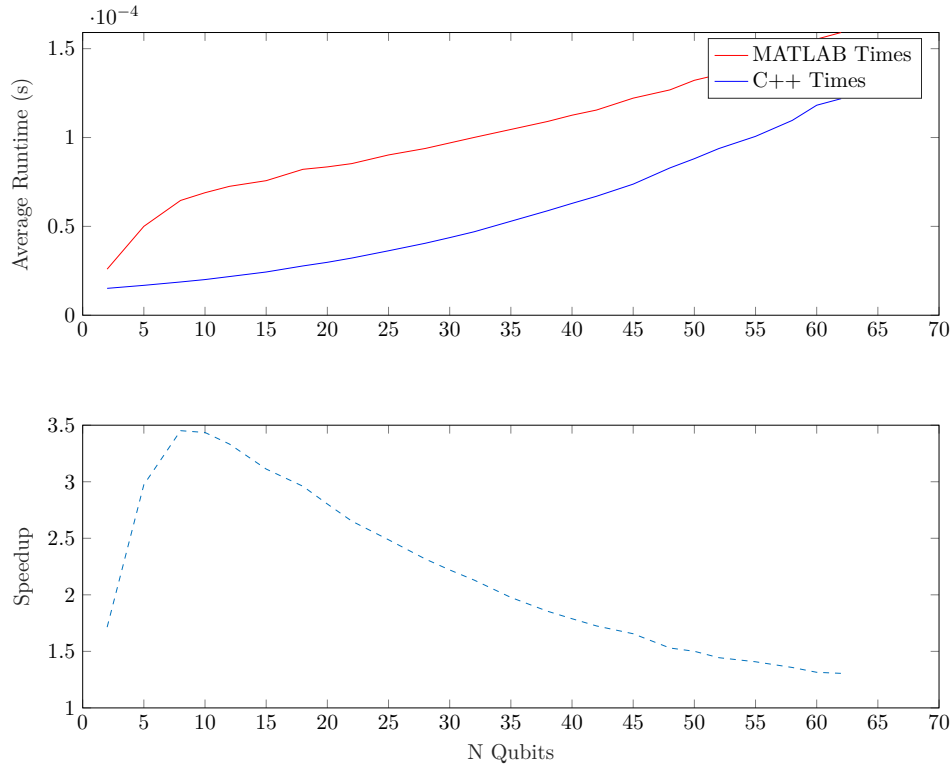
(a) Average runtime and resulting speedup of the `Shrink` routine.

(b) Average runtime and resulting speedup of the `Extend` routine.
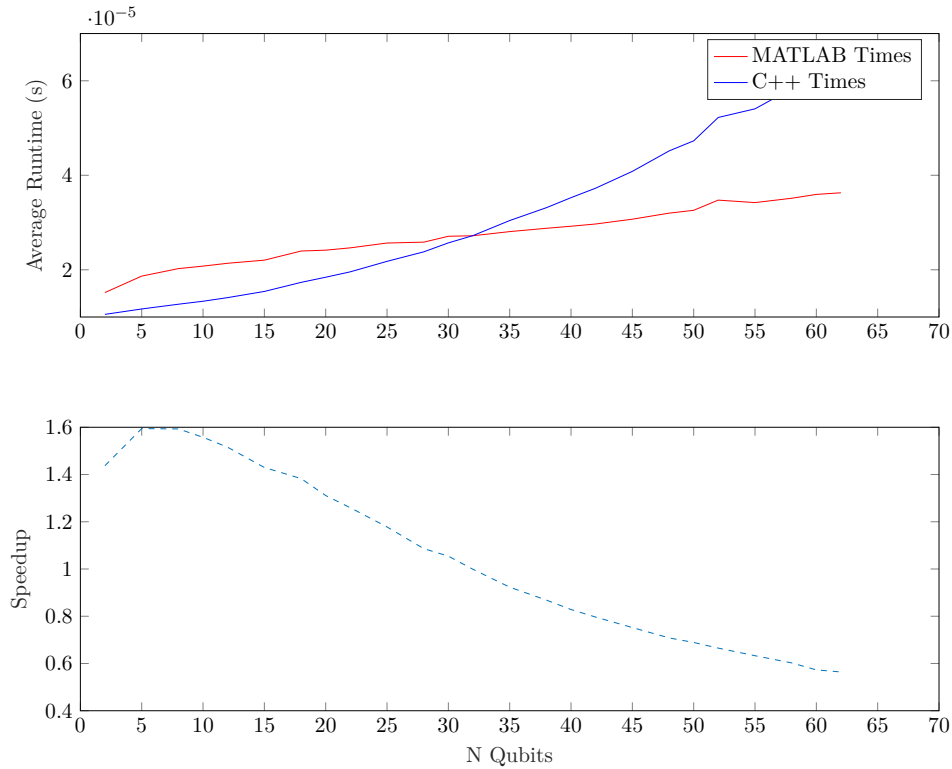
(c) Average runtime and resulting speedup of Pauli measurements.
(d) Average runtime and resulting speedup of stabilizer inner products.

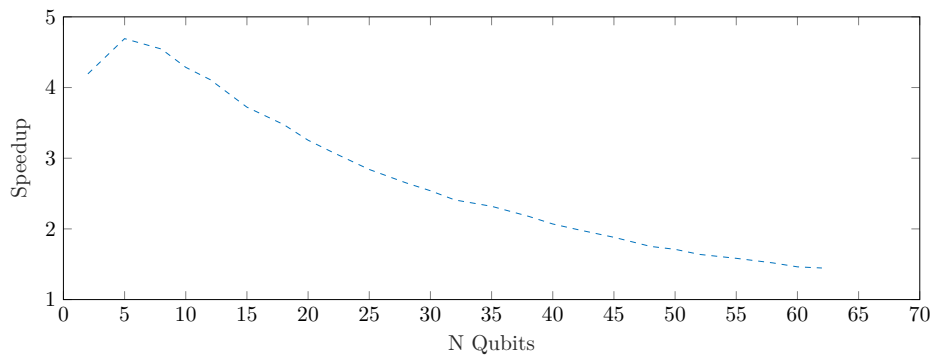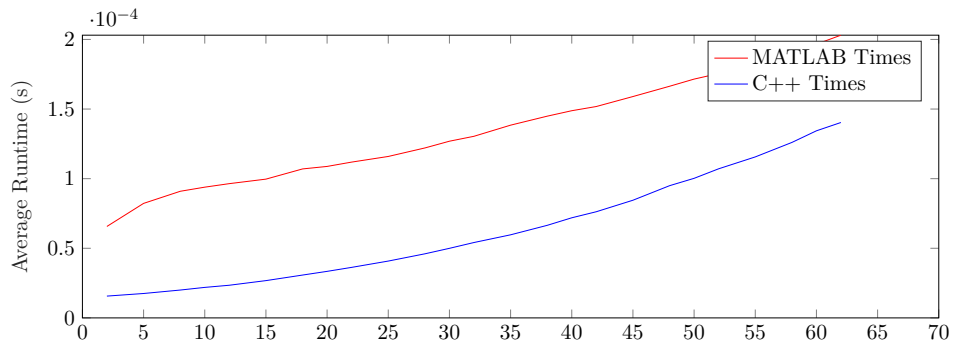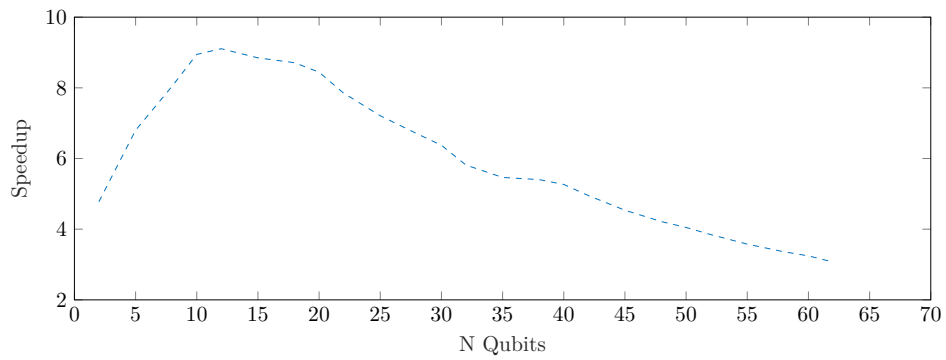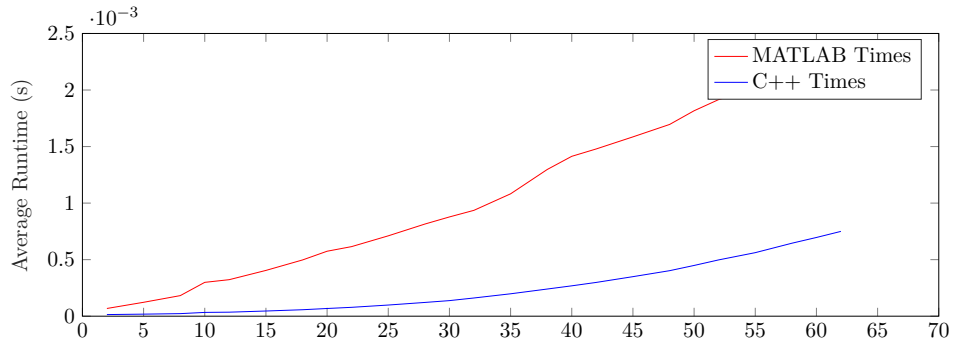`Extent` routine, which actually performs worse than the `MATLAB` version above 35 qubits. All benchmarks have a cutoff below 64 qubits, which is enforced by the use of 64 bit integers for bitpacking in the `C++` simulator.

Specific Optimizations for the CH and DCH Forms

We make use of bitpacking to efficiently store the CH and DCH forms. As many subroutines require computing vector-matrix multiplications of the form aM, we store the matrices in 'column format' where each bitpacked variable stores one column of the binary matrix. This allows us to make use of intrinsic functions to speedup these multiplications.

Transposed matrices are computed using 'lazy evaluation'. When the transposed matrix is required, we compute it and store it. We then additionally store a flag to indicate if the transposed matrix is up to date. If later function calls change the values of the transposed matrix, the flag is set to false and the transpose will be recomputed only when required.

Whenever the result of a calculation is expected to be symmetric, we an halve the number of operations by copying values across. This gives a constant factor speedup in, for example, computing the phase matrices K as part of inner product calculations. We can also make use of this symmetric structure to avoid transposing a matrix when accessing a row.

Typically, phase matrices are stored as binary matrices with 0 diagonal, and then a separate pair of bitpacked variables storing the diagonal entries which are modulo 4. When required, we update the diagonals separately using an explicit expansion of the matrix multiplications.

Some updates for the DCH form are further optimised by using explicit expansions of the matrix multiplications. For example, when commuting a Pauli Z through the CNOT layer as in Eq. 2.47, we avoid a call to the transpose

W^T by noting that

$$[zW^T]_i = \sum_j z_j W^T_{j,i} = \sum_j z_j W_{i,j}$$

i.e. each entry $[zW^T]_i$ is a sum of some entries in row i. We can thus build up the new vector $z' = zW^T$ by repeatedly doing $z' \leftarrow z' \oplus \mathrm{col}_j(W)$ for each $j : z_j = 1$.

2.2.4 Performance Benchmarks

To establish the performance of the DCH and CH implementations, we benchmark them against two existing stabilizer circuit simulators, which are available publicly online. The first is the `C` implementation of the CHP method, developed by Scott Aaronson [9]. This uses a variant of bitpacking based on 32-bit integers. The second method is a radically different representation of stabilizer states, based on the fact that any stabilizer state can be generated by a local Clifford circuit (single qubit Clifford gates), acting on a special class of stabilize state called a graph state [18, 19].

Graph states are named as their structure is described by a mathematical graph of vertices V and edges E, where each qubit is a vertex. From this graph, a graph-state is then built-up as

$$|(V,E)\rangle = \left(\prod_{i,j \in E} CZ_{i,j} \right) |+^{\otimes n}\rangle,$$

by performing a CZ gate between every pair of qubits connected by an edge of the graph [19].

The so called 'Anders & Briegel' simulator describes a stabilizer state by its corresponding graph, and by sequences of local Clifford operators acting at each vertex. A `C++` implementation of this simulator also exists, called `GraphSim` [20]. This stores a graph as a list of vertices, each with local information about the vertices connected to it.

The expected runtime of different routines using the Anders & Briegel method

are also given in Table 2.1. Importantly, in their analysis, routines are quoted with a runtime that scales as d, the maximum 'degree' or number of edges involving a given vertex. By definition, $d \leq n$, the number of vertices in the graph, and thus the simulator has a worst case performance comparable to the DCH, CH and tableau methods. However, this analysis makes explicit a feature of stabilizer circuit simulators; their runtime in practice depends on the state/circuit being considered.

This phenomenon was first described in [2], who observed that the runtime for Pauli measurements seemingly varied between linear and quadratic scaling in the number of qubits, despite the expected asymptotic quadratic scaling. In particular, the algorithm for computing a given measurement in the CHP representation requires between 1 and n calls to a subroutine which takes $O(n)$ to evaluate, and the exact number is determined by the sparsity of the X-bits of the stabilizers, which is in turn related to the number of entangling gates in the circuit.

Similar results hold in detailed analysis of the CH and DCH representations, where the exact number of calculations required will depend on the sparsity of the matrices/vectors encoding different features of the stabilizer circuits. Consider for example the inner product algorithm of Proposition 2, where we need to apply $|v|$ H gates at a cost of $O(n^2)$ each.

As a result, Aaronson & Gottesman introduced a heuristic for evaluating stabilizer circuit simulators. We begin by applying a random stabilizer circuit to the state, choosing H, S and $CNOT$ gates at random, before applying the operation we are benchmarking and recording the runtime. Using an argument based on message passing, the authors claim that in general we need $O(n \log n)$ gates in the circuit to observe this transition between easier and harder instances of stabilizer circuit simulation, and so we apply $\beta n \log n$ gates where β is a parameter that varies between 0.5 and 1.2. This heuristic is also employed by Garcia et al. in their paper presenting an algorithm for computing stabilizer inner products, where they observe a transition between quadratic

and cubic scaling with varying β [7].

Here we present results comparing the performance of different operations between the DCH, CH, CHP and GraphSim methods, for different values of the parameter β. All run-times are averages taken over 100000 repetitions, where we first apply a random stabilizer circuit of $\beta n \log n$ gates, and then record the time taken by the particular operation.

We also present data for routines specific to the DCH and CH routines. In particular, we present data demonstrating the runtime of arbitrary n-qubit Pauli measurements, and for the specialized 'equatorial' inner product defined in Claim 1. We also consider the effect of weight on the complexity of Pauli measurements.

2.3   Discussion

In this chapter, we have introduced two new representations for simulating stabilizer circuits, including their implementation in software, and presented data evaluating their performance against previous methods.

In particular, we make use of bitpacking techniques to try and further improve their runtime. Figure 2.3 introduced results comparing a bitpacked simulator with a prior `MATLAB` implementation. In general, we see a broad speedup over the `MATLAB` version across the full parameter range, though the exact degree of this speedup decreases with increasing n. The main exception is the `Extend` routine, where we observe the `C++` implementation scaling roughly quadratically with the input size, whereas the `MATLAB` version exhibits a closer to linear scaling.

One possible explanation for this effect is an unfortunate side-effect of the use of MEX files, namely that the `C++` version additionally needs to convert the MATLAB data into a C++ data-structure. This adds an additional $O(n^2)$ overhead to the runtime of the `C++` simulator. Otherwise as coded, the `Extend` algorithm has only $O(n)$ steps. In more complex functions like measurement, `Shrink` and inner products, which have run-times $10-100$ times longer than
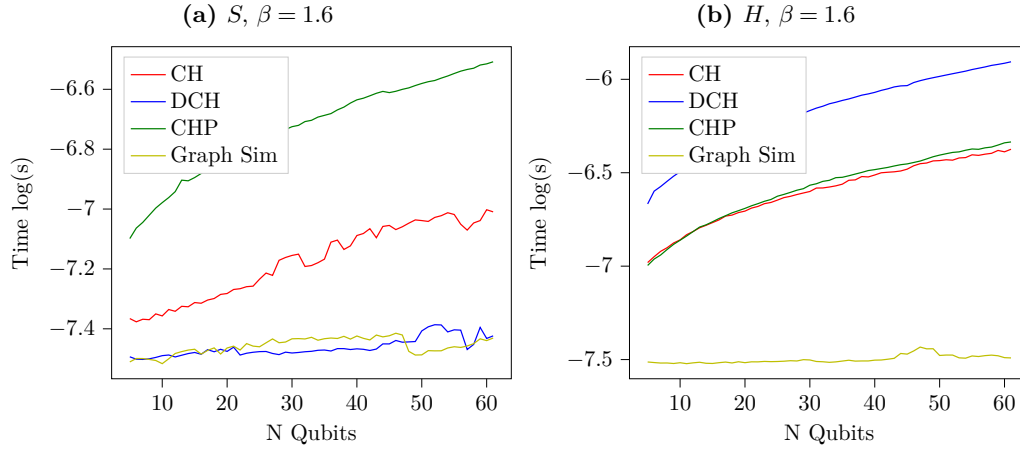
Figure 2.4: Average runtime of the single qubit H and S gates as a function of the number of qubits across different stabilizer simulators. Single qubit gates show no dependence on length of the preceding circuit, encoded as the β parameter.

Figure 2.5: Average runtime of entangling $CNOT$ and CZ gates as a function of the number of qubits for different stabilizer simulators, for extremal values of β. The Anders & Briegel method shows a significant dependence on circuit length.
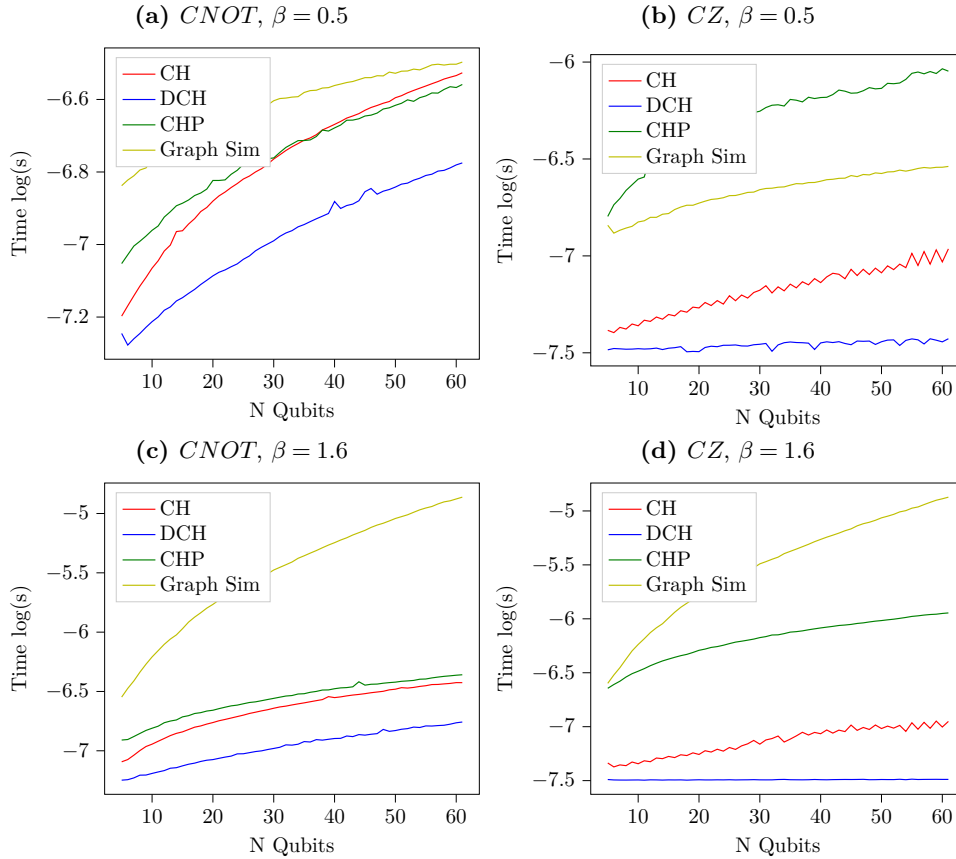
Figure 2.6: Average runtime of single qubit measurements in the X and Z basis, as a function of the number of qubits and the length of the preceding stabilizer circuit, for 4 stabilizer simulators.

(a) Z measurement, $\beta = 0.5$ **(b)** X measurement, $\beta = 0.5$

(c) Z measurement, $\beta = 0.8$ **(d)** X measurement, $\beta = 0.8$

(e) Z measurement, $\beta = 1.2$ **(f)** X measurement, $\beta = 1.2$

(g) Z measurement, $\beta = 1.6$ **(h)** X measurement, $\beta = 1.6$

(a) Computing Computational Amplitudes

(b) Equatorial Stabilizer Inner Products
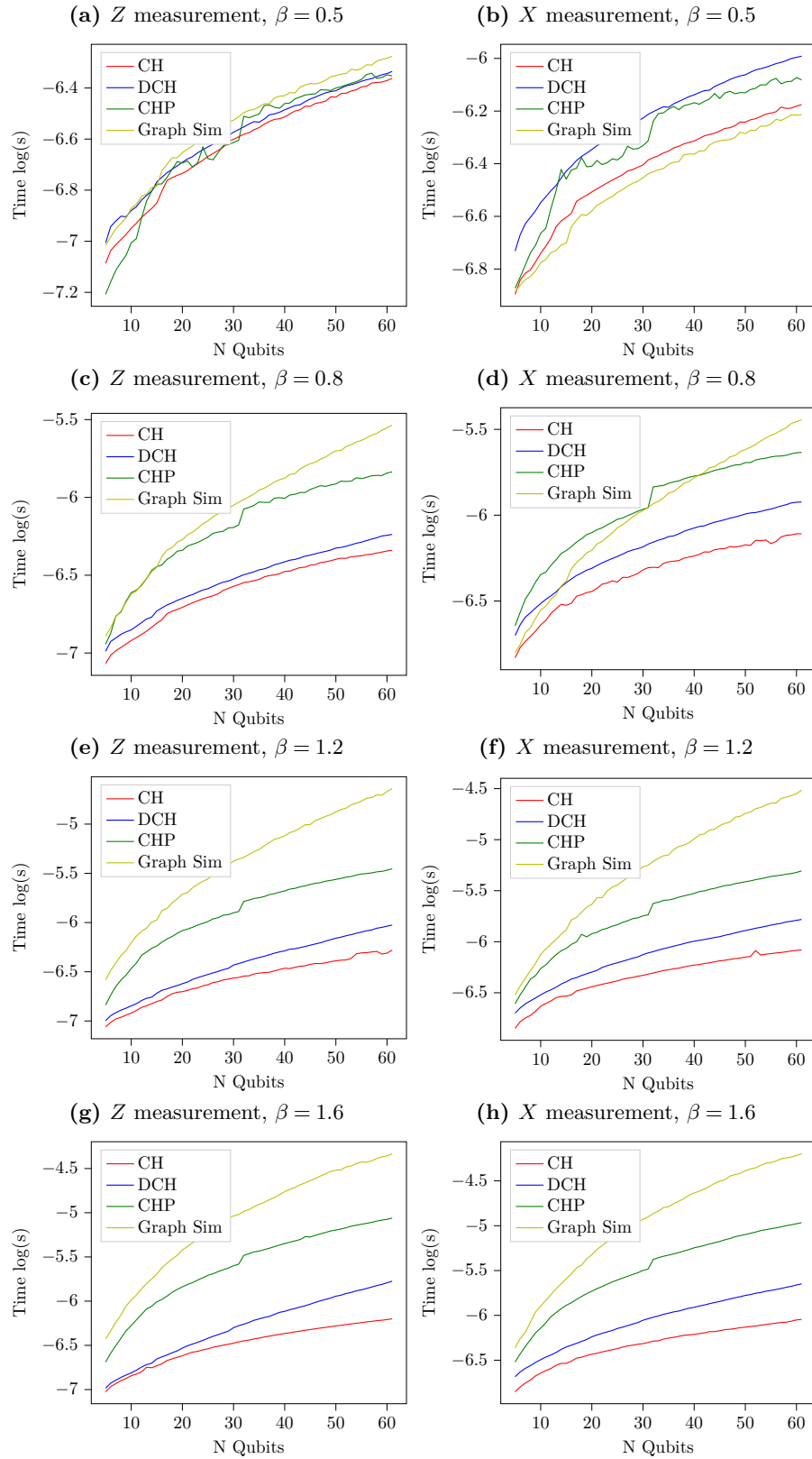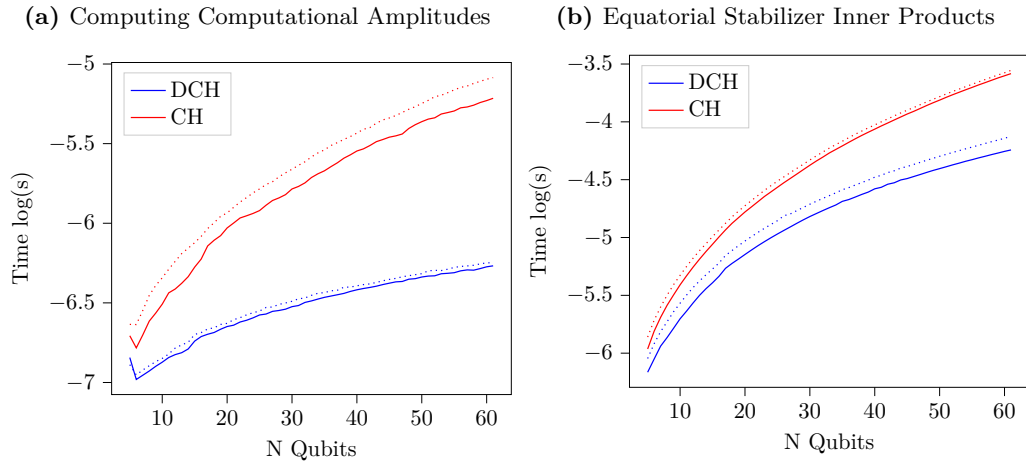
Figure 2.7: Average runtime of two routines specific to the DHC and CH routines, as a function of the number of qubits. Solid lines are for $\beta = 0.5$, and dash lines for $\beta = 1.6$. A slight dependence on circuit length is observed.

Figure 2.8: Average runtime of Pauli measurements for the CH and DCH simulators. A solid line represents a single Pauli Z measurement. The dashed lines represent n-qubit Pauli Z measurements, and the dotted line random n-qubit Paulis.
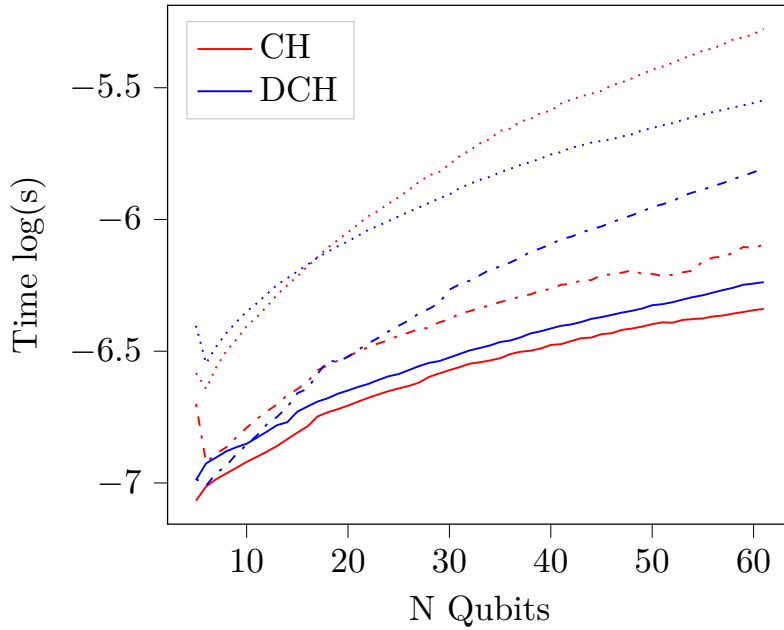
`Extend`, this effect is less significant, but nonetheless likely contributes to the steeper gradient of the `C++` scalings.

The difference in performance is most significant for the inner product routine, which has an overall complexity that scales as $O(n^3)$ resulting from up to n calls to the `Shrink` routine, and a call to Sergey Bravyi's Exponential Sum routine which also has runtime $O(n^3)$. In this case, the effect of the additional data-copying is suppressed by the overall runtime of the algorithm.

It is important to note that the `MATLAB` implementations also benefit from a degree of parallelization, through a combination of multi-threading, and so called 'Single Instruction stream Multiple Data stream' (SIMD) operations [21]. Matrix and vector multiplications are intrinsically parallelisable, as each element in the result is computed from a unique set of multiplication and addition operations. One option for optimising parallel code is to make multiple 'threads' available to the program, which each tackle a different part of the computation. However, as we are frequently performing lots of identical operations over different inputs, they can also benefit from SIMD CPU instructions. These are optimizations which speedup computations by loading multiple values into a special shared binary registers, applying a common operation to the entire register, and then reading the result back out [22]. `MATLAB` is built atop the long established `LAPACK` and `BLAS` libraries for linear algebra, which implement these types of optimization [23, 24, 25].

The effect of these optimizations becomes apparent when we try to extend a bitpacked simulation beyond 64 qubits. In this case, we need to use an array of integer values to encode each binary vector, and each operation now incurs the overhead of looping over these arrays. As an example, Figure 2.9 shows the runtime of the Exponential Sum algorithm of [12], extended up to 150 qubits. We choose Exponential Sum for this benchmark as it has a complexity that scales as $O(n^3)$, reducing the impact of the MEX interface on performance. As before, the speedup shown by the `C++` implementation continually decreases with increasing n. Given that some measure of performance improvement is
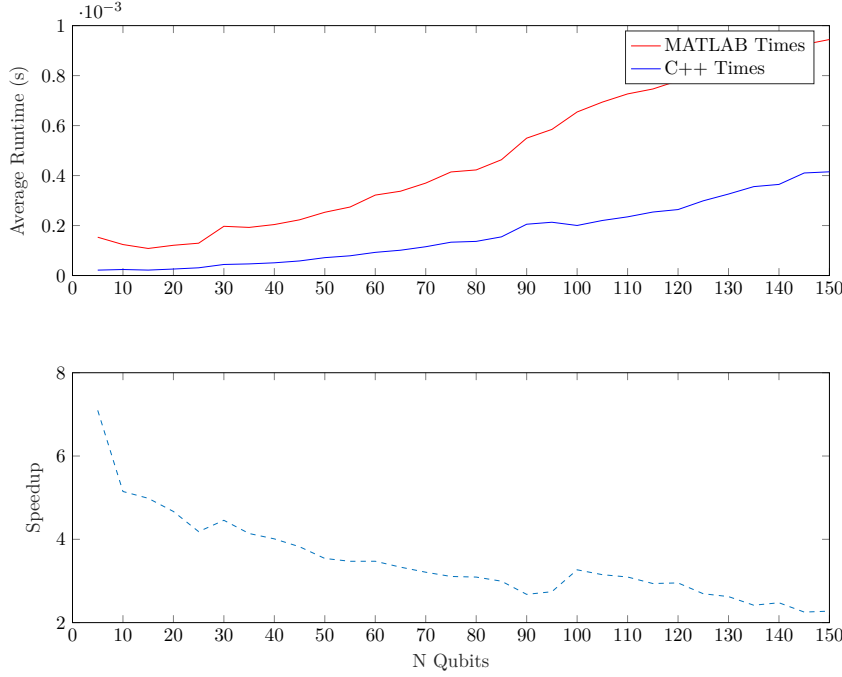
Figure 2.9: Figure comparing the runtime of the `C++` and `MATLAB` implementations of Sergey Bravyi's Exponential Sum routine, up to 150 qubits.

expected by virtue of using a compiled language, compared with the dynamic language `MATLAB`, we can see that the bitpacking method is no longer providing significant speedup.

It would also be possible to further optimize the implementation developed here with the addition of SIMD operations. Instead of looping over each integer variable used to encode large bitpacked vectors, the variables could instead be loaded into SIMD registers. THis would significantly optimize the computations up to 512 qubits, as 512 bits is the largest register currently supported [22]. An SIMD implementation is outside the scope of this thesis, but would be a significant performance upgrade to the CH and DCH simulators.

CH and DCH Performance

Comparisons between the DCH and CH forms and previous stabilizer simulators are shown in Figures 2.4, 2.5 and 2.6. Broadly, we see that the DCH and CH representations are competitive with previous techniques, in spite of tracking additional phase information and offering additional 'functionality'.

Specifically, for single qubit Clifford gates, we see that the Graph Sim method

has the best overall performance. Because applying a single qubit operator in this picture only requires updating 'local' information, it can be implemented using a lookup table and thus has constant complexity. This is a significant advantage over the other methods.

However, as mentioned in Table 2.1, the graph based data-structure employed by Anders & Breigel has a runtime that scales as the maximum degree d of the graph for entangling gates, as they alter this underlying graph. This effect becomes clear with increasing β, where the complexity of graph and subsequently the runtime of entangling gates significantly increases. At the largest tested value, 61 qubits, the runtime of an entangling gate grew from $\approx 3\text{x}10^{-7}$ at $\beta = 0.5$, to $\approx 1\text{x}1^{-5}$ at $\beta = 1.6$. In contrast, we note that the CHP, CH and DCH methods also show no apparent dependence on β. This would be expected from the update algorithms, which rely on binary operations that are independent of the sparsity of the data structures.

The DCH also benefits from a constant time complexity for all phase gates, leading to its improved performance for the 'CZ' gate. The CH representation has no constant time operations, but is broadly competitive in terms of single qubit gate performance. This is especially true in the case of the Hadamard gate, in spite of the theoretical $O(n^2)$ complexity of this operation. However, the DCH representation shows a significantly increased overhead in simulating Hadamard gates. This suggests the simulator is a poor choice for circuits involving many basis changes.

The origin of this increased overhead can potentially be explained by comparing the performance of Pauli measurements, where the CH simulator also out-performs the DCH method. This suggests that the additional overhead is incurred when commuting Pauli operators through the circuit layers. We might also expect that applying the circuit correction of Proposition 1 is slower for the DCH form, as it involves explicit matrix operations. In contrast, the CH form here requires only column updates, which take a single time-step as we store binary matrices as bitpacked column matrices.

The effect of commuting Paulis can be clarified by also considering Figure 2.8. We see that the CH method has a significant advantage for both single and n qubit Z-rotations, but that the DCH method shows slightly better performance for arbitrary Pauli operators. This likely follows from the need to compute a transpose of the F and M matrices, whereas the DCH method is optimized to avoid then need for transposition.

Transposition is also likely the cause of the increased overhead incurred by the CH representation in computing the equatorial inner products, and in computing computational state amplitudes, shown in Figure 2.7. Importantly, as discussed before, transposed matrices are stored 'lazily', computed only when required and then cached until outdated. Thus, in computing multiple amplitudes or inner products as is likely in a practical simulation, this performance gap between the two representations would likely decrease.

An interesting feature of computing computational basis state amplitudes and equatorial inner products is that they do not show only a small dependence on the length of the preceding stabilizer circuit. This is in contrast to the results of [7], which observed a transition from quadratic to cubic scaling in the number of qubits when computing stabilizer inner products, even for computational state amplitudes. This would be expected from the implementation of both routines, making use of intrinsic functions. These allow us to avoid inspecting matrices and vectors element-wise, instead operating on rows and columns at a time, and thus makes us less sensitive to the sparsity of the DCH/CH encoding.

Finally, if we consider simulating of Pauli measurements, we again observe that as implemented the DCH and CH forms have little apparent dependence on the sparsity of the underlying data-structures. At low values of β, each method shows a similar performance for Pauli X and Z measurements, with a slight advantage for the CH and GraphSim methods when simulating X measurements. However, as previously mentioned, Pauli measurements in the CHP method have a scaling that increases with the number of non-zero entries

in the tableau. The measurement routine of the GraphSim method, like the entangling gates, also depends on the maximal degree of the underlying graph. Thus, both routines see a significant increase in runtime as β increases. The GraphSim method in particular sees an almost 100 times increase in runtime between the smallest and largest values of β at $n = 60$.

Again, likely as a result of the bitpacked implementation, the DCH and CH methods are mostly unaffected by increasing β, with their runtime growing by a factor of $1.33 - 2$ between the extremal values. This small shift can be attributed to an increase in the number of non-zero entries, and thus the number of operations required in commuting a Pauli through the circuit and applying Proposition 1.

If we were to extend the CH and DCH methods above 64 qubits, we might expect this effect to become slightly more pronounced, as we would also incur the overhead of checking multiple binary variables. This effect can in fact be observed in the CHP data, which employs a version of bitpacking based on 32-bit integers. Above 32 qubits, we see a sharp jump in the runtime, which arises from the need to employ two integers for each bitpacked variable.

In conclusion then, we have developed two novel stabilizer simulators which are performant, and offer improved 'functionality' over previous methods. To further develop these tools, it would be important to extend them beyond the current 64 qubit limit, and to finish the implementation of arbitrary stabilizer inner products. With the addition of these routines, this software would form a very versatile tool-set for simulating different aspects of stabilizer circuits.

Chapter 3

Stabilizer Decompositions of Quantum States

3.1   Introduction

In the previous chapter, we discussed in detail efficient simulations of stabilizer circuits. Recalling the discussion in Section**Please insert your reference later**, this classical simulability in turn implies that non-stabilizer states are a resource for quantum computation. In this section, we will introduce a particular model of quantum computation that makes explicit the computational role of 'magic' states, Pauli Based Computation [26, 27].

This model forms the basis for the definition of Stabilizer Rank, a quantity which tries to relate the computational power of non-stabilizer states to the task of classical simulation. This chapter will be focused on extending the stabilizer rank method, whereas the following chapter will focus on its implementation for the task of classical simulation.

3.1.1   Pauli Based Computations

A Pauli Based Computation (PBC) is a measurement-based model of quantum computing, whereby a computation is realised by applying a sequence of Pauli measurements to a set of non-stabilizer magic states, and post-processing of the measurement outcomes. In general, this sequence will be 'adaptive', and the choice of measurement operator will depend on the outcome of previous measurements.

It is well known that quantum circuits built out of Clifford gates and the T gate are universal for quantum computation [28]. Thus, any arbitrary computation
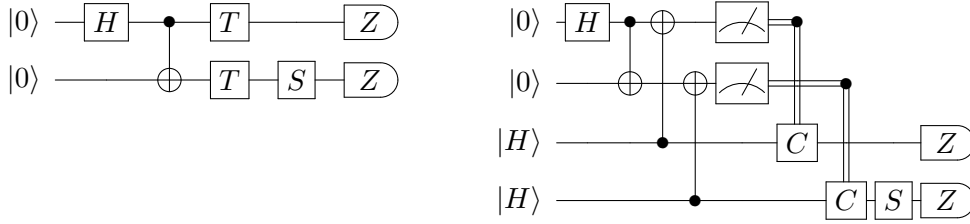
Figure 3.1: Figure illustrating two equivalent forms of a small circuit built form the Clifford $+ T$ gate set. The lower circuit is obtained from the former by replacing each T gate with a teleportation or 'state-injection' gadget that consumes one magic state $|H\rangle = \cos\frac{\pi}{8}|0\rangle + \sin\frac{\pi}{8}|1\rangle$. This performs a T gate (up to a measurement controlled correction operation C which is a Clifford gate) [29].

U acting on a computational input state can be expressed as a circuit with m Clifford operations and t T gates.

By replacing each T gate in a Clifford+T circuit with a state-injection gadget [28], we instead end up with a circuit built exclusively from Clifford gates and Pauli measurements, acting on n qubits in a computational basis state, and t qubits in a non-stabilizer state. Once in this form, we can convert the circuit to a PBC [26, 27].

In the following discussion, we assume that the only intermediate measurements in the circuit arise from the state-injection gadgets. Circuits with clasically controlled gates condition on intermediate measurements are called 'adaptive'. We note that the PBC construction works for both adaptive and non-adaptive circuits, so this assumption can be made without loss of generality [26, 27].

Once in this form, we can commute every Clifford operator through the circuit and past the final Pauli measurement layer. As we do, each measurement operator $P \to P'$ under conjugation, and the Clifford gate can then be discarded as it happens after the measurement layer and thus has no effect on the outcome. These updates can be efficiently computed using the methods discussed in Chapter 2. The result is some new sequence of Pauli measurements $P_1, \ldots, P_r$, acting on $n + t$ qubits.

It is then possible to show that these measurements can be rearranged such that

all measurements commute, and act non-trivially on only the t magic states. The key technique is a lemma showing that if any pair P_j, P_k anticommute, they can be updated by sampling a measurement outcome $\lambda_k = \pm 1$ uniformly at random, replacing the P_j with a Clifford operator $V_{j,k} = \frac{\lambda_j P_j + \lambda_k P_k}{\sqrt{2}}$, where λ_j was the outcome of measuring P_j. This Clifford can then be commuted through the rest of the measurement layer [27].

Now consider prepending the circuit with Pauli Z measurements on the n computational qubits. By definition, these measurements are deterministic and do not change alter the computation. Application of the above Lemma ensures that these computational measurements all commute with the final measurement operators P_i, and thus that the P_i act trivially on the n computational qubits [26].

Overall then, the PBC model allows us to realise quantum computation using only a supply of non-stabilizer resource states, Pauli measurements, and probabilistic classical computation, used to compute and update the Pauli measurement sequence [27]. The classical component of the computation is efficient, that is to say the measurement sequence can be computed with a runtime that scales polynomially in the number of qubits.

A PBC $\mathcal{C}$, obtained from some Clifford $+ T$ circuit U, can be said to efficiently simulate the original circuit, in both the weak [27] and strong sense [26]. Weak simulation follows immediately as, given a method to sample from the measurement operators of the PBC, this also corresponds to a sample of the output distribution of the original circuit [27]. Strong simulation then follows from the result that an adaptive circuit with postselection has a corresponding PBC with postselected Pauli measurements [27]. In particular, we can fix both the measurement outcomes of the circuit, and the measurement-controlled correction operations introduced by state-injection. The result is a non-adaptive circuit, which is translated to a non-adaptive PBC with a fixed Pauli projector $\Pi_{x,s}$ [27], where x and s are the postselected binary bits corresponding to the measurement outcome and the state-injection gadgets, respectively [26, 8].

The corresponding probability amplitude is thus given by

$$\langle x|U|0^{\otimes n}\rangle \equiv 2^t \langle T^{\otimes t}|\Pi_{x,s}|T^{\otimes t}\rangle \tag{3.1}$$

where we reweight the probability to account for the fact that each of the 2^t different outcomes on the state-injection gadgets is equiprobable.

3.1.2   Stabilizer State Decompositions

In the PBC model of quantum computation, the role of non-stabilizer states as a resource for quantum computation is made explicit. It is also clear that the PBC would require exponential time to simulate clasically, as Pauli expectation values on non-stabilizer states cannot in general be efficiently computed [1].

In the context of resource theories for quantum computation, we can consider studying quantum computations by decomposing computations in terms of the 'free' set of operations. This is what Bravyi, Smith & Smolin did when considering stabilizer state decompositions of magic states. We define a stabilizer state decomposition of a general state $|\psi\rangle$ as

$$|\psi\rangle = \sum_{i=1}^{\chi} c_i |\phi_i\rangle, \tag{3.2}$$

where each $|\phi_i\rangle$ is a stabilizer state and the total number of terms in the decomposition, χ, is called the *Stabilizer Rank* of the state $|\psi\rangle$.

Given a PBC, and a stabilizer state decomposition of the magic states $|T\rangle^{\otimes t}$, then strong simulation of a PBC reduces to computing a Pauli expectation value for each term in the decomposition. As these are stabilizer states, this expectation value can be computed efficiently. Using that fact that Pauli projectors map stabilizer states to stabilizer states, we can write

$$\Pi\left|H^{\otimes t}\right\rangle = \sum_{i=1}^{\chi} c_i \Pi |\phi_i\rangle = \sum_{i=1}^{\chi} c_i \left|\phi_i'\right\rangle = \left|psi'\right\rangle$$

and thus, the overall expectation value is given by

$$\left\langle H^{\otimes t}\middle|\Pi\middle|H^{\otimes t}\right\rangle = \left\langle H^{\otimes t}\middle|\psi'\right\rangle = \sum_{i,j} c_i^* c_j \left\langle \phi_i\middle|\phi_j'\right\rangle, \tag{3.3}$$

a sum of χ^2 stabilizer inner products. Thus, the overall runtime of the simulation scales as $O\left(\chi^2 \text{poly}(n)\right)$ [26].

An explicit method for weak sampling using stabilizer state decompositions was also outlined in [26], based on computing individual measurement probabilities and using them to sample marginals. In particular, consider sampling the jth bit of an output string x, given outcomes for bits $x_1, x_2, \ldots x_{j-1}$. We can sample x_j but computing two probability terms, as [8]

$$P(x_j|x_1, x_2, \cdots x_{j-1}) = \frac{P(x_1, \ldots x_j)}{P(x_1, \ldots x_{j-1})} \equiv \frac{\left\langle H^{\otimes t}\middle|\Pi_{x_1,\ldots x_j}\middle|H^{\otimes t}\right\rangle}{\left\langle H^{\otimes t}|\Pi_{x_1,\cdots x_{j-1}}|H^{\otimes t}\right\rangle}. \tag{3.4}$$

Fixing $x_j = 0$, and computing the conditional probability, we can thus sample the jth bit by generating uniform random numbers. If $r \leq P(0|x_1, x_2, \cdots x_{j-1})$, we return 0, else we return 1.

Importantly, the authors were able to show that stabilizer rank decompositions of magic states can be smaller than expected. As a simple example, consider two copies of the $|T\rangle$ magic state:

$$\begin{aligned} |H\rangle &= \cos\tfrac{\pi}{8}|0\rangle + \sin\tfrac{\pi}{8}|1\rangle & \chi\left(|H\rangle\right) &= 2 \\ \left|H^{\otimes 2}\right\rangle &= \tfrac{1}{2}\left(|00\rangle + \mathrm{i}|11\rangle\right) + \tfrac{1}{2\sqrt{2}}\left(|01\rangle + |10\rangle\right) & \chi\left(\left|H^{\otimes 2}\right\rangle\right) &= 2 \end{aligned} \tag{3.5}$$

This is a quadratic reduction in the number of terms in the decomposition, compared to an expansion in the computational basis. The authors in fact improved this asymptotic bound by using random walk methods to search for other stabilizer state decompositions. They were able to set an upper bound $\left|H^{\otimes 6}\right\rangle \leq 7$, and thus

$$\chi\left(\left|H^{\otimes t}\right\rangle\right) = 7^{t/6} = 2^{\frac{\log_2(7)}{6}t} \approx 2^{0.47t} \tag{3.6}$$

giving strong simulation with stabilizer state decompositions a smaller exponential overhead than state-vector methods, even with the dependence on χ^2 in the runtime.

Previous works have also explored stabilizer decompositions of universal quantum computations, containing non-Clifford gates. In their original paper, Aaronson & Gottesman explored expanding gates in the Pauli operator basis. Each branch in the expansion will produce a different stabilizer state [2].

$$U \ket{\phi} = \sum_i a_i P_i \ket{\phi} = \sum_i a_i \ket{\phi_i'}$$

In general, this will require up to 4^m stabilizer states for each m-qubit non-Clifford gate. For the T gate in particular, we can write

$$T \equiv \begin{pmatrix} 1 & 0 \\ 0 & \frac{1}{\sqrt{2}}(1+i) \end{pmatrix} = \frac{\sqrt{2}+i}{\sqrt{2}} I - \frac{i}{\sqrt{2}} Z$$

and thus this extension of the CHP method requires 2^t stabilizer states for t T gates.

A different method was also proposed by Garcia et al., which they call stabilizer frames [10]. These are stabilizer state decompositions built out of so-called 'cofactors', made from post-selecting the results of single qubit computational basis measurements. For example, the action of a controlled-S gate can be expanded into two stabilizer state terms, by post-selecting on the control bit being $\ket{0}$ or $\ket{1}$. For the T gate, stabilizer frames similarly require a number of terms that that scales as 2^t.

Norm Estimation and Approximate Decompositions

The stabilizer rank method as introduced in [26] already compares favourably to similar methods of simulating quantum circuits through stabilizer state decompositions. However, the method was further refined in a successive paper, which extended its results to the case of approximate simulation [8].

The first development of [8] was an algorithm for estimating the norm of sta-

bilizer states that could be used to optimize the computation of Pauli expectation values on stabilizer state decompositions. A detailed discussion of this norm estimation routine will be given in Chapter 4. Importantly however, this method allows Pauli expectation values to be approximated to within ϵ error in total variation distance, with a runtime that scales as $O(\chi t^3 \epsilon^{-2})$, a quadratic reduction in terms of the stabilizer rank [8].

The second component was a method for construction approximate stabilizer state decompositions

$$\left|\tilde{\psi}\right\rangle = \sum_{i=1}^{\chi_\epsilon} c_i \left|\phi_i\right\rangle \,:\, F\left(\left|\tilde{\psi}\right\rangle, \left|\psi\right\rangle\right) \geq 1 - \epsilon \tag{3.7}$$

where F is the fidelity and χ_ϵ is called the approximate stabilizer rank. Using a method which we will discuss in detail in Section 3.2.2, the authors showed that

$$\chi_\epsilon\left(\left|H\right\rangle^{\otimes t}\right) \approx 2^{0.23t}\epsilon^{-2}. \tag{3.8}$$

Thus giving a further quadratic reduction in the number of terms in the stabilizer state decomposition.

3.2   Results

As established, the stabilizer rank method offers reasonably efficient decompositions of universal quantum circuits. Importantly however, these results only apply to the T magic state. While Clifford+T is known to be a universal gate set for quantum computation, in practice the number of T gates required to synthesize a circuit grows rapidly. For example, synthesising arbitrary-angle Pauli Z rotations from Clifford+T gates can quickly result in a T count on the order of 100 per gate [30, 31]. In the rest of this chapter, we seek to extend our understanding of stabilizer state decompositions beyond the $|H\rangle$ magic state, and discuss the interpretation of the stabilizer rank as it relates to quantum computation.

3.2.1   Exact Stabilizer Rank

As well as having an interpretation in terms of classical simulations, the stabilizer rank of a state has three properties that make it interesting as a potential measure of 'magic' as a resource in quantum computation [4, 32].

Claim 2 *Properties of the exact stabilizer rank:*

1. **Faithfulness:** $\chi(|\psi\rangle) = 1$ *iff* $|\psi\rangle$ *is a stabilizer state.*

2. **Submultiplicativity:** $\chi(|\psi\rangle \otimes |\Psi\rangle) \leq \chi(|\psi\rangle)\chi(|\Psi\rangle)$.

3. **Monotonicity:** χ *is invariant under Clifford gates and monotonically decreasing under Pauli measurements.*

Proof of Claim 2. The faithfulness property of χ follows from its definition (see Eq. 3.2).

Given a tensor product of two states, we can expand out their stabilizer state decompositions as

$$|\psi\rangle \otimes |\Psi\rangle = \sum_{i=1}^{\chi(|\psi\rangle)} \sum_{j=1}^{\chi(|\Psi\rangle)} c_i c_j |\phi_i\rangle \otimes |\phi_j\rangle\,.$$

A tensor product of two stabilizer states is also a stabilizer state, and thus we obtain a potential stabilizer state decomposition with $\chi(|\psi\rangle) \cdot \chi(|\Psi\rangle)$ terms. However smaller decompositions, including entangled stabilizer states rather than these separable states, may exist. Thus, the stabilizer rank is submultiplicative under tensor product.

Invariance under Clifford unitaries follows from the linearity of quantum mechanics, and the definition of the Clifford group. Expanding out the decomposition, we have

$$V|\psi\rangle = \sum_i c_i V|\phi_i\rangle = \sum_i c_i |\phi_i'\rangle$$

where the new states in the decomposition can be efficiently computed [1]. After performing a Pauli measurement, the decomposition will be updated by

applying a projector $\frac{1}{2}(\mathbb{I} + \lambda P)$, where $\lambda = \pm 1$ is the outcome of the measurement.

$$\frac{1}{2}(I + \lambda P)|\psi\rangle = |\psi'\rangle = \sum_i c_i (|\phi\rangle + \lambda P |\phi\rangle)$$

As discussed in the previous chapter, applying a Pauli projector to a stabilizer state either produces a new stabilizer state, or the null-vector if $\lambda P |\phi\rangle = -|\phi\rangle$. If no states are orthogonal to the Pauli projector applied, then the stabilizer rank is unchanged and the decomposition is updated. Otherwise, $\chi(|\psi'\rangle) < \chi(|\psi\rangle)$. $\square$

No general method is known for finding low rank stabilizer state decompositions of general quantum states. The number of stabilizer states grows exponentially with the number of qubits [2], even before considering the combinatoric growth in the number of candidate decompositions. Additionally, checking the validity of a candidate stabilizer state decomposition has a computational complexity that also scales exponentially in the number of qubits.

n copies	1	2	3	4	5	6
χ_n	2	2	3	4	6	7

Table 3.1: Optimal rank of stabilizer state decompositions for the $|H\rangle$ magic state, from [26].

In [26], the authors made use of computational searches to find the upper bounds on the stabilizer rank of the $|H\rangle$ magic state shown in Table 3.1. They also make the following conjecture, called Conjecture 1 in the paper.

Conjecture 1 *Let $\chi_n = \chi\left(\left|H^{\otimes n}\right\rangle\right)$. Then for a single qubit state $|\phi\rangle$*

$$\chi\left(\left|\phi^{\otimes n}\right\rangle\right) = 1 \quad \text{If } |\phi\rangle \text{ is a stabilizer state}$$
$$\chi\left(\left|\phi^{\otimes n}\right\rangle\right) = \chi_n \quad \text{If } |\phi\rangle \text{ is a magic state}$$
$$\chi\left(\left|\phi^{\otimes n}\right\rangle\right) > \chi_n \quad \text{Otherwise.}$$

The $|H\rangle$ state is one of a family of 12 single qubit magic states, which can be transformed into each other by applying Clifford gates. Thus, they also have

equivalent stabilizer rank. We refer to these magic states as 'edge states', from their location on the Bloch sphere [28]. However, there also exist a second set of 8 single qubit magic states that cannot be generated from the edge states by Clifford unitaries. In this text, we call these 'face states'.

$$|F\rangle = \cos\beta\,|0\rangle + \mathrm{e}^{\mathrm{i}\pi/4}\sin\beta\,|1\rangle \ : \ 2\beta = \cos^{-1}\frac{1}{\sqrt{3}} \tag{3.9}$$

Denoted $|R\rangle$ in [26], the authors comment that numeric results appear to show it has the same stabilizer rank as the edge type-states, and thus put forward Conjecture 1.
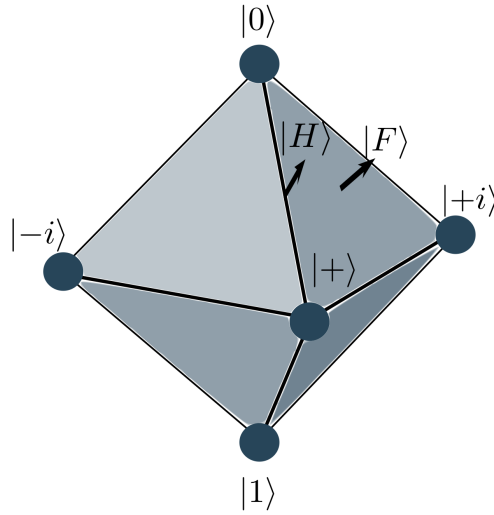
Figure 3.2: Diagram showing the location of single-qubit stabilizer states and magic states on the Bloch sphere. Single qubit Clifford gates act as the symmetry group of an octahedron in the Bloch sphere, who's vertices are the individual stabilizer states. 'Edge' and 'face' magic states are named for their positions relative to this octahedron. Based on diagrams given in from [28].

We further examined the stabilizer rank for different quantum states by extending the computational searches of [26].

Computation Searches for Decompositions

We employ a combination of brute force and random walk searches for stabilizer state decompositions to establish the stabilizer rank of different families of quantum states, using a custom program developed in Python.

To test a candidate decomposition of χ stabilizer states $\Phi = \{|\phi_i\rangle\}$, we compute

the projector on to the subspace generated by the states Π_Φ, and the compute the projection of the target state into this subspace $\|\Pi_\Phi |\psi\rangle\|$. If the norm is equal to 1, then the state lies within this subspace and we terminate the search.

Given a collection of χ stabilizer states, we can build their projector by first constructing a $2^n \times \chi$ matrix A where each column is one of the χ stabilizer states. We then apply the QR decomposition, a standard linear algebra technique, to compute χ orthogonal basis-vectors for the subspace spanned by these stabilizer states. Given the column matrix Q built from these orthogonal basis-vectors, we then have $\Pi_\Phi \equiv QQ^\dagger$. This was implemented using the `Numpy` library, with additional optimization provided by using the `Numba` Just-In-Time compiler [33, 34].

The random walk method follows the description in Appendix B of [26]. The search algorithm takes as input a state $|\psi\rangle$ to decompose, and a candidate stabilizer rank χ. We begin with a candidate decomposition $\Phi = \{|\phi_i\rangle\}$, and compute the 'distance' from the generated subspace $F = 1 - \|\Pi_\Phi |\psi\rangle\|$. We then update one state, chosen uniformly at random, by applying a random Pauli operator P. We then compute the updated distance $F' = 1 - \left\|\Pi_{\tilde{\Phi}} |\psi\rangle\right\|$ using this updated set of stabilizer states. If $F' < F$, we accept the move and proceed. Otherwise, we accept the move with a probability given by the Boltzmann distribution $p = \mathrm{e}^{-\beta(F'-F)}$, where β is a parameter we set. As the search continues, we gradually increase β. This method is thus similar to the simulated annealing approach in optimization, where we are seeking to minimize the distance between $|\psi\rangle$ and the generated subspace.

Our random walks were run using the same parameters of [26], testing 100 values of the inverse-temperature parameter $\beta \in [100, 4000]$, and running for 1000 steps for each value of β. For any given candidate and value of χ, we repeated the random walk 5 times. The smallest decomposition found across all runs was taken as an upper bound on the stabilizer rank. As with the brute force searches, $\chi = 2$ was taken as a lower bound, and the largest value tested

was either $2^n - 1$, or else a value derived using submultiplicativity and results for fewer copies of the target state.

The brute force method, in contrast, takes as input a target state $|\psi\rangle$, and an upper and lower bound of stabilizer rank to test. The typical lower bound given is 2. The upper-bound is set by either the computational basis expansion, which is a valid stabilizer state decomposition, or else a bound based on submultiplicativity and known results for fewer copies of a state.

Pseudocode descriptions of the search methods are given in Algorithms 1 and 2. We also note an additional optimisation that, in the case where the target state has only real coefficients, we can restrict ourselves to considering decompositions built only from stabilizer states with real values. In the random walk case, we additionally restrict the moves we generate such that they do not introduce any imaginary coefficients. We do this by requiring that the random Pauli operators have an even number of Pauli Y operators.

As mentioned above, the number of stabilizer states grows exponentially with the number of qubits. In particular, we have [2]

$$N_\phi = 2^n \prod_{k=1}^{n-1} \left(2^{n-k} + 1 \right). \tag{3.10}$$

In practice, brute force searches were tractable up to about 3 qubits. Some examples of the growth in possible combinations are given in Table 3.2.

n Qubits	1	2	3	4
N_ϕ	6	60	1080	36720
$\binom{N_\phi}{2^n-1}$	6	33240	3.33×10^{17}	2.27×10^{56}

Table 3.2: Table showing how the number of combinations of stabilizer states grows as a function for the number of qubits. We consider $2^n - 1$ as this is the largest possible stabilizer rank that is below the trivial computational basis bound.

Generating Stabilizer States

As an input for Algorithms 1 and 2, we need a way to quickly generate random stabilizer states, as well as a library of all stabilizer states for small n. To

---

Algorithm 1 Random Walk Search for Stabilizer State Decomposition

---

Require: $\beta_{init}, \beta_{max}, M$, target integer χ
Require: PROJECTOR(Φ)   ▷ Returns projector onto subspace spanned by Φ
 1: $\Phi \leftarrow (\phi_1, \cdots \phi_\chi)$ where each ϕ_a is chosen at random.
 2: $\beta \leftarrow \beta_{init}$
 3: **while** $\beta < \beta_{max}$ **do**
 4:     **for** $i = 0$ to 1000 **do**
 5:         $\Pi_\Phi \leftarrow$ PROJECTOR(Φ)
 6:         $F(\tilde{\phi}) = 1 - \|\Pi_\phi |\psi\rangle\|$
 7:         **if** $F(\tilde{\phi}) = 1$ **then**
 8:             **return** $\tilde{\phi}$
 9:         **end if**
10:         Pick random integer $a \in [1, n]$ and random Pauli $P \in \mathcal{P}_n$
11:         $|\phi_a\rangle' \leftarrow c(\mathbb{I} + P)|\phi_a\rangle$ ▷ If $|\phi_a\rangle' = 0$, pick new a and P.
12:         $\tilde{\Phi} \leftarrow (|\phi_1\rangle, \cdots, |\phi_a\rangle', \cdots |\phi_\chi\rangle)$
13:         $\Pi_{\tilde{\Phi}} \leftarrow$ PROJECTOR($\tilde{\Phi}$)
14:         $F' \leftarrow 1 - \|\Pi_{\tilde{\Phi}} |\psi\rangle\|$
15:         **if** $F' < F$ **then**
16:             $|\phi_a\rangle \leftarrow |\phi_a\rangle'$
17:         **else**
18:             $p_{accept} \leftarrow \exp[-\beta(F' - F)]$
19:             Pick random $r \in [0, 1]$
20:             **if** $r < p_{accept}$ **then**
21:                 $|\phi_a\rangle \leftarrow |\phi_a\rangle'$
22:             **end if**
23:         **end if**
24:     **end for**
25:     $\beta \leftarrow \beta + \left(\frac{\beta_{\max} - \beta_{\text{init}}}{M}\right)$
26: **end while**
27: **return** No decomposition found.

Algorithm 2 Brute Force Search for stabilizer rank

Require: $\{\phi\}_n$ ▷ The set of n qubit stabilizer states
Require: PROJECTOR(Φ)   ▷ Returns projector onto subspace spanned by Φ.
 1: $\chi = 2$
 2: **while** $\chi < (2^n - 1)$ **do**
 3:     **for**   **do** $\Phi = \{|phi_1\rangle, \ldots, |\phi_\chi\rangle$ ▷ For all combinations of i states.
 4:         $\Pi_\Phi \leftarrow$ PROJECTOR(Φ)
 5:         **if** $\|\Pi_{\tilde{\Phi}} |\psi\rangle\| = 1$ **then**
 6:             **return** χ, Φ
 7:         **end if**
 8:     **end for**
 9:     $\chi \leftarrow \chi + 1$
10: **end while**
11: **return** 2^n ▷ The computational basis expansion is the best found.

---

accomplish this, we make use of the canonical form for stabilizer tableaux introduced by Garcia et al., and discussed in Section 2.1 [7].

Like the CHP method, a canonical stabilizer tableau is a $n \times (2n+1)$ matrix, where each row encodes a Pauli operator

$$P(s) = -1^{s_0} \otimes_{i=1}^{n} X^{s_i} Z^{s_{i+n}}, \; : \; s \in \mathbb{Z}_2^{2n+1}.$$

There are in general multiple tableau corresponding to a given stabilizer state, but using Algorithm 1 of [7] any tableau can be converted to a standard form.

To quickly generate random stabilizer states then, we generate a random $n \times (2n+1)$ binary matrix. We then apply the canonical form algorithm. If any rows of the tableau are the all-0 string, then the tableau does not correspond to a stabilizer state and so we discard it. Else, we build up a Pauli projector from the rows of the tableau, and compute the stabilizer state as the unique $+1$ eigenstate.

To generate a complete library of stabilizer states, first recall that Pauli operators in a stabilizer group have only phase of ± 1. For a stabilizer group with n generators, there are thus 2^n possible combinations of phase for each generator, each of which correspond to a given stabilizer state. We can thus focus on generating just the $N_\phi / 2^n$ stabilizer groups with all positive phase.

We begin by generating all $2^{2n} - 1$ possible binary strings, which correspond to all possible choices of Pauli operator. We ignore the all 0 string, as this corresponds to the identity operator which cannot generate a stabilizer group. Then, for all $\binom{2^{2n}-1}{n}$ possible combinations of n strings, we build the stabilizer tableau and convert it to canonical form. If it is not full rank, or corresponds to a tableau already found, we discard it. Otherwise we store the tableau. We terminate after generating $N_\phi / 2^n$ groups. For each group then, we test all 2^n possible phase combinations, and then compute the stabilizer state as described above. This process was quite computationally intensive, but overall we were able to generate a library of stabilizer states on up to 4 qubits.

Both the random stabilizer state generation and the deterministic stabilizer state generation were implemented in Python. Stabilizer tableau were stored as bitpacked `Numpy` arrays. Computing the corresponding Pauli projector and stabilizer state made use of `Numpy` linear algebra routines, including the optimised eigensovler for hermitian matrices, with additional optimization using `Numba` [33, 34].

Results of Computational Searches

We extend the computational searches for copies of single-qubit magic states up to $n = 10$, and give explicit results for the face-type magic states. We used brute force searches for $n \leq 3$ qubits. Otherwise, we made use of random walk searches.

For all values of n tested, the edge and face type magic states had the same observed stabilizer rank. Despite extending the range of the numeric search, however, above $n = 6$ copies we found no decomposition smaller than the sub-multiplicative bound. Thus, the asymptotic scaling shown in [26] remains the best result known for single-qubit magic states..

As a means of probing Conjecture 1, we also explored the stabilizer rank of 'typical' single qubit states, generated uniformly at random. The target states were prepared by applying a Haar random single-qubit unitary to the $|0\rangle$ states [35]. We began by applying brute force searches to 1000 typical states up to 3 copies, and observed that all states tested had the same stabilizer rank, and also that their stabilizer rank grew more slowly than the computational basis expansion. All results for single qubit states are shown in Table 3.3.

Applying the argument of Eq. 3.6, then for typical single qubit states their stabilizer rank is upper bounded by

$$\chi\left(\left|\phi^{\otimes t}\right\rangle\right) \leq 8^{t/6} = 2^{\log_2 8t/6} = 2^{0.5t}. \tag{3.11}$$

To further explore the claim in Conjecture 1, we also performed computational searches for specific states with a structure related to the magic states. In par-

ticular, we performed computational searches for the $|CS\rangle$ and $|CCZ\rangle$ magic states, which can be used to inject the two-qubit CS gate and the three-qubit CCZ gate, respectively. Both of these gates, like the T gate, belong to the third level of the Clifford hierarchy. We also considered the single qubit resource states $T^{\frac{1}{2}}|+\rangle$ and $T^{\frac{1}{4}}|+\rangle$. These resource states can be used to inject gates from the 4th and 5th levels of the Clifford hierarchy, though potentially requiring a non-Clifford correction operation. We limited our searches up to 6 qubits, which meant considering up to 3 copies of the $|CS\rangle$ state and just two copies of the CCZ state The results are show in table 3.4.

Interestingly, we observe that the single qubit resource states corresponding to gates in higher levels of the Clifford hierarchy show no difference from the stabilizer rank of typical single qubit states. However, magic states on 2 and 3 qubits also show significantly reduced stabilizer rank. In fact, the asymptotic scaling of the $|CS\rangle$ and $|CCZ\rangle$ is significantly smaller when compared to the naive computational basis expansion, scaling as $\approx 2^{0.79t}$ and 2^t versus 2^{2t} and 2^{3t}, respectively.

t Copies	2	3	4	5	6	7	8	9	10
$\chi\left(|T^{\otimes t}\rangle\right)$	2	3	4	6	7	12	14	21	28
$\chi\left(|F^{\otimes t}\rangle\right)$	2	3	4	6	7	12	14	21	28
χ (Typical)	3	4	5	6	8	14	24	30	36

Table 3.3: Results of computational searches for stabilizer rank decompositions of different single-qubit quantum states. The results would appear to agree with Conjecture 1, that stabilizer rank is smaller for magic states.

t Copies	1	2	3	4
$T^{\frac{1}{2}}|+\rangle$	2	3	4	5
$T^{\frac{1}{4}}|+\rangle$	2	3	4	5
$|CS\rangle$	2	3	6	-
$|CCZ\rangle$	2	4	-	-

Table 3.4: Results of computational searches for stabilizer rank decompositions of different types of non-stabilizer resource state. We extended the searches for the $T^{\frac{1}{2}}$ and $T^{\frac{1}{4}}$ gate resource states up to 6 copies, but found no decompositions smaller than the results for typical single qubit states.

Decompositions of the Symmetric Subspace

When taking multiple copies of any given n-qubit state $|\psi\rangle$, the result will always lie within the symmetric subspace $\mathrm{Sym}_{n,t} \subseteq \mathbb{C}^{2^n}$. This is a subspace of the full n-qubit Hilbert space with dimension

$$\dim\left(\mathrm{Sym}_{n,t}\right) = \binom{2^n + t - 1}{t} \tag{3.12}$$

We can thus consider searching for stabilizer state decompositions of a subspace. We define the exact stabilizer rank of a subspace P as

$$\chi\left(P\right) = |\Phi| : P \in \mathrm{span}[\Phi]. \tag{3.13}$$

Computationally, we employ the Random Walk method, to build decompositions of the subspace $\mathrm{Sym}_{1,t}$. As our objective function, we replace the projection into the subspace Π_Φ with the largest principle angle between two subspaces Π_Φ and $\Pi_{\mathrm{Sym}_{1,t}}$. If $\mathrm{Sym}_{1,t} \subseteq \mathrm{Span}\left(\Phi\right)$, this angle is zero. The formula for the largest principle angle is shown in Eq. 3.14 [36]. The projector onto the symmetric subspace, $\Pi_{\mathrm{Sym}_{1,t}}$, was computed using the method based on superpositions of computational basis states with equal Hamming weight, outlined in [37].

$$\theta\left(\Pi_\Phi, \Pi_{\mathrm{Sym}_{1,t}}\right) = \sin^{-1}\left(\left\|\left(I - \Pi_\Phi\right)\Pi_{\mathrm{Syn}_{1,t}}\right\|\right) \tag{3.14}$$

For all values tested, the best decomposition found for the projector onto the single qubit symmetric subspace were equal to the results for typical single qubit states. Additionally, we note that for $t \leq 5$

$$\chi\left(\mathrm{Sym}_{1,t}\right) = \dim\left(\mathrm{Sym}_{1,t}\right) \leq t + 1 = \binom{2 + t - 1}{t}, \tag{3.15}$$

the stabilizer rank found for the single qubit symmetric subspace is equal to its dimension.

In fact, in [12], we make the following claim

Claim 3 $\chi\left(Sym_{n,t}\right) = dim\left(Sym_{n,t}\right) : \forall n,\ t \leq 5$

For $t \leq 3$, this claim follows from the property that stabilizer states form a projective 3 design [38]. Thus, for a given n qubits and $t \leq 3$

$$\frac{1}{N_\phi} \sum_i |\phi_i\rangle\langle\phi_i| = \frac{\Pi_{\mathrm{Sym}_{n,t}}}{\dim\left(\mathrm{Sym}_{n,t}\right)}, \tag{3.16}$$

a superposition of t copies of all n-qubit stabilizer states is proportional to the projector onto the symmetric subspace.

From this, we can conclude that $\mathrm{Span}\left(\left\{\left|\phi_i^{\otimes t}\right\rangle\right\}\right) \subseteq \Pi_{\mathrm{Sym}_{n,t}}$. We can thus find a minimal spanning set of vectors $\{|\phi_j^{\otimes t}\rangle\}$ such that $\mathrm{Span}\left(\{|\phi_j^{\otimes t}\rangle\}\right) = \mathrm{Sym}_{n,t}$, and $\left|\{|\phi_j^{\otimes t}\rangle\}\right| = \dim\left(\mathrm{Sym}_{n,t}\right)$, completing the claim for $t \leq 3$. In [12], we present a proof by Earl Campbell that also extends this result up to $t = 5$ using the fact that stabilizer states are 'almost' a projective 4-design [38].

Clifford Symmetries

The results of computational searches, and the proof for the decomposition of the symmetric subspace, are consistent with Conjecture 1. In Table 3.5, we compare the bounds for the symmetric subspace with the stabilizer rank decompositions found for different magic states, and show that in general the magic states exhibit a smaller stabilizer rank.

(a)

n Copies	2	3	4	5
$\dim\left(\mathrm{Sym}_{n,t}\right)$	3	4	5	6
$\chi\left(|T,F\rangle\right)$	2	3	4	6

n Copies	1	2	3
$\dim\left(\mathrm{Sym}_{n,t}\right)$	4	10	20
$\chi\left(|CS\rangle\right)$	2	3	6

(b)

n Copies	1	2
$\dim\left(\mathrm{Sym}_{n,t}\right)$	8	36
$|CCZ\rangle$	2	4

(c)

Table 3.5: Tables comparing the dimension, and thus stabilizer rank, of the symmetric subspace up to 5 copies with that of magic states, for 1, 2 and 3 qubits.

A property common to all the magic states tested is that they each have an associated Clifford symmetry. This is in fact always true for a magic state

that can be used to inject a gate from $\mathcal{C}_3$. These magic states have the form $|U\rangle = U|\phi\rangle$, where $|\phi\rangle$ is a stabilizer state [29]. Updating the stabilizer group under conjugation, we obtain a new set of operators that stabilizer the resource state $|U\rangle$

$$S|\phi\rangle = |\phi\rangle \rightarrow USU^\dagger|U\rangle = USU^\dagger U|\phi\rangle = U|\phi\rangle \ \forall S \in \mathcal{S}_\phi. \tag{3.17}$$

From the definition of $\mathcal{C}_3$, these operators are then Clifford as $USU^\dagger \in \mathcal{C}_2$, and also form a group which we call $\mathcal{M}$. We introduce the following nomenclature.

Definition 3.1 (Clifford Magic State). Consider a magic state $|R\rangle$, with an associated group of Clifford symmetries $\mathcal{M}$ such that

1. $\mathcal{M} \subseteq \mathcal{C}_2$

2. $m|R\rangle = |R\rangle \ \forall m \in \mathcal{M}$

3. $|R\rangle\langle R| = \frac{1}{|\mathcal{M}|}\sum_{m \in \mathcal{M}} m$

Then $|R\rangle$ is a Clifford magic state.[1]

Any state that can be consumed in a state-injection gadget is also a Clifford magic state.. For example, the $|H\rangle$ magic state is so labeled as it has the property that $H|H\rangle = |H\rangle$, and thus has the group $\{I, H\}$ as its Clifford symmetry. We note however that the face-type magic states are also Clifford magic states. The state $|F\rangle$, for example, is fixed by a group generated by the Clifford gate F. The F gate corresponds to a rotational symmetry of the faces of the stabilizer octahedron, as can be seen by its action on the single qubit stabilizer states.

$$F|0\rangle = |+\rangle \quad F|+i\rangle = |+\rangle \quad F|+\rangle = 0 \tag{3.18}$$

It was shown by Earl Campbell that quotient groups of Clifford symmetries

---

[1]Note that this differs from the definition in [12]. We introduce this definition in this thesis as we consider slightly broader classes of magic state which nonetheless share the property of Clifford symmetries.

can be used to find the stabilizer rank of Clifford magic states $|R\rangle$.

Lemma 3 *Consider a stabilizer state $|\phi_0\rangle : \langle\phi_0|\psi\rangle \neq 0$. We will denote by $\mathcal{M}$ the group of Clifford symmetries of $|\phi\rangle$. Let $\mathcal{N} \subseteq \mathcal{M}$ be the subgroup of $\mathcal{M}$ such that $n|\phi_0\rangle = |\phi_0\rangle \forall n \in \mathcal{N}$, and define $\mathcal{Q}$ as the quotient group $\mathcal{M}/\mathcal{N}$. Then*

$$\chi\left(|\phi\rangle\right) \leq \frac{|\mathcal{M}|}{|\mathcal{M}|} \tag{3.19}$$

with stabilizer state decomposition

$$|\psi\rangle \propto \sum_{q \in \mathcal{Q}} q\,|\phi_0\rangle \tag{3.20}$$

Proof of Lemma 3. We can expand out $|\phi_0\rangle$ as

$$|\phi_0\rangle = \frac{1}{|\mathcal{N}|} \sum_{n \in \mathcal{N}} n\,|\phi_0\rangle.$$

Making this substitution for $|\phi_0\rangle$, we thus have

$$\sum_{q \in \mathcal{Q}} q\,|\phi_0\rangle = \sum_{q \in \mathcal{Q}} \sum_{n \in \mathcal{N}} qn\,|\phi_0\rangle$$

$$= \sum_{m \in \mathcal{M}} m\,|\phi_0\rangle$$

where on the last line we use the definition of the quotient group. From the definition of $\mathcal{M}$, we can write

$$\sum_{m \in \mathcal{M}} = \langle\psi|\psi\rangle$$

and thus

$$\sum_{q} q\,|\phi_0\rangle = \frac{|\mathcal{M}|}{|\mathcal{N}|} |\psi\rangle\,\langle\psi|\phi_0\rangle$$

$$\implies |\psi\rangle = \frac{|\mathcal{N}|}{|\mathcal{M}|\,\langle\psi|\phi_0\rangle} \sum_{q \in \mathcal{Q}} q\,|\phi_0\rangle$$

completing the proof. $\qquad\qquad\square$

As an example, consider the state $\left|H^{\otimes 2}\right\rangle$. This state has the Clifford symmetry group $\{I, H \otimes I, I \otimes H, H \otimes H\}$. We can build a 2-element normal subgroup $\{I, H \otimes H\}$, which stabilizes the state $|0\rangle |+\rangle + |1\rangle |-\rangle$. This give a stabilizer rank of $|\mathcal{M}| / |\mathcal{N}| = \frac{4}{2} = 2$, as expected.

One interesting extension of this result is that any resource state used to inject controlled diagonal Clifford gate, such as CCZ or CS, also has a stabilizer rank of 2, which agrees with the results of the computational searches in Table 3.5. The stabilizer state decompositions for these states can in fact be found by considering the resource state itself. Expanding out the action of the control, we have

$$U \equiv |0\rangle\langle 0| \otimes I + |1\rangle\langle 1| \otimes C \implies U\left|+^{\otimes n}\right\rangle \propto |0\rangle |+\rangle^{\otimes n-1} + |1\rangle C\left|+^{\otimes n-1}\right\rangle \quad (3.21)$$

which is a stabilizer state decomposition with $\chi = 2$ as C is a Clifford operator, and thus $C\left|+^{\otimes n-1}\right\rangle$ is a stabilizer state.

However, here we show that this method does not always produce optimal stabilizer state decompositions. For example, consider the $|F\rangle$ state. A single copy has Clifford symmetry group $\{I, F, F^2\}$, which has no non-trivial subgroups. This would suggest $\chi(|F\rangle) \leq 3$, which is larger than just the computational basis bound.

For two copies, $\left|F^{\otimes 2}\right\rangle$ has the 9-element symmetry group

$$\{I, FI, IF, F^2 I, IF^2, FF, F^2 F, FF^2, F^2 F^2\}, \quad (3.22)$$

where we omit the tensor product symbol for brevity. From the Lagrange theorem, we know that the order of any subgroup $\mathcal{N} \subseteq \mathcal{M}$ must divide the order of the group [39]. Thus, the smallest possible quotient group has $|\mathcal{Q}| = 3$. Again, this is larger than the known optimal decomposition $\chi\left(\left|F^{\otimes 2}\right\rangle\right) = 2$.

We can further consider extending this method to include permutation symmetries. For t copies of single qubit states, the permutation symmetries corre-

spond to the symmetric group $S(t)$, and can be generated using swap permutations [39]. In terms of quantum gates, these permutations correspond to the $SWAP$ gate, which is a Clifford operator as it can be realised by a sequence of 3 $CNOT$ gates.

Extending the groups to incorporate these permutation symmetries allows us to generate subgroups with the correct index. For example, for the $\left|H^{\otimes 2}\right\rangle$ state, incorporating permutations gives an order 8 symmetry group, with a subgroup of order 4 and thus index 2. This subgroup $\mathcal{N} = \{I, SWAP, HH, SWAPHH\}$, fixes the same stabilizer state $|0\rangle|+\rangle + |1\rangle|-\rangle$, and thus we again have $\chi = 2$.

Similarly, for the $\left|F^{\otimes 2}\right\rangle$ state, we obtain an order 18 Clifford symmetry group by incorporating permutations, and can construct a subgroup of order 9 and thus index 2. However, this subgroup $\mathcal{N}$ corresponds to the group given in Eq. 3.22, which fixes the state $\left|F^{\otimes 2}\right\rangle$. Thus, there is no stabilizer state $|\phi_0\rangle$: $n|\phi_0\rangle = |\phi_0\rangle \ \forall n \in \mathcal{N}$, and we cannot use this result to build a stabilizer state decomposition.

3.2.2   Approximate Stabilizer Rank

In this section, we show how to construct approximate stabilizer state decompositions for Clifford magic states, and more generally. Both methods start with an exact stabilizer state decomposition, which is not required to be optimal, and show how to construct an approximate decomposition by discarding terms.

Clifford Magic States

A method for constructing approximate stabilizer state decompositions of the $|H\rangle$ magic state was described in [8]. Here, we outline their argument, showing how it can naturally be extended to any Clifford magic state, such as $|F\rangle$ or $|CCZ\rangle$.

The authors begin by considering an exact stabilizer state decomposition of

$\left| H^{\otimes t} \right\rangle$ in terms of the states $|0\rangle$ and $|+\rangle$.

$$\left| H^{\otimes t} \right\rangle = \frac{1}{2\cos(\pi/8)^t} \sum_{\tilde{x} \in \mathbb{Z}_2^t} |x\rangle \qquad (3.23)$$

where $|\tilde{x}\rangle$ is a t-qubit state such that

$$|\tilde{x}\rangle = \otimes_{i=1}^t H^{\tilde{x}_i} |0\rangle. \qquad (3.24)$$

Each term in the decomposition is a tensor product of stabilizer states, generated by a subgroup of the Clifford group. Recalling Eq. 3.20, we can construct a stabilizer state decomposition for a Clifford magic state $|R\rangle$ from a group $\mathcal{Q} \subseteq \mathcal{C}_2$, and a state $|\phi_0\rangle : \langle \phi_0 | R \rangle > 0$. We can write

$$|R\rangle \propto \sum_{q \in \mathcal{Q}} |\phi_q\rangle \; : \; |\phi_q\rangle = q|\phi_0\rangle.$$

To normalize the decomposition, we note that $\langle \phi_q | R \rangle = \langle \phi_0 | q^{-1} | R \rangle = \langle \phi_0 | R \rangle$. Thus,

$$|R\rangle = \frac{1}{|Q| \langle \phi_0 | R \rangle} \sum_{q \in \mathcal{Q}} |\phi_q\rangle$$

$$\implies |R\rangle^{\otimes t} = \frac{1}{(|\mathcal{Q}| \langle \phi_0 | R \rangle)^t} \sum_{\vec{\mathbf{q}} \in \mathbb{Z}_{|\mathcal{Q}|}^t} \left| \phi_{\vec{\mathbf{q}}} \right\rangle \qquad (3.25)$$

where $|\phi\rangle_{\vec{\mathbf{q}}} \equiv \otimes_{i=1}^t \left| \phi_{\vec{\mathbf{q}}_i} \right\rangle$ and $\vec{\mathbf{q}}$ is t-element vector where each entry denotes a member of the group. Setting $|\mathcal{Q}| = 2$ and $|\phi_0\rangle = |0\rangle$, gives the same decomposition for $\left| H^{\otimes t} \right\rangle$ given in Eq. 3.23.

We can also define states $|\mathcal{L}\rangle$, built from subspaces $\mathcal{L} \subseteq \mathbb{Z}_{|\mathcal{Q}|}^t$

$$|\mathcal{L}\rangle = \frac{1}{\sqrt{|\mathcal{L}| Z(\mathcal{L})}} \sum_{\vec{\mathbf{q}} \in \mathcal{L}} \left| \phi_{\vec{\mathbf{q}}} \right\rangle, \qquad (3.26)$$

where $|\mathcal{L}|$ is the number of elements in the subspace, and $Z(\mathcal{L})$ is a normali-

sation factor, given by

$$\langle \mathcal{L}|\mathcal{L}\rangle = 1 = \frac{1}{|\mathcal{L}|\, Z(\mathcal{L})} \sum_{\vec{\mathbf{p}},\vec{\mathbf{q}} \in \mathcal{L}} \langle \phi_p | \phi_q \rangle$$

$$= \frac{1}{|\mathcal{L}|\, Z(\mathcal{L})} \sum_{\vec{\mathbf{p}}\vec{\mathbf{q}}} \langle \phi_{\vec{\mathbf{0}}} | \phi_{\vec{\mathbf{p}}^{-1}\vec{\mathbf{q}}} \rangle$$

$$= \frac{1}{Z(\mathcal{L})} \sum_{\vec{\mathbf{q}}} \langle \phi_{\vec{\mathbf{0}}} | \phi_{\vec{\mathbf{q}}} \rangle$$

where in the last line we have used the group properties of $\mathcal{Q}$ to simplify the sum, and where $\left|\phi_{\vec{\mathbf{0}}}\right\rangle = \left|\phi_0^{\otimes t}\right\rangle$.

How well does a given subspace with $|\mathcal{L}| < 2^t$ approximate the full stabilizer state decomposition? Each term in the subspace state has overlap $(\langle \phi_0 | R \rangle)^t$, and thus

$$\left|\left\langle R^{\otimes t} \middle| \mathcal{L} \right\rangle\right|^2 = \frac{|\mathcal{L}|^2 \, f_{\phi_0}^t(R)}{|\mathcal{L}|\, Z(\mathcal{L})} = \frac{|\mathcal{L}|\, f_{\phi_0}(R)}{Z(\mathcal{L})} \tag{3.27}$$

where we define $f_{\phi_0}(R) \equiv |\langle \phi_0 | R \rangle|^2$, the fidelity of $|\phi_0\rangle$ with $|R\rangle$.

The fidelity of the $\mathcal{L}$ approximate thus depends on the size of the subspace, the initial overlap, and the quantity $Z(\mathcal{L})$ which depends on the subspace we choose. Bravyi & Gosset then showed for the case of the $|H\rangle$ state that we can achieve $Z(\mathcal{L}) \sim 1 + |\mathcal{L}|\, f_{\phi_0}(H)^t$ by choosing subspaces at random [8].

This argument also extends to the more general case of Clifford symmetries. Choosing subspaces uniformly at random, we can compute the expectation value of the weight $Z(\mathcal{L})$. Every subspace must contain $\left|\phi_{\vec{\mathbf{0}}}\right\rangle$, which contributes $\left\langle \phi_{\vec{\mathbf{0}}} \middle| \phi_{\vec{\mathbf{0}}} \right\rangle = 1$ to the weight. Otherwise, each state $\left|\phi_{\vec{\mathbf{q}}}\right\rangle$ is equiprobable, and occurs with probability $\frac{|\mathcal{L}-1|}{|Q|^t - 1}$. Thus,

$$\mathbb{E}\left[Z(\mathcal{L})\right] = 1 + \frac{|\mathcal{L}| - 1}{|Q|^t - 1} \left(\sum_{\vec{\mathbf{q}} \in \mathbb{Z}_{|\mathcal{Q}|}^t - 1} \left\langle \phi_{\vec{\mathbf{q}}} \middle| \phi_{\vec{\mathbf{0}}} \right\rangle \right). \tag{3.28}$$

By replacing $\sum_{\vec{\mathbf{q}} \in \mathbb{Z}_{|\mathcal{Q}|}^t - 1} \left\langle \phi_{\vec{\mathbf{q}}} \middle| \phi_{\vec{\mathbf{0}}} \right\rangle$ with $\sum_{\vec{\mathbf{q}} \in \mathbb{Z}_{|\mathcal{Q}|}^t} \left\langle \phi_{\vec{\mathbf{q}}} \middle| \phi_{\vec{\mathbf{0}}} \right\rangle - 1$, and substituting

Eq. 3.25, we can write

$$\mathbb{E}\left[Z\left(\mathcal{L}\right)\right] = 1 + \frac{|\mathcal{L}| - 1}{|Q|^t - 1}\left(|\mathcal{Q}|^t f_{\phi_0}\left(R\right) - 1\right) \approx 1 + \left(|\mathcal{L}| - 1\right)f^t \approx 1 + |\mathcal{L}|\,f^t, \quad (3.29)$$

where we have assumed t and $\mathcal{L}$ are large.

Following the argument in [8], there is thus at least one subspace $\mathcal{L}$ such that $Z\left(\mathcal{L}\right) \leq 1 + |\mathcal{L}|\,f_{\phi_0}(R)^t$. Substituting this value into Eq. 3.27 gives

$$\left|\left\langle R^{\otimes t} \middle| \mathcal{L}\right\rangle\right|^2 \approx \frac{|\mathcal{L}|\,f^t}{1 + |\mathcal{L}|\,f^t}$$

, which can be rearranged to solve for how large we require $|\mathcal{L}|$ to obtain a given fidelity. More formally, and again extending the argument of [8], we can use Eq. 3.29 and Markov's lemma to show that

$$P\left[\frac{Z\left(\mathcal{L}\right)}{\left(1 + |\mathcal{L}|\,f_{\phi_0}(R)^t\right)\left(1 + \frac{\epsilon}{2}\right)} \geq 1\right] \leq \frac{\mathbb{E}\left[Z(\mathcal{L})\right]}{\left(1 + |\mathcal{L}|\,f_{\phi_0}(R)^t\right)\left(1 + \frac{\epsilon}{2}\right)} \leq 1 - \frac{\epsilon}{2 + \epsilon}.$$

Thus, with $O(\frac{1}{\epsilon})$ samples, we can generate a subspace $\mathcal{L}' : Z\left(\mathcal{L}'\right) \leq \left(1 + |\mathcal{L}|\,f_{\phi_0}(R)^T\right)\left(1 + \frac{\epsilon}{2}\right)$ [8].

If we now fix the size of the subspace such that

$$2 \leq \left|\mathcal{L}'\right| f_{\phi_0}^t \epsilon \leq 4$$
$$\implies \left|\mathcal{L}'\right|^{-1} f_{\phi_0}^{-t} \leq \frac{\epsilon}{2}$$

then the corresponding subspace state $|\mathcal{L}'\rangle$ achieves a fidelity

$$\begin{aligned}\left|\left\langle R^{\otimes t} \middle| \mathcal{L}'\right\rangle\right|^2 &= \frac{|\mathcal{L}'|\,f_{\phi_0}(R)}{\left(1 + |\mathcal{L}'|\,f_{\phi_0}(R)\right)\left(1 + \frac{\epsilon}{2}\right)} \\ &= \frac{1}{(1 + |\mathcal{L}'|^{-1} f_{\phi_0}^{-t})(1 + \frac{\epsilon}{2})} \\ &\geq \frac{1}{\left(1 + \frac{\epsilon}{2}\right)^2} \approx 1 - \epsilon. \quad\quad (3.30)\end{aligned}$$

We can thus generate an approximate stabilizer state decomposition that is ϵ

close in fidelity by choosing a random subspace, provided that we have sufficiently many terms in the decomposition. Again applying the inequality from above, we have

$$\chi_\epsilon\left(\left|R^{\otimes t}\right\rangle\right) = |\mathcal{L}| \leq 4f_{\phi_0}^{-t}\epsilon^{-1} = O\left(f_{\phi_0}^{-t}\epsilon^{-1}\right), \tag{3.31}$$

where the asymptotic scaling depends on the term f_{ϕ_0}. Thus, we introduce the concept of stabilizer fidelity

Definition 3.2 ((Stabilizer Fidelity)). $F\left(\psi\right) = \max_{\phi \in \mathcal{S}_n} |\langle\phi|\psi\rangle|^2$

with the corollary that

Corollary 1 *The approximate stabilizer rank of a Clifford magic state*

$$\chi_\epsilon\left(\left|R^{\otimes t}\right\rangle\right) = O\left(F^{-t}\left(R\right)\right).$$

We refer to this method of generating an approximation stabilizer state decomposition as the 'random codes' method, because it can be conceptualised as approximately encoding the state using a code-space of dimensionality $|\mathcal{L}|$.

Sparsification

The method outlined above works by taking exact, even potentially 'over-complete' stabilizer state decompositions, and dropping terms to obtain an approximate decomposition with a given fidelity. This principle is similar to approximate classical simulation methods based on quasiprobability representations of quantum states [40]. In these models, the number of terms that must be sampled scales as the 'negativity' of the state, given by the the one-norm of the coefficients with respect to the phase-space under consideration.

It was shown by David Gosset that a similar strategy can be applied to stabilizer state decomposition [12]. Given any valid stabilizer state decomposition, we can sample terms at random using a probability distribution based on their coefficients to build an approximate decomposition. We can rewrite a given

stabilizer state decomposition as

$$|\psi\rangle = \sum_i c_i |\phi_i\rangle = \sum_i \frac{|c_i|}{\|\vec{c}\|} |w_i\rangle = \sum_i p_i |w_i\rangle \tag{3.32}$$

where $|w_i\rangle \equiv \frac{c_i}{|c_i|} |\phi_i\rangle$. The new coefficients $\frac{|c_i|}{\|\vec{c}\|}$ are positive, real-valued, and also have the property that $\sum_i p_i = 1$. Thus, they define a probability distribution. Let $|\omega\rangle$ be one of the $|w_i\rangle$ states, sampled with probability p_i. It can be shown that$\mathbb{E}[|\omega\rangle] \propto |\psi\rangle$ and, by taking multiple samples $|\omega_i\rangle$, we can obtain an approximate state

$$|\tilde{\psi}\rangle = \frac{\|c\|_1}{\chi_\epsilon} \sum_{i=1}^{\chi_\epsilon} |\omega_i\rangle \ : \ \left\| |\tilde{\psi}\rangle - |\psi\rangle \right\| \le \epsilon \tag{3.33}$$

with high-probability, provided that we set [12]

$$\chi_\epsilon(|\psi\rangle) = O\left(\|c\|_1^2 \epsilon^{-2}\right), \tag{3.34}$$

Importantly, we note that this method guarantees an approximation that is ϵ close in the one-norm, as opposed to fidelity as in Eq. 3.31.

Based on this approximation, we subsequently introduce the notion of 'Stabilizer Extent':

Definition 3.3 ((Stabilizer Extent))**.** For a normalised quantum state $|\psi\rangle$, the stabilizer extent $\xi(\psi)$ is defined as the minimum value of $\|c\|_1^2$ over all stabilizer state decompositions $|\psi\rangle = \sum_i c_i \phi_i$.

The one-norm is a convex quantity, and thus we can be computed efficiently using convex optimisation techniques [41]. However, as the search space scales with the number of stabilizer states, which in turn scales exponentially with the number of qubits, in practice extent is difficult to compute for more than a few qubits. An equivalent quantity to extent was also introduced in Section 5.4 of [42], a general study of convex resource measures for quantum computing. It follows from [42] stabilizer extent is a faithful measure, such that $\xi(\psi) = 1$ if and only if $|\psi\rangle$ is a stabilizer state.

Stabilizer Fidelity

Interestingly, as a convex optimization problem, it is also possible to use the 'dual' convex problem to find a lower bound on the stabilizer extent. The proof was given by Earl Campbell in Section VI.A of [12], but we quote the key result here, namely

$$\xi(\psi) \geq \frac{1}{F(\psi)}, \tag{3.35}$$

where $F(\psi)$ is the stabilizer fidelity introduced in Definition 3.2. It can also be shown that this lower-bound is tight for injectable Clifford magic states [12]. Thus, despite the slightly different definition of approximation, the approximate stabilizer rank of Clifford magic states coincides under both the random codes and the sparsification methods.

An important question is whether stabilizer extent is multiplicative. As extent is lower bounded by the stabilizer fidelity, we can thus ask if the stabilizer fidelity is multiplicative, namely

$$F\left(\left|\psi^{\otimes t}\right\rangle\right) \stackrel{?}{=} F(\psi)^t$$

This can also be expressed as asking if there exists some entangled stabilizer state $|\varphi\rangle$, such that

$$\left|\left\langle\varphi\right|R^{\otimes t}\right\rangle\right| > \left|\left\langle\phi^{\otimes t}\right|R^{\otimes t}\right\rangle\right| = \left|\langle\phi|R\rangle\right|^t.$$

Lemma 4 *For single qubit states $|S\rangle$, the stabilizer fidelity of t copies $F\left(S^{\otimes t}\right) = F(S)^t$*

Proof of Lemma 4. Consider a single qubit state $|S\rangle$. Using the Bloch-vector representation, we can write this state as $|S\rangle = \frac{1}{2}\left(1 + \vec{\mathbf{r}} \cdot \vec{\mathbf{P}}\right)$, where $\vec{\mathbf{P}} = (X, Y, Z)$, and $\vec{\mathbf{r}} = (r_x, r_y, r_z)$ is the Bloch-vector with coefficients $r_i = \langle S|P_i|S\rangle$. We also consider a single qubit stabilizer state $|P\rangle$, with corresponding stabilizer group $\mathcal{S}_\phi = \{I, \pm P\}$, where $P \in \{X, Y, Z\}$.

The fidelity between $|S\rangle$ and a single qubit stabilizer state can be written in terms of the stabilizer group as

$$|\langle P|S\rangle|^2 = \langle S|P\rangle\langle P|S\rangle = \frac{1}{2}\langle P|(I\pm P)|S\rangle$$
$$= \frac{1}{2}(1+|r_P|)$$

where r_P is the Bloch-vector coefficient associated with P, and we use the result that $|\phi\rangle\langle\phi| = \frac{1}{2^n}\sum_{s\in\mathcal{S}_\phi} s$ for an n-qubit stabilizer state. Thus, the stabilizer fidelity of $|S\rangle$ is given by

$$F(S) = \frac{1}{2}\left(1 + \max_i |r_i|\right).$$

Let us assume throughout the following that

$$|r_z| \geq |r_y| \geq |r_x|.$$

This assumption can be made without loss of generality, substituting X or Y for Z through the following argument. We will also assume that $r_z > 0$, otherwise the argument follows but replacing Z with $-Z$. We define $|\phi\rangle$ to the be single qubit stabilizer state with maximum fidelity with $|S\rangle$. For t copies, the stabilizer group of $|\phi^{\otimes t}\rangle = \{Z(\vec{\mathbf{z}})\}$, where $\vec{\mathbf{z}}$ is a t-bit binary string and we employ the same notation for tensor products of Pauli operators as in Chapter 2. The fidelity of $|\phi^{\otimes t}\rangle$ with $|S^{\otimes t}\rangle$ is given by

$$\left|\left\langle\phi^{\otimes t}\middle|S^{\otimes t}\right\rangle\right|^2 = \frac{1}{2^t}\sum_{\vec{\mathbf{z}}\in\mathbb{Z}_2^t}\left\langle S^{\otimes t}\middle|Z(\vec{\mathbf{z}})\middle|S^{\otimes t}\right\rangle$$
$$= \frac{1}{2^t}\left(\sum_{i=0}^{t}\binom{t}{i}|r_z|^i\right)$$
$$= \frac{1}{2^t}\left(1 + t|r_z| + \sum_{i=2}^{t}\binom{t}{i}|r_z|^i\right) \tag{3.36}$$

where we have joined together the expectation values for elements of the group with equal numbers of Pauli Z operators, and used the fact that $|r_z| \leq 1$.

Assume now that stabilizer fidelity is multiplicative up to $t-1$ copies. We will prove $\nexists |\varphi\rangle$, a t qubit stabilizer state, such that $\left|\left\langle \varphi | S^{\otimes t} \right\rangle\right|^2 > F(S)^t$.

For a general t-qubit stabilizer state, we have the stabilizer group $\mathcal{S}_\varphi$, and the corresponding fidelity with $\left|S^{\otimes t}\right\rangle$ is given by

$$\left|\left\langle \varphi | S^{\otimes t} \right\rangle\right|^2 = \frac{1}{2^t} \left(\sum s \in \mathcal{S}_\varphi \left\langle S^{\otimes t} \middle| s \middle| S^{\otimes t} \right\rangle \right).$$

For a t-qubit Pauli operator Q, we define the weight $|Q| = \otimes_{i=1}^{t} P_i$ as the number of qubits where $P_i \neq I$ [43]. Using the assumption above, we can write the expectation value of Q on $|S\rangle$ in terms of the weight as

$$\left\langle S^{\otimes t} \middle| Q \middle| S^{\otimes t} \right\rangle = \prod_{i=1}^{n} \langle S|P_i|S\rangle \leq |r_z|^{|Q|}$$

and thus

$$\left|\left\langle \varphi | S^{\otimes t} \right\rangle\right|^2 \leq \frac{1}{2^t} \left(\sum_{s \in \mathcal{S}_\varphi} |r_z|^{|s|} \right).$$

All t-qubit stabilizer states are equivalent to a graph state, up to a sequence of local Clifford operations. As this is a local circuit, the weight of the stabilizers is left unchanged, and thus we can characterize the weights of $\mathcal{S}_\varphi$ using the stabilizer group of a graph states.

The stabilizer group of a graph state is generated from the underlying graph $G = (V, E)$. The jth generator is given by

$$g_j = \bigotimes_{i=1}^{t} X^{\delta_{ij}} Z^{\mathbf{1}_E(i,j)}$$

where $\mathbf{1}_E(i,j)$ is an indicator function that returns 1 if qubits/vertices i and j are connected by an edge. A product of m generators has weight $\geq m$, arising from the Pauli X term acting on each qubit, and there are $\binom{t}{m}$ elements which are the product of m generators. We can also limit ourselves to considering only fully-connected graphs, as otherwise the state $|\varphi\rangle$ is separable with respect

to some bipartition, and thus

$$\left|\left\langle\varphi\middle|S^{\otimes t}\right\rangle\right| = \left|\left\langle\varphi_A\middle|S^{\otimes|A|}\right\rangle\right|\left|\left\langle\varphi_B\middle|S^{\otimes|B|}\right\rangle\right| \leq F(S)^{|A|}F(S)^{|B|}$$

as stabilizer fidelity is multiplicative up to $t-1$ copies. Thus, every generator must have $|g_j| \geq 2$.

Splitting up the sum, we thus have

$$\begin{aligned}\left|\left\langle\varphi\middle|S^{\otimes t}\right\rangle\right|^2 &\leq \frac{1}{2^t}\left(1 + \sum_j |r_z|^{|g_j|} + \sum_{s\in\mathcal{S}_\varphi\setminus\{I,g_j\}} |r_z|^{|s|}\right)\\ &\leq \frac{1}{2^t}\left(1 + t|r_z|^2 + \sum_{i=2}^t \binom{t}{i}|r_z|^i\right)\\ &\leq \frac{1}{2^t}\left(1 + t|r_z| + \sum_{i=2}^t \binom{t}{i}|r_z|^i\right),\end{aligned} \qquad (3.37)$$

where in the final line, we have brought down the expression from Eq. 3.36.

For $t = 2$, we can verify explicitly that

$$\frac{1}{4}\left(1 + 2|r_z|^2 + |r_z|^2\right) \leq \frac{1}{4}\left(1 + 2|r_z| + |r_z|^2\right)$$

for all $|r_z| \leq 1$. Thus, from Eq. 3.37 and using proof by induction, stabilizer fidelity is multiplicative for all single qubit states. □

It was subsequently shown by David Gosset that stabilizer fidelity is multiplicative for 1, 2 and 3 qubit states, but that in fact for typical states with $n \geq 4$ qubits the stabilizer fidelity is not multiplicative [12]. This in turn suggests that in general, stabilizer extent is submultiplicative.

3.3 Discussion

In this chapter, we have presented a number of results that extend our understanding of both exact and approximate stabilizer rank beyond just the 'edge-type' family of single qubit magic states.

In the case of exact stabilizer rank states, we focused on examining Conjec-

ture 1, which asserts that the exact stabilizer rank of single-qubit states is smallest for the Clifford magic states. Explicit computational searches up to 3 copies, and an upper bound based on groups of Clifford symmetries, both provide evidence in favor of this being true. However, for other families of states, stabilizer rank has proven difficult to quantify precisely. The performance of numeric searches breaks down as the number of qubits increases. However, we were able to provide explicit upper bounds for the stabilizer rank of up to 5 copies of any quantum state, by considering the properties of the symmetric subspace.

Nonetheless, our results would suggest that in general the stabilizer rank is smallest for Clifford magic states on any number of qubits, as both the $|CS\rangle$ and $|CCZ\rangle$ magic states have stabilizer ranks significantly smaller than either their computational basis expansion, or the upper bounds obtained from the symmetric subspace.

It is also interesting to note that the $|T\rangle$, $|CS\rangle$ and $|CCZ\rangle$ magic states, all of which can be used to inject an operator from $\mathcal{C}_3$, also all have the same stabilizer rank. Given the properties of exact stabilizer rank discussed at the beginning of Section 3.2.1, in particular invariance under Clifford unitaries, this equal stabilizer rank might appear to suggest that, for example, there exists some Clifford circuit V and stabilizer states $|\phi\rangle$ such that $V(|T\rangle \otimes |\phi\rangle) = |CCZ\rangle$. This would in turn suggest that a $|CCZ\rangle$ gate can be realsied using just Clifford gates and a single T gate. However, the best known unitary circuit for synthesising a CCZ gate from Clifford+T operations requires 7 T-gates [44].

Smaller circuits, have also been shown to exist that allow a CCZ gate to be synthesised using Clifford gates, T-gates, and Pauli measurements. Again, appealing to the properties of the exact stabilizer rank, we might expect that as $\chi\left(\left|T^{\otimes 3}\right\rangle\right) > \chi(|CCZ\rangle)$, we could find such a circuit with a T-count of 3. However, the current optimal circuit know has a T-count of 4 [45]. Similar results exist for the CS gate, for which the optimal circuit known requires 3

T-gates.

Additionally, there is evidence from alternative resource formulations of 'magic' that these circuits are in fact optimal. For example, in the 'Robustness of Magic' picture, it can be shown that $R\left(\left|T^{\otimes 3}\right\rangle\right) < R\left(\left|CCZ\right\rangle\right) < R\left(\left|T^{\otimes 4}\right\rangle\right)$ [32]. It is also important to note that no circuits with smaller T-counts have been found since these circuits were first proposed, despite continued research into gate-synthesis by the community. This includes efforts employing computational searches [46].

This has important consequences for the interpretation of the exact stabilizer rank as a resource measure. In particular, it is clear that the exact stabilizer rank is not a useful quantifies of magic as it relates to problems of gate synthesis. While Clifford equivalent states naturally have the same stabilizer rank, equal stabilizer rank does not imply Clifford equivalence.

However, this observation does have an important consequence for how we interpret other resource measures of magic. As previously mentioned, for example, the $|CCZ\rangle$ state has a greater robustness of magic than the $|T\rangle$. However, both states have equivalent stabilizer rank, and subsequently given an appropriate algorithm a circuit with either a single CCZ or a single T gate would be broadly equivalently difficult to simulate. Phrased another way, large 'magic' does not guarantee that a circuit shows significant non-classical behaviour. We also present results showing how to construct approximate stabilizer state decompositions for broad classes of states. This is especially true of the sparsification method and the associated quantity of stabilizer extent. As a convex resource measure [42], it lends itself to easier explicit computation than the exact stabilizer rank, which as a form of sparse optimization is NP-hard even non-withstanding the exponentially growing search space [47]. As mentioned previously, the number of stabilizer states grows exponentially with the number of qubits and so in practice extent is difficult to compute for more than a few qubits. However, in some cases stabilizer rank calculations can be sped up by taking into account features of the state like all-real amplitudes.

Recent work by Gross et al. looked and optimizing a similar computation for Robustness of Magic, using symmetries in the Clifford group to significantly reduce the number of states to be considered [48].

As a convex measure, extent is also well behaved as a magic monotone [42]. For example, unlike in the case of the exact stabilizer rank, subsequent work has used the stabilizer extent to find lower bounds on the 'non-Clifford' resources required for different quantum computations [49].

From a simulation perspective, we can compare the impact of building direct stabilizer state decompositions by directly comparing the stabilizer fidelity of states. As quoted above, the current optimal T-counts known to be required for synthesing the CS and CCZ gates are 3 and 4, respectively. Comparing the stabilizer fidelities, we can show that

$$
\begin{aligned}
F(T)^{-2} \approx 1.373 < \quad & F(CS)^{-1} = 1.6 \quad & < F(T)^{-3} \approx 1.608 \\
F(T)^{-3} \approx 1.608 < \quad & F(CCZ)^{-1} \approx 1.778 \quad & < F(T)^{-4} = 1.884.
\end{aligned}
\tag{3.38}
$$

Asymptotically, these savings become significant. For example, a circuit built out of 40 CCZ gates would require $\sim 11\%$ of the resources compared to an equivalent circuit built in the Clifford+T basis. At 80 CCZ gates, a direct decomposition needs just 1.1% of the terms that a synthesised decomposition would require. We also note that, like in the case of robustness, these inequalities support the claim that 3 and 4 T-gates is the optimum number required to synthesise CS and CCZ.

The comparison becomes even more significant if we consider resource states that could be used to realise gates from outside of the 3rd level of the Clifford hierarchy. For example, consider a state

$$
|\theta\rangle = \frac{1}{\sqrt{2}} \left(|0\rangle + e^{i\theta/2} |1\rangle \right).
\tag{3.39}
$$

These resource states can be used to realize single-qubit rotations around the Pauli Z axis through an angle θ. As previously discussed, such rotations can

require up to 100 T-gates to synthesize [31] as $\theta \to 0$. However, the stabilizer fidelity of $|\theta\rangle$ actually increases as θ gets smaller. In fact, any rotation smaller than a T gate will require multiple T gates to synthesize, but has a smaller approximate stabilizer rank.

A caveat of this method is that to be used in a state-injection circuit, resource states like $|\theta\rangle$ require non-Clifford 'correction operations'. In the approximate simulation case, however, we cannot post-select on the measurement gadgets to avoid these additional non-Clifford gates [8]. Thus, to be used in a simulation scheme, we need a different formulation than the PBC method discussed in Section 3.1.1. We will discuss the problem of applying the sparsification method to simulation in the following chapter.
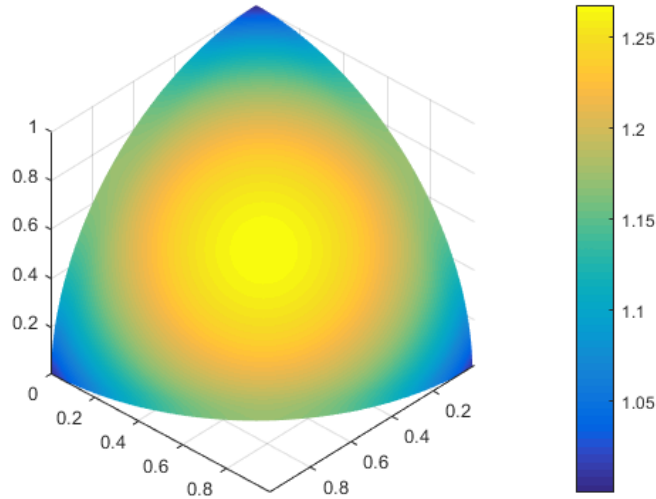

Figure 3.3: Heatmap showing the inverse stabilizer fidelity, $F(\psi)^{-1}$, for all single-qubit states lying in a single quadrant of the Bloch sphere. We note that the state with the largest inverse fidelity, and thus largest stabilizer extent, is the face-type magic state. Figure taken from [12].

It is interesting to note that there is a tension between trying to minimize the exact or the approximate stabilizer rank. For example, consider the two classes of single-qubit magic state. While the face state has a smaller stabilizer fidelity that the edge-type states — in fact it has the smallest possible stabilizer fidelity, c.f. Fig 3.3 — both states have equivalent exact stabilizer

rank. Alternatively, single-qubit states exponentially close to a stabilizer state will have a small approximate stabilizer rank, but have a larger exact stabilizer rank. In fact, for any single qubit state with stabilizer fidelity $\geq \frac{1}{\sqrt{2}}$, its approximate stabilizer rank will have an asymptotic scaling smaller than $2^{0.5t}$, the upper bound obtained from computational searches in Section 3.2.1.

Finally, we note that all the results shown here serve only as upper bounds on the stabilizer rank. While stabilizer fidelity is capable of lower bounding the stabilizer extent, this is itself also an upper bound on the approximate stabilizer rank. Currently, the only lower bounds that have been explicitly proven apply to the case of the $|T\rangle$ state. It was argued in [26] that $\chi\left(\left|H^{\otimes n}\right\rangle\right) = \Omega\left(\sqrt{n}\right)$, based on constructing states with finite stabilizer rank but which require a large number of T gates to create. In [12], it was also shown that the approximate stabilizer rank $\chi_\epsilon\left(\left|H^{\otimes n}\right\rangle\right) = \Omega\left(F(H)^{-n}\epsilon^{-2}\right)$, but only under the assumption that the decomposition is built from the states $|0\rangle$ and $|+\rangle$, as used in the random codes construction.

Part of this difficulty likely arises from the fact that, as a sparse optimization problem, even approximately computing the optimal stabilizer rank is NP-hard [47]. Currently, the best explicit lower bound is a complexity theoretic argument. It was shown by Dalzell that for any classical simulation of a Clifford+T circuit must have a runtime that scales asymptotically as $2^{\gamma t}$, where $\gamma > \frac{1}{128}$, otherwise the polynomial hierarchy would collapse to the third level [50]. This result acts as a lower-bound on the approximate stabilizer rank of the $|T\rangle$ magic states, and is significantly looser than the current best known decompositions with $\gamma \approx 0.23$. It is a open question if this complexity theoretic argument can be tightened.

In the case of approximate stabilizer rank, we might also ask if alternative strategies for building decompositions could be yield a smaller approximate stabilizer rank.

For example, inspired by the random codes method, we might consider us-

ing Schumacher compression to efficiently encode many copies of a resource state [51]. In [8], the authors compared the Shannon entropy of the $|H\rangle$ state with the asymptotic $2^{0.23t}$ scaling obtained using random codes, showing that it outperforms Schumacher compression. Figure 3.4, taken from [13], shows a similar analysis comparing the Shannon entropy with the stabilizer extent for $|\theta\rangle$ states as a function of the angle θ. We can see that in fact, at small angles, Schumacher compression can achieve a smaller decomposition than sparsification. However, over most of the parameter range, the difference between sparsification method performs significantly better.

Alternatively, we could consider techniques that construct an approximate stabilizer state decomposition by discarding only the terms which contribute least to the overall decomposition. Indeed, an interesting feature of both the random codes and sparsification methods is that the resulting decompositions are uniform mixtures of the sampled stabilizer states.

In the most general case, the simulation overhead achieved by discarding terms is related to the notion of ϵ-sparsity, namely how many terms in the decomposition can be discarded while retaining an additive error ϵ in the output distribution [52]. The notion of ϵ-sparsity is closely related to the smooth max entropy H_{max}^{ϵ}, the logarithm of the number of terms with coefficients $|c_i| > \epsilon$. An ideal truncation method of this type would have approximate stabilizer rank $2^{H_{max}^{\epsilon}}$, but as previously stated computing optimal sparse decompositions of this type constitutes an NP-hard problem.

In some tensor network methods for classical simulation, such as `Rollright` and `qFlex`, the output state of the computation before measurement is broken up into a decomposition of largely independent states, which contribute roughly equally to the norm [53, 54]. Thus, they can achieve an approximate fidelity f by dropping all but a fraction f of the states [53]. In practice, this method does slightly worse than the target fidelity due to small overlaps $\sim 10^{-6}$ between states [54], but the reduction in the number of terms achieved is significant.

The overlap between general n-qubit stabilizer states, in contrast, varies significantly from 0 to $2^{-s} : s \in [1, n]$. The sparsification method works around this, using the fact that sampling states according to $\frac{c_j}{\|\vec{c}\|_1}$, the expectation value

$$\mathbb{E}\left[|\omega\rangle\right] = \frac{|\psi\rangle}{\|c\|},$$

i.e. the sampled states have equal norm on average [12]. Additionally, grouping like terms, we can see that in the sampled state

$$\mathbb{E}\left[|\tilde{\psi}\rangle\right] = \mathbb{E}\left[\frac{\|c\|}{\chi_\epsilon} \sum_{i=1}^{\chi_\epsilon} |\omega_i\rangle\right] = \mathbb{E}\left[\|c\| \sum_j \frac{\#|w_j\rangle}{\chi_\epsilon} |w_j\rangle\right] = \|c\| \sum_j p_j |w_j\rangle.$$

On average, then, building uniform decompositions in this way does effectively weight each stabilizer state according to its contribution to the decomposition. It might however be interesting to test alternative sampling strategies, such as sampling without replacement or excluding terms with a coefficient below some small threshold value.
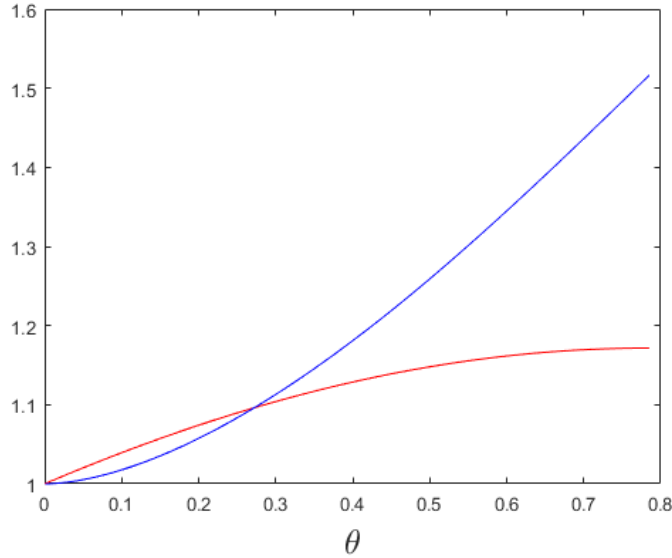

Figure 3.4: Graph comparing the Shannon entropy (blue) and stabilizer extent (red) of $|\theta\rangle$ states, defined in Eq. 3.39, as a function of the angle $|\theta\rangle$.

Chapter 4

Simulating Quantum Circuits with the Stabilizer Rank Method

4.1 Introduction

Previously, we have discussed decompositions of quantum computations, where each individual term can be efficiently simulated classically. This connection to classical simulation gives an easy operational interpretation to these decompositions, and suggests a way of building a classical simulator along these lines. In this chapter, we will make this connection explicit, introducing methods that can be used to simulate universal quantum circuits, and discussing their implementations.

As discussed, efficient classical simulation of quantum effects is broadly believed to be intractable. Nonetheless, classical simulations play an important role in the research and development of quantum technologies. In recent years, fas quantum hardware has continued to improve, an increasingly important role of simulations has been to support the transition and adoption of quantum technology. Providing classical simulators as a test bed enables the development of software engineering, protocols and applications that take into account non-classical features, even while access to actual quantum devices is still limited.

For example, `SimulaQron` and `NetSquid` are classical simulations of quantum communications networks, developed as part of an effort to promote the development of practical quantum communications [55, 56]. These tools have been used to develop proposals for link layer protocols in quantum networks, which can then be tested in the lab [57].

In the context of quantum computing, many classical simulators in use today form part of 'Quantum Development Kits' (QDKs), software environments for the development of quantum software. These tools broadly follow a similar architecture to that of `ProjectQ`, described in [58]. Typically, the user-facing component is a 'high-level' description of a quantum programme, either as an API or with a domain-specific language (DSL), which is agnostic to how it will be evaluated. These programmes can be built out of algorithms and meta-algorithms, such as the Variational Quantum Eigensolver; subroutines and operations, such as the quantum Fourier transform; or even individual gates. The resulting description of the programme can then be compiled to a quantum circuit, and either simulated clasically, or else dependent on requirements further compiled and dispatched to a quantum processor. Multiple such QDKs have been developed over the past 5 years, and a brief summary of the some of the available options is shown in Table 4.1.

Framework	High-level Description	Classical Methods	Supported Hardware
Microsoft QDK [59]	`Q#` [60]	State vector	None
`ProjectQ` [61]	DSL	State vector	IBMQ [62]
`Qiskit` [63]	QASM [64], Python API	Various	IBMQ [62]
`Circ` [65]	Python API	State vector, density matrix	Bristlecone[1] [66]
`Forest` [67]	Quil, Python API [68]	State vector density matrix	Rigetti QPU [69]

Table 4.1: A non-exhaustive list of different quantum software frameworks or QDKs. We note that many of these frameworks have additional components aimed at supporting application development that are not mentioned here.

In practice, most of the QDKs mentioned above make use of what could be described as 'textbook' classical simulations of quantum computing, where a circuit is simulated by matrix multiplication of the unitary associated with each gate, acting on either a state-vector or a density matrix description [44].

These simulators have the advantage that they are relatively straightforward to

implement, and can leverage mature computational libraries for matrix maths such as `Numpy` [33]. Probabilities in the computational basis can also be trivially obtained, either by reading off the right diagonal entry in the density matrix or computing the absolute value squared of the corresponding amplitude in a state-vector. Noise in these models is also relatively straightforward to model, either by using a stochastic noise model inserting extra operators into the circuit in the state-vector case, or else applying Kraus operators directly in the density matrix case [44].

However, the main drawback to these simulators is their spatial complexity. A state-vector requires 2^n complex numbers to define, and a density matrix requires up to 2^{2n}, where n is the number of qubits. As each complex number requires two 64-bit floating point numbers to specify, the memory requirements can quickly approach the limits of personal computing. A simulation on 30 qubits requires 16GB of memory, and up to 45 qubits this requires 0.5PB [70]. The current top-ranked supercomputer in the world has access to 2.7PB of memory, meaning it could simulate up to 47 qubits using these methods [71].

These classical representations also have a significant temporal overhead. In the most straightforward implementation, applying gates requires multiplying $2^n \times 2^n$ matrices. These updates require time 2^{2n} in the state-vector case, and $2^{4.746n}$ for density matrices. In practice though, significant optimizations are possible that can make state-vector simulators reasonably performant at accessible sizes. For example, the $2^n \times 2^n$ matrices representing single qubit gates are sparse, with the vast majority of entries being 0. Other optimizations that have been applied include parallelising single-qubit gate updates [72, 73, 72, 74], optimising permutation operations such as CNOT and Pauli X [73], replacing certain arithmetic operations with classical equivalents [70], and accelerating algorithms using parallel execution via `OpenMP`, `MPI` or GPUs [75, 72, 73, 74].

In practice, this limit of approximately 30 qubits when simulating circuits with personal computers roughly corresponds to the kind of quantum programmes that can be run on current publicly accessible devices, which have anywhere

from 5-20 qubits [62, 69]. However, with continued development of quantum hardware into the 50–72 qubit range [76, 77], classical simulations need to be pushed further, to continue in their other role in the verification and benchmarking of quantum devices.

Given the expected intractability of classical simulations at large enough system sizes, the question of verifying quantum computations without simulation constitutes a separate branch of research based on the idea of 'interactive proofs' [78, 79]. Nonetheless, classical simulations offer a unique opportunity in verification as at any point the simulation can be paused and the system state inspected. Large-scale classical simulations also provide a performance baseline, as part of attempts to establish Quantum Supremacy.

Recent work has focused on tensor-network methods in particular to push classical simulations up past 45 qubits, and have achieved some of the largest scale classical simulations to date [80, 81, 82, 53, 83]. Tensor networks are undirected graphs, where tensors represent input and output states, and quantum gates, and edges represent qubit wires [84]. Tensors are combined or contracted by summing over shared indices, with a runtime that scales as the product of the dimensions of the indices to be contracted. For fixed input and output states x and y, contracting the entire network results in a rank-0 tensor or scalar value which corresponds to the amplitude $\langle x|u|y \rangle$ [85].

These papers on large classical simulations focus on on simulating quantum circuits on grids of qubits with local connectivity. This restriction is motivated by the designs of current quantum processors, and also allows for specific optimizations that reduce the temporal complexity of the simulation. State of the art methods typically split this grid into sub-blocks, which are locally contracted leaving only connections between blocks [80, 82, 53, 54]. The remaining s contractions are then 'sliced', fixed to one of 2^s values and then contracted fully [80]. This has a natural operational interpretation in terms of a sum-over-paths expansion [53], and has the advantage that the contractions within blocks can be parallelised.

These methods all achieve runtimes that scale as $\max\left[2^{dl}, 2^n\right]$, where l is the length of the longest edge of the grid [85]. They also have exponential spatial requirements, though these are reduced compared to a state-vector method by virtue of tensor slicing. Through application of supercomputing resources, these methods have simulated random universal circuits of up to depth 40 on 72 qubits [54], depth 35 on 100 qubits [81], and depth 24 on 121 qubits [83].

Because this generated of quantum hardware aims to maximize qubit count, it will not employ full error-correction routines. As a result, noise is a significant factor in the system, and limits the depth of circuits that can be run. We refer to this regime of quantum computing as 'Noisy Intermediate Scale Quantum' or NISQ [86]. Thus, much like system size for the state-vector simulator, the exponential simulation overhead in the depth does not render the simulations intractable. In fact, simulators can benefit from the increased noise level, by dropping terms from the simulation and reducing the overall computational time required by a constant factor, as discussed in Section 3.3.

4.2   Results

In the rest of this chapter, we will discuss a distinct method for simulating universal quantum circuits, based on stabilizer state decompositions. We will present simulation results for several types of quantum circuit, and argue that this method has a great potential for simulating circuits on current and near-term quantum hardware.

4.2.1   Methods for Manipulating Stabilizer Decompositions

At a high level, simulating a quantum circuit U using a decomposition into efficiently simulable terms requires two main stems. Firstly, we need to build a representation of the circuit state $U\left|x\right\rangle$ for an input state $\left|x\right\rangle$, which is itself part of our efficiently representable set of states. Then, we need a routine for computing output variables from the distribution, either computing explicit probabilities if we interested in strong simulation, or else sampling from the output distribution if we are interested in weak simulation.

In the following, we will use U to denote a classical description of the quantum circuit U. We store U as a sequence of gates, where each gate includes its label, e.g. 'H', and the labels of the qubits it acts on.

Stabilizer states will be encoded classically using either the CH or the DCH representations, introduced in Chapter 2.

Building Decompositions

The main method for constructing a stabilizer state decomposition, given a description of a quantum circuit U, is the PBC method introduced in [26] and [8], and outlined previously in Sections 3.1.1 and 3.1.2. We will review the method briefly here, with a focus on implementation in software.

Implementing a PBC requires rewriting U as an equivalent Clifford circuit V. We achieve this by walking through the circuit U, and replacing each of the m non-Clifford gate with an appropriate magic state or states, and state-injection gadget, such as the example shown in Figure 3.1. We note that this requires a library of known gadgets for implementing different gates. The result is a new circuit U', acting on n qubits and m magic states.

State-injection gadgets include additional, measurement controlled 'correction' operations. By post-selecting on these measurement-outcomes, we can expand out U' as a sum of different Clifford circuits V_y

$$ U\left|x\right> = \sum_y \left<y|V_y|x\otimes\psi\right> $$

where y is the post-selection string with length $O(m)$, and $\left|\psi\right>$ is the joint state of all the magic states.

It was shown in [8] that given some approximate stabilizer state decomposition of the magic states $\left|\tilde{\psi}\right>$, we can construct a PBC to sample from the output distribution of the circuit by sampling the post-selection string at random. Thus, for each gadget, we sample the measurement outcomes appropriately to build-up the Clifford circuit V.

As previously discussed, when injecting a gate U the correction operation has the form $UPU^\dagger$ for some Pauli operator P. If $U \in \mathcal{C}_3$, then by definition $UPU^\dagger$ is a Clifford operator and we are done. Otherwise, we will need to introduce additional layers of state-injection until we build an all-Clifford circuit $\mathtt{V}$.

Finally, we need to construct an approximate stabilizer state decomposition for the magic states $|\psi\rangle$. In general, $|\psi\rangle$ will be a tensor-product of different 'species' of magic state, and so we build the full approximation using the multiplicative upper bound

$$\chi_\epsilon\left(|\psi\rangle\right) = \chi_\epsilon\left(|T\rangle^{\#T}\right)\chi_\epsilon\left(|CCX\rangle^{\#CCX}\right)\chi_\epsilon\left(|\theta\rangle^{\#\theta}\right)\cdots$$

For Clifford magic states, we can make use of the random codes construction. Otherwise, we can use sparsification. We note that this again implies a library of best-known decomposition strategies for each magic-state we introduce.

Overall then, the gadgetization method takes as input a classical description of an n-qubit circuit $\mathtt{U}$ and target error ϵ, and returns a new description of a Clifford circuit $\mathtt{V}$ acting on n qubits and m magic states, the corresponding post-selection string $\vec{\mathbf{y}}$, and an approximate stabilizer state decomposition $|\tilde{\psi}\rangle$. A pseudo-code description of this method is given in Algorithm 3.

The Sum-over-Cliffords picture

The PBC model has an interesting feature where the number of qubits in the stabilizer state expansion depends only on the magic states, and not on the number of qubits in the circuit. Stabilizer circuits are efficient to simulate in terms of the number of qubits, but the $O(n^3)$ overhead is still considered significant in practice. Thus, if there are fewer magic states, the PBC can reduce the number of variables in the simulation. But, in general, universal quantum computations have a number of gates that scales as $\mathrm{poly}\,(n)$, and gadgetization will result in more qubits.

An alternative strategy for building stabilizer state decompositions makes use

of the equivalence between stabilizer circuits and stabilizer states. If we consider a Clifford gate decomposition $Q = \sum_i \alpha_i V_i$, then the action of Q on a stabilizer state results in a stabilizer state decomposition

$$Q\,|\phi\rangle = \sum_i \alpha_i V_i\,|\phi\rangle = \sum_i \alpha_i\,|\phi_i\rangle, \qquad (4.1)$$

which we can then turn into an approximation stabilizer state decomposition with sparsification, giving a decomposition with a rank $O(\|\vec{\alpha}\|^2)$.

From this, we can define a notion of 'extent' for a unitary

$$\xi\,(Q) = \min_V \|\vec{\alpha}\|^2 \ : \ Q = \sum_i \alpha_i V_i. \qquad (4.2)$$

For example, considering single-qubit rotations in around the Z axis of a Bloch sphere with $\theta \in [0, \pi/2$, we can expand them into two Clifford branches

$$R_Z\,(\theta) = \left(\cos\frac{\theta}{2} - \sin\frac{\theta}{2}\right) I + \mathrm{e}^{-\mathrm{i}\pi/4}\sqrt{2}\sin\frac{\theta}{2}S, \qquad (4.3)$$

with corresponding extent $\xi\,(R\,(\theta)) = \left(\cos\frac{\theta}{2} + \tan\frac{\pi}{8}\sin\frac{\theta}{2}\right)^2$ [12]. Similar results can be found for all Z rotations, where we slightly adjust the phase and the Clifford operations on each branch.

This expansion corresponds with the stabilizer extent of the $|T\rangle$ state by setting $\theta = \frac{\pi}{4}$. In fact, it was shown by Earl Campbell that for injectable Clifford magic states, such as $|T\rangle$ and $|CCZ\rangle$, that the extent-optimal stabilizer state decomposition can be used to 'lift' a Clifford gate expansion of the corresponding unitary (i.e. T and CCZ), that is also optimal [12].

Using submultiplicativty, we can thus upper-bound the stabilizer extent of the circuit U as

$$\xi\,(U) = \prod_{i=1}^{m} \xi\,(U_i) \qquad (4.4)$$

for each non-Clifford gate U_i. We can then build up a term in the stabilizer state decomposition by iterating through U. If the gate is Pauli or Clifford,

we just apply it and update the state. Otherwise, for each non-Clifford gate U_i we sample a branch from the Clifford expansion with $p_{i,j} = \frac{|\alpha_{i,j}|}{\|\vec{\alpha_i}\|}$ as in the sparsification method, and apply the corresponding Clifford gate $V_{i,j}$. We can repeat this $O(\xi(U))$ times, to produce a stabilizer state decomposition of the $U|x\rangle$. This algorithm is outined in Algorithm 4.

Output Variables

There are two main methods for computing output variables from a given stabilizer state decomposition. The first is the 'norm estimation' routine, introduced in [8] and refined in [12]. Norm estimation can be used to compute measurement probabilities, and also to sample as described in Section 3.1.2. The second is a Metropolis-style Monte Carlo method, which can be used to return samples in the computational basis. Both methods were developed by Sergey Bravyi, and we introduce them here with a view to their implementation. The two methods are also outlined in Algorithms 5 and 6, respectively.

Norm Estimation

This routine allows us to quickly compute an approximation to $\|\psi\|$. Importantly, given a projector Π, we can compute the probability of that outcome as

$$p(\Pi) = \frac{\|\Pi\psi\|^2}{\|\psi\|^2}.\tag{4.5}$$

In particular, it is possible to show that if we generate equatorial stabilizer states $|\eta\rangle$ uniformly at random, then the random variable $\eta \equiv 2^{n/2}|\langle\eta|\psi\rangle|$ has the property that

$$\mathbb{E}\left(\eta^2\right) = \|\psi\|^2 \quad \mathbb{E}\left(\eta^4\right) \leq 2\|\psi\|^4$$

and thus, the average inner product of $|\psi\rangle$ with equatorial stabilizer states is the norm, with variance at most $\|\psi\|^4$ [12].

The number of samples we need depends on the accuracy desired. It can be shown that given an estimate

$$\bar{\eta} = \frac{1}{L}\sum_i \eta_i^2$$

Algorithm 3 Pseudocode description of the computational routine for construction a stabilizer state decomposition of a quantum circuit using state-injection gadgets.

Require: Known set of gadgets for non-Clifford gates.

  function GADGETDECOMPOSITION($\mathtt{U}, \epsilon$)

      $\mathtt{V} \leftarrow \emptyset$ ▷ Output Clifford circuit

      $|\psi\rangle \leftarrow \emptyset$ ▷ Magic states

      for $U_i \in \mathtt{U}$ **do**

          if $U_i \notin \mathcal{C}_2$ **then**

              Sample a measurement outcome z

              $\mathtt{V} \leftarrow \mathtt{V} \cap \mathtt{G} \cap \mathtt{V}_z$ ▷ $\mathtt{G}$ is the gadget for U_i.

              $|\psi\rangle \leftarrow |\psi\rangle \otimes \psi_G$ ▷ Magic state associated with $\mathtt{G}$

          else

              $\mathtt{V} \leftarrow \mathtt{V} \cap \mathtt{U}_i$

          end if

      end for

      Reorder qubits in $\mathtt{V}, |\psi\rangle$ to join common species of magic state

      $\left|\tilde{\psi}\right\rangle = \emptyset$

      for $\left|\psi_{U_j}^{\otimes \#U_j}\right\rangle \in |\psi\rangle$ **do**

          $\left|\tilde{\psi}\right\rangle \leftarrow \left|\tilde{\psi}\right\rangle \otimes \left|\tilde{\psi_{U_j}}\right\rangle$ ▷ Rank is set by ϵ.

      end for

      return $\mathtt{V}, \left|\tilde{\psi}\right\rangle$

  end function

Algorithm 4 Pseudocode description of building stabilizer state decompositions in the sum-over-Cliffords picture.

Require: Clifford decompositions of non-Clifford gates.

  function SUMOVERCLIFFORDDECOMPOSITION($\mathtt{U}, \epsilon, |x\rangle$)

      $\left|\tilde{\psi}\right\rangle = \emptyset$

      $\xi \leftarrow$ COMPUTEEXTENT($\mathtt{U}$)

      $i \leftarrow 0$

      while $i < \chi_\epsilon = O\left(\xi \epsilon^{-2}\right)$ **do**

          $|\phi\rangle \leftarrow |x\rangle$

          $c \leftarrow 1$

          for $U_i \in \mathtt{U}$ **do**

              if $U_i \notin \mathcal{C}_2$ **then**

                 Sample Clifford branch j of gate U_i

                 $|\phi\rangle \leftarrow V_{i,j} |\phi\rangle$

                 $c \leftarrow \frac{\alpha_{i,j}}{|\alpha_{i,j}|} c$

              else

                 $|\phi\rangle \leftarrow U_i |\phi\rangle$

              end if

          end for

          $\left|\tilde{\psi}\right\rangle \leftarrow \left|\tilde{\psi}\right\rangle + c |\phi\rangle$

          $i \leftarrow i + 1$

      end while

      return $\left|\tilde{\psi}\right\rangle$

  end function

Algorithm 5 Pseudocode outline of the Norm Estimation routine for computing expectation values of Pauli projectors.

Require: L, number of samples to take, n, number of qubits, Π, Pauli projector
   function NORMESTIMATION(Π, $\left|\tilde{\psi}\right\rangle$)
        $\vec{\eta} \leftarrow \{\eta_i = 0\}$
        $\{|\eta_i\rangle\} \leftarrow$ RANDOMEQUATORIALSTATE(n)
        for $\alpha_i, |\phi_i\rangle \in \left|\tilde{\phi}\right\rangle$ **do**
            $\Gamma \leftarrow 1$
            for $P \in \Pi$ **do**
                $\Gamma_P, |\phi_i\rangle \leftarrow$ MEASUREPAULI(P,$|\phi\rangle$)
                if $\Gamma_P = 0$ **then**
                    $\Gamma \leftarrow 0$, Break loop
                end if
                $\Gamma \leftarrow \Gamma\Gamma_P$
            end for
            if $\Gamma \neq 0$ **then**
                for $|\eta_i\rangle \in \{|\eta_i\rangle\}$ **do**
                    $\eta_i \leftarrow \Gamma\alpha_i \langle\eta_i|\phi_i\rangle$
                end for
            end if
        end for
        return $\frac{2^n}{L}\sum_i |\eta_i|^2$
   end function

Algorithm 6 Pseudocode description of the Metropolis-style Monte Carlo method for sampling a computational basis string x from the output distribution of a stabilizer state decomposition.

Require: n, number of qubits
   function METROPOLISSAMPLING($\left|\tilde{\psi}\right\rangle$, m)
        $\vec{x} \leftarrow$ Random initial n-bit binary string
        $p_x \leftarrow |\sum_i \alpha_i \langle x|\phi_i\rangle|^2$
        for $j \in [1,\ldots,m]$ **do**   ▷ m repetitions of the random walk step
            $j \leftarrow$ Random integer $\in [1,\ldots,n]$
            $\vec{x}' \leftarrow \vec{x} \oplus \vec{e}_j$
            $p_{x'} \leftarrow |\sum_i \alpha_i \langle x'|\phi_i\rangle|^2$
            if $p_x = 0$ **then**   ▷ Always move away from 0 amplitudes
                $x \leftarrow x'$, $p_x \leftarrow p_{x'}$
            else
                Generate $r \in [0,1)$ uniformly at random
                if $r < \frac{p_{x'}}{p_x}$ **then**   ▷ Always accept if $p_{x'} > p_x$
                    $x \leftarrow x'$, $p_x \leftarrow p_{x'}$
                end if
            end if
        end for
        return $\vec{x}$
   end function

---

then $\bar{\eta}$ approximates $\|\psi\|$ to within multiplicative error ϵ with probability $\frac{3}{4}$ if $L = 4\epsilon^{-2}$ [12]. We can of course increase this probability to $1 - \delta$ by taking $\log \delta^{-1}$ estimates of $\bar{\eta}$.

In Section 2.2.2, we introduced an algorithm for computing inner products between stabilizer states $|\phi\rangle$ and equatorial stabilizer states. This method has computational complexity $O(n^3)$. Thus, given a stabilizer state decomposition $\left|\tilde{\psi}\right\rangle$, we can use compute $\left\|\tilde{\psi}\right\|$ in time $O(L\chi n^3)$, where L is the number of samples of η.

As part of the sampling routine described in Section 3.1.2, we want to compute marginal probabilities $P(x_1, x_2, \ldots x_j)$ for some j-bits. These marginals correspond to fixing j qubits, and projecting the rest onto a 2^{n-j} dimensional codespace, generated by j Pauli operators [8]. This codespace can be generated by j Pauli operators, giving

$$\Pi = \prod_{i=1}^{j} \frac{1}{2}\left(I + P_i\right)$$

where P_i are n qubit Pauli operators. We can thus apply this projector by measuring each of the Pauli generators in turn. Recall that each Pauli measurement takes time $O(n^2)$, (c.f. 2.2.2) and thus computing $\left\|\Pi\tilde{\psi}\right\|^2$ also has runtime $O\left(L\chi n^3\right)$.

To avoid accumulation of errors, each marginal probability needs to be computed with multiplicative error $O(w^{-1})$ when sampling from w output bits. Using the bound on the approximation accuracy above, this implies $L = O(w^2)$. As there are w marginals to compute, sampling with the norm estimation method thus takes time $O(\chi n^3 w^3)$.

In the gadgetized picture, we can employ norm estimation by first setting the measurement projector Π, and then updating it to obtain the corresponding PBC Π_s by conjugating the projector with the Clifford circuit V_y. These Pauli updates can be computed efficiently classically, using similar update rules as for a stabilizer tableau [2]. Otherwise, for decompositions obtained using the

sum-over-Cliffords method, no further preprocessing is required.

We note that norm estimation is required to compute individual computational basis amplitudes, and to convert a stabilizer state decomposition into the state vector picture. Recalling that in the CH and DCH representations, we can compute $\langle x|\phi\rangle$ in time $O(n^2)$, this means that for a given stabilizer state decomposition we can compute $\langle x|\tilde{\psi}\rangle$ in time $O(\chi n^2)$. To avoid potential floating point errors, stabilizer states in the decomposition are stored only with their relative phase coefficients. Thus, these amplitudes needs to be reweighted by $\|\tilde{\psi}\|$.

Metropolis Estimation

One advantage of norm estimation is that it can be used to compute the probability of arbitrary Pauli measurements. However, as discussed, while technically polynomial it has a runtime up to $O(n^6)$ in the number of qubits. THus, an alternative strategy based on Metropolis Monte Carlo methods was proposed by Sergey Bravyi, that also makes use of the ability to compute individual computational basis amplitudes in time $O(n^2)$.

The idea is to define a random walk through the set of computational basis strings, flipping one bit at a time and computing the amplitude of the new string. If at some time-point we have computational basis string x and amplitude $\left|\langle x|\tilde{\psi}\rangle\right|$, then we obtain x' by flipping a single bit at random, and compute $\left|\langle x'|\tilde{\psi}\rangle\right|$. If the new amplitude is larger, we accept the move. Otherwise, we accept with fixed probability

$$p = \frac{\left|\langle x'|\tilde{\psi}\rangle\right|}{\left|\langle x|\tilde{\psi}\rangle\right|}.$$

It can be argued that, assuming that for all strings x, y there exists a path of single-bit moves between them, the steady state distribution of this walk converges to the output distribution of the circuit in time poly$n$ [12].In practice, we have used this method to obtain samples from the output distribution on

50 qubit circuits with mixing time of ~ 2000 steps [12]. Importantly, once the chain has been mixed, we can then obtain samples by continuing to run the core random-walk step (contained within the `For` loop in Algorithm 6) for a further s repetitions, recording the string $\vec{\mathbf{x}}$ at the end of each step as one sample.

In general, computing amplitudes requires time $O\left(\chi n^2\right)$, and so we might expect the Metropolis method to have a runtime that scales as $O\left(\chi n^2\right)$. However, we can actually remove a factor of n from the runtime of the random-walk step by exploiting the fact we are flipping single bits at a time.

Recall from Section 2.2.2 that we compute the computational amplitudes $\vec{\mathbf{x}}$ in the CH and DCH picture by commuting a Pauli $X(\vec{\mathbf{x}})$ past the CH/DCH layers which we denote here as a Clifford circuit W. We can store this resulting Pauli operator $P' = W^\dagger X(\vec{\mathbf{x}})W$, which takes $O(n^2)$ to compute, for a constant memory cost. We can then compute the operator Q', obtained by commuting $X(\vec{\mathbf{x'}})$, as

$$Q' = WX(\vec{\mathbf{x'}})W^\dagger = WX(\vec{\mathbf{e}}_j)X(\vec{\mathbf{x}})W^\dagger = WX(\vec{\mathbf{e}}_j)W^\dagger P'.$$

Because $X(\vec{\mathbf{e}}_j)$ acts as the identity everywhere except qubit j, commuting this operator through the Clifford layer can be optimised to ignore any terms except for those involving qubit j. By inspection of Eqs. 2.46, 2.47, 2.48 and 2.49, this takes time $O(n)$ as each vector-matrix multiplication will involve only a single row or column.

Thus, overall then, if we run the Metropolis method for time $m + s = T$ to obtain s samples, the runtime scales as $O\left(\chi n^2\right) + O\left(T\chi n\right)$.

4.2.2   Implementation of the Simulator

To implement these simulation methods, the fundamental data-structures we consider are arrays of stabilizer states, and their complex coefficients. The stabilizer states themselves are encoded using either the CH or the DCH representation, as each encoding supports the necessary update routines including

fast inner-product calculations with equatorial states.

Building on the existing implementations of the CH and DCH simulators discussed in Section 2.2.3, the simulator was written in `C++`. In the previous section, we introduced two distinct approaches for building stabilizer state decompositions, and two distinct methods for computing output variables. Thus, the simulator was designed using the 'strategy' design pattern [87], which allows different algorithms for the same task to be used interchangeably.

The core of the simulator is a class we call `Runner`, which is responsible for maintaining the stabilizer state decomposition. The `Runner` class is initialized with the target stabilizer rank, the number of qubits and, optionally, the initial stabilizer state $|x\rangle$.

Because the specifics of building a stabilizer state decomposition will depend extensively on the circuit, including factors like the choice of gadget or Clifford decomposition, the `Runner` accepts user-defined strategies. These can be implemented using 'function objects', classes that can be called like functions [88]. This allows the decomposition strategy to have internal state information, e.g. the choice of 'subspaces' used to decompose Clifford magic states, which is kept separate from the resulting stabilizer state decomposition. The user defines their decomposition strategy by sub-classing the `DecompositionBuilder` class, and at runtime the `Runner` class simply calls the function object χ times to build up the decomposition. The `Runner` method then also implements both the norm estimation and metropolis methods.

Details of the specific strategies used to build stabilizer state decompositions will be given as part of the descriptions of the method in Section 4.2.3.

In their implementation, the DCH and CH classes have the same set of public methods, differing only in their internal representation of the stabilizer state. We formalise this using the notion of 'template' programming [87, 89]. Templates allow the implementation of the simulator to be agnostic to the choice of internal representation. The choice of encoding is made at compile-time, by

specifying either the `CHState` or `DCHState` classes.

Parallelization

An important feature of all the routines outline in Algorithms 3–6 is that they each include a step where we operate on every single term in the stabilizer state decomposition independently. In the decomposition routines, each stabilizer state term is built up separately. Similarly, in the output routines, we use a 'map-reduce' model where the same calculation is applied to every state before combining the results at the end; for example, computing a probability amplitude requires summing the value of $\langle x|\phi_i\rangle$ for every state.

These kind of computations are called 'embarrassingly parallelisable', as there is little to no dependency between the tasks, and thus they can be easily sped-up by providing multiple parallel workers. Importantly, these loops are also they only parts of the computation where the complexity scales as $O(\chi)$; other steps, such as gadgetizing a circuit or computing a PBC, are efficiently computable. Thus, these parallelisable loops dominate the runtime, and by Amdahl's law we can significantly reduce the runtime of the programme by adding parallel workers [90].

In contrast to 'data parallelism', such as the SIMD methods discussed in Section 2.3, this kind of computation is called Multiple Instruction Multiple Data(MIMD) computation [21]. MIMD programmes can be further subdivided into 'shared memory' execution, where parallel threads run on a single computer, or 'distributed' execution, where multiple separate processes run independently on multiple processing units.

Shared memory parallelism is the most straightforward to implement. The programme is mainly executed by a single thread, with additional parallel threads 'forked' from the programme for specific subroutines [91]. In `C++`, this can be implemented using `OpenMP`, which allows parallelising loops and 'map-reduce' operations with single-line annotations [92].

However, the benefits of shared memory parallelism are limited by the kind

of hardware available, in particular the maximum memory and number of threads. While this kind of parallelism is sufficient for personal computers, scaling the simulator to large problem sizes requires distributed memory techniques.

We used a 'message passing' model of distributed memory parallelism, where multiple processes each execute a unique copy of the programme, and synchronise and share results through inter-process communication [91]. In particular, we use `Open-MPI`, an open source implementation of the Message Passing Interface standard [93, 94].

We implement a subclass of `Runner`, called `MPIRunner`, for distributed memory computations. On initialization, each process is assigned a 'rank' in the group, with the rank-0 process designated the 'master' [94]. All processes run the same setup steps to initialize the simulation, and the 'master' process then splits the decomposition, allocating a unique fraction of states f_i to each of the 'worker' processes. The worker processes then perform computations locally on their share of the decomposition. Initialization is done entirely locally, with the only communication being to pause the programme until all processes have computed their terms [94]. For output variables, processes again apply the 'map-reduce' model locally, before broadcasting their results to the master process which performs a final reduction step [94]. We can also allow for 'hybrid' parallelism, where each distributed process also uses local, shared-memory execution to speed up its part of the simulation task.

Through distributed memory execution, the stabilizer rank simulator can be scaled up to even larger problem sizes. In this thesis, the largest simulation we considered used 108GB of memory, running on UCL's Myriad supercomputing cluster, but this method could be scaled to even larger instances.

Integration with `Qiskit-Aer`

Using the `Runner` class outlined above, we were also able to integrate our simulation method with `Qiskit-Aer`, the component of IBMs `Qiskit` QDK that is responsible for classical simulations. Here, we briefly outline the `Qiskit`

execution model, and show how our simulator can be incorporated with it.

The fundamental data-structure in `Qiskit` is the `Qobj` or 'Quantum Object', which contains information about a quantum programme in the form of the available quantum and classical registers, and the circuits to be run. The `Qobj` is then converted to Javascript Serial Object Notation (JSON), such that it can be transmitted over the internet to the IBM Quantum Experience, or dispatched to the `Aer` suite of classical simulators.

This classical backend also employs a version of the strategy pattern. The `Qobj` is first parsed by a `Controller`, which is responsible for setting up the simulation, including configuring the shared-memory parallel execution, and creating an internal representation of the quantum circuit as an sequence of `Gate` objects. This includes reading configuration options related to the choice of strategy, or else picking a strategy automatically by inspecting the memory requirements for the circuit. The `Controller` class is also responsible for implementing noisy simulations using a stochastic noise model, where additional random gates and measurements are inserted according to a specified noise model. It does this by sampling additional gates, and inserting them into the circuits. The controller then initializes a `State` class for each circuit in the `Qobj`, passing in the details of the circuit and quantum and classical registers.

We integrate the stabilizer rank simulator by creating a custom `State` class. These objects are responsible for parsing the quantum circuit, and maintaining an internal representation of the quantum state called a `qreg` or 'quantum register' object. In our case, the `qreg` object is a version of the `Runner` class. We begin by first iterating through the circuit, checking it contains only gates we now how to decompose, computing the (multiplicative upper-bound) on the circuit extent ξ, and initializing the `Runner` with $\chi_\epsilon = \lceil \xi \epsilon^{-2} \rceil$ copies of the initial stabilizer state $|x\rangle$.

The simulation strategy then depends on whether the circuit contains intermediate measurements, whether as a result of sampled noise operators or just

as part of the circuit to be run. If there are no intermediate measurements, then the simulation is embarrassingly parallel up until the final measurement stage. Thus, we can iterate through the circuit in parallel, building up each term in the decomposition using the sum-over-Cliffords method.

Otherwise, we need to coordinate the simulator at each measurement operation. Thus, we instead build up the circuit one gate at a time. For each gate, we then begin a parallel loop, taking χ_ϵ samples of the Clifford branches for that gate. When we reach a measurement step, we then run the metropolis method to produce a single sample, and apply the corresponding Pauli projector to decomposition, again parallelising over the $\chi\epsilon$ terms. This model is less performant than the previous case, as it requires blocking the computation until all parallel workers have finished, and also as there it requires entering and exiting parallel execution multiple times, which has some associated overhead.

The current integration as part of `Qiskit-Aer` only uses the metropolis method, as this is the most general method for sampling from the output distribution of the circuit. However, the output distribution of some circuits will not satisfy the irreducibility requirement. We can in practice achieve good performance, passing the benchmark suite of test circuits for `Qiskit`, by re-mixing the metropolis method for each sample. This avoids us becoming stuck in a non-zero amplitude, and returning the same bit-string for 100% of the samples.

This version of the simulator was made public in April, 2019, in the `0.1.0` release of `Qiskit-Aer`. As an example of the capabilities of our simulator, we ran a small random circuit benchmark using both the default `Qasm` simulator of `Qiskit-Aer`, which is based on the state-vector method, and our simulator, which is called `extended_stabilizer` in the `Qiskit-Aer` package. We used the default paramters for the stabilizer rank-based method, which sets $\epsilon = 0.05$ and mixes the Metropolis method for 3000 steps.

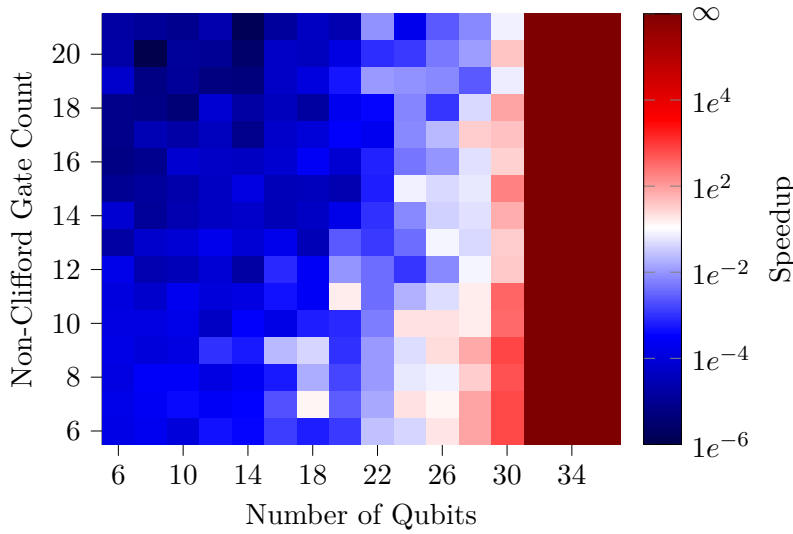We generated random circuits with a fixed number of non-Clifford gates, and

Figure 4.1: Figure comparing the runtime of stabilizer rank-based simulations to the
`Qiskit` state-vector simulation for random circuits, using `Qiskit-Aer`. The
solid red region corresponds to the regime where quantum circuits required
too much memory to simulate with state-vector methods.

simulated these circuits 10 times each with both methods, running on the UCL
Myriad cluster with access to 4 2.3GHz processors and 16GB of RAM, and
a maximum of 90 minutes of compute time. These conditions are intended
to simulate typical personal computers. We then recorded the runtime, and
plotted the 'speedup' as the ratio of $\frac{\text{Extended Stabilizer Runtime}}{\text{Qasm Runtime}}$. The results are
shown in Figure 4.1. As we can see, the runtime of the stabilizer-rank based
methods increases with the number of non-Clifford gates, which we expect
as the extent also increases. However, even for circuits with small extent,
below 20 qubits the stabilizer rank method requires significantly increased
runtime compared to the state-vector approach. However, as the number of
qubits continues to increase, the stabilizer rank method becomes increasingly
efficient.

Above a hard upper limit of 30 qubits, the spatial requirements of the state-
vector simulator exceed the available memory, and so the circuits cannot be
simulated. The stabilizer rank simulator, however, is still capable of running
the simulation. it is also important to note that, as expected, the runtime of
the stabilizer state method does not increase significantly with the number of
qubits. For example, a circuit on 50 qubits and with 20 non-Clifford gates

required on average 246 seconds to simulate with the stabilizer-rank method, compared to the 213 seconds required by the state-vector method to simulate a similar circuit on 30 qubits.

4.2.3 Simulations of Quantum Circuits

In this section, we will present results using the stabilizer rank method to simulate three common classes of quantum circuit: 'oracle' or black-box circuits, variational methods, and random circuits.

Hidden Shift Circuits

Oracle-based circuits are a very common technique for designing quantum algorithms, encompassing everything from toy methods such as the Deutsch-Jozsa algorithm up to famous algorithms like Grover search and Shor's algorithm [95]. These methods generally involve initializing the quantum state in a superposition of computational basis states, and then applying a black-box unitary O_f that computes some classical function f [44].

The hidden-shift problem is an example of a computational task where quantum algorithms require fewer invocations or queries to the oracle than any classical method [96]. Consider a 'bent' boolean function $f(\vec{\mathbf{x}}) : \mathbb{Z}_2^n \to \pm 1$, which has the property that its Fourier coefficients $\hat{f}(\vec{\mathbf{w}}) = \frac{1}{2^n} \sum_{\vec{\mathbf{x}}} (-1)^{\vec{\mathbf{w}} \cdot \vec{\mathbf{x}} + f(\vec{\mathbf{x}})}$ are equal for all n-bit strings w.

For any boolean function, we can also define a shifted function f_s as $f_s(x) = f(x \oplus s)$, where $\vec{\mathbf{s}} \in \mathbb{Z}_2^n$ is a fixed binary string. Finally, we can also define the Fourier transformed dual of the bent function as [96]

$$\tilde{f}(\vec{\mathbf{x}}) = 2^{-n/2} \sum_{\vec{\mathbf{y}} \in \mathbb{Z}_2^n} (-1)^{\vec{\mathbf{x}} \cdot \vec{\mathbf{y}}} f(y)$$

Given oracles O_{f_s} and $O_{\tilde{f}}$ that will evaluate both the shifted function and its unshifted dual for some input string $\vec{\mathbf{x}}$, it will take a classical method $O(n)$ queries to determine the hidden-shift string $\vec{\mathbf{s}}$. However, a quantum algorithm can determine $\vec{\mathbf{s}}$ in just two queries.

$$|0^{\otimes n}\rangle \; -\boxed{H^{\otimes n}}-\boxed{O_{f_s}}-\boxed{H^{\otimes n}}-\boxed{O_{\tilde{f}}}-\boxed{H^{\otimes n}}- \; |s\rangle$$
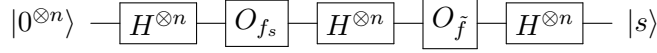
Figure 4.2: Circuit diagram of the quantum method for solving the hidden-shift problem, described in [96].

It is interesting to note that, if we further restrict this problem to only have access to f_s and f, and not the dual bent function, there nonetheless exists an alternative quantum algorithm capable of solving for $\vec{s}$ in $O(n)$ queries. The authors conjecture that in this case a classical method would require an exponential number of queries [96].

The specific class of bent functions considered in [96] are called Majorana-McFarland functions. In practice, we can construct a quantum oracle for random bent functions from this family using a fixed number of CCZ gates. This method was outlined in Appendix F of [8], which used the hidden-shift problem to benchmark the performance of the stabilizer rank simulation method. Because we specify the string s in the construction of the oracle, this method has 'built-in' verification that the simulator is running correctly.

In particular, [8] detail how to construct a bent function starting from a random boolean function $g : \mathbb{Z}_2^{n/2} \to \pm 1$, which they generate using a random sequence of Z and CZ gates and a fixed number of CCZ gates. If we denote this circuit O_r, then the oracles for the hidden-shift problem are defined as

$$O_g = \left(\Pi_{i=1}^{n/2} CZ_{i,i+n/2} \right) O_r \otimes I \quad O_{\tilde{f}} = \left[\left(\Pi_{i=1}^{n/2} CZ_{i,i+n/2} \right) I \otimes O_r \right] Z(\vec{s}) \tag{4.6}$$

For m CCZ gates, the overall circuit thus contains $2m$ non-Clifford gates. In [8], they simulate these circuits by using a gadget for CCZ gates built out of 4 T gates. Here, we use the hidden-shift circuits on 40 qubits as a way to test our results on decomposing alternate Clifford magic states, and the sum-over-Cliffords picture. In particular, we simulate the hidden-shift circuits using four distinct methods

- A gadgetized decomposition, using 4 T gates to synthesis each CCZ gate

- A gadgetized decomposition, using $|CCZ\rangle$ magic states

- A sum-over-Cliffords decomposition, using 4 T gates per CCZ gate

- A sum-over-Cliffords decomposition, using CCZ gates

This allows us directly compare the sum-over-Cliffords and gadgetized methods, and to compare direct decompositions over Clifford+T synthesis.

The simulation was developed in collaboration with Mark Howard, based on the previous simulations developed by David Gosset in [8]. The setup for the simulation, including constructing the oracle circuits, and constructing the PBC projectors in the gadgetized method, are implemented in `MATLAB`.

As previously stated, sampling from n output bits with the norm estimation routine has a runtime that scales as $O\left(\chi_\epsilon n^6\right)$. To circumvent this, we exploit the fact that we can clasically cache the state of the simulation before measurement, and that the output state of the simulation is an approximation of single output string $|s\rangle$, and learn the string $\vec{\mathbf{s}}$ by sampling single qubits a time. An example of this is shown in Figure 4.3. Overall, this method takes time $\left(\chi_\epsilon n^4\right)$ to sample from all n bits.

To more easily the decomposition between each norm estimation step, we build up the decompositions in MATLAB. We then make use of the `MEX` API to pass the decomposition and Pauli projectors to the `C++` simulator, which computes and returns the probability $p_{x_i=1}$.

In the gadgetized case, the number of terms in the decomposition depends on the stabilizer fidelity and the target infidelity, which we will denote here as δ. Using the stabilizer fidelity of the $|T\rangle$ and $|CCZ\rangle$, then for a bent function using m CCZ gates the size of the decomposition χ scales as

$$
\begin{aligned}
F\left(T\right) &\approx 0.853 & \chi &= \lfloor \tfrac{4F(T)^{-8m}}{\delta} \rfloor \approx \lfloor 4\left(\tfrac{3.57^m}{\delta}\right) \rfloor \\
F\left(CCZ\right) &\approx \tfrac{9}{16} & \chi &= \lfloor \tfrac{4F(CCZ)^{-2m}}{\delta} \rfloor \approx \lfloor 4\left(\tfrac{3.16^m}{\delta}\right) \rfloor
\end{aligned}
\tag{4.7}
$$

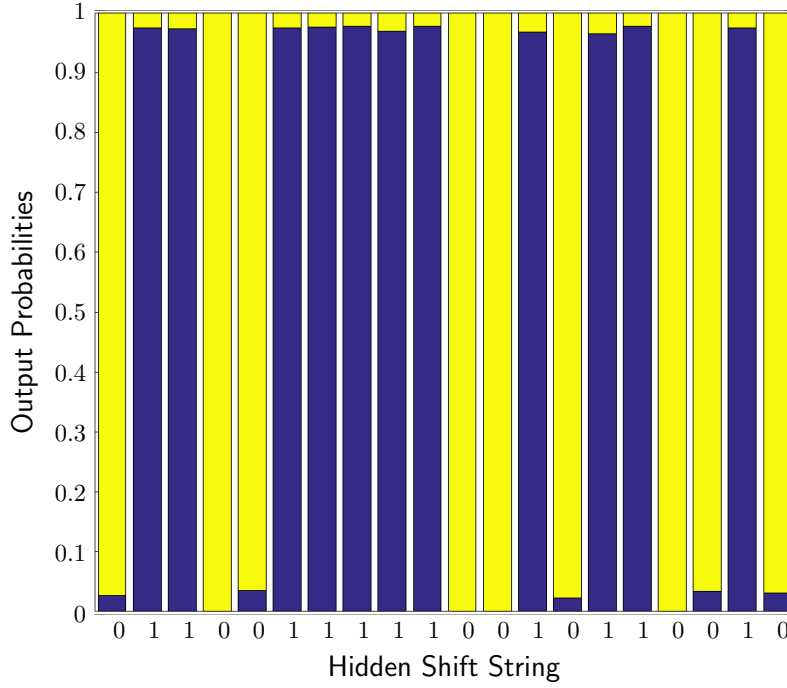Similarly, for the sum-over-Cliffords method, the number of terms is given by

Figure 4.3: Figure showing the probability $P(x_i = 1)$ for 20 bits, obtained using the sum-over-Cliffords methods and synthesizing the CCZ gate with 4 T gates. Each output probability is computed individually.

the stabilizer extent, and the target error ϵ. For $m\ CCZ$ gates, the number of terms is given by

$$
\begin{aligned}
\xi(T) &\approx 1.17 \quad \chi = \lceil 1.17^{8m}\epsilon^{-2} \rceil = \lceil 3.57^m \epsilon^{-2} \rceil \\
\xi(CCZ) &= \tfrac{16}{9} \quad \chi = \lceil 1.78^{2m}\epsilon^{-2} \rceil = \lceil 3.16^m \epsilon^{-2} \rceil
\end{aligned}
\tag{4.8}
$$

Recall that for Clifford magic states, the stabilizer fidelity and stabilizer extent coincide, which explains the correspondence in the scaling between the random codes and sum-over-Cliffords method. In all the simulations, we set $\delta = \epsilon = 0.3$. Due to platform limitations, the `C++` component was executed serially, though decompositions were built in parallel using `MATLAB`'s built in parallel execution. All simulations were run on a dual-core 1.9GHz Intel Xeon, with 32GB of RAM. The results of the simulations are shown in Figure 4.4.

QAOA

As mentioned in Section 4.1, current NISQ computers lack full error correction and thus accumulate noise as the circuit depth increases. Thus, there is a great deal of interest in relatively low-depth quantum algorithms that can run

Figure 4.4: Figures demonstrating the performance of the stabilizer rank method on simulating the hidden shift problem, using 4 methods of building the stabilizer state decomposition. Figures originally created for [12]
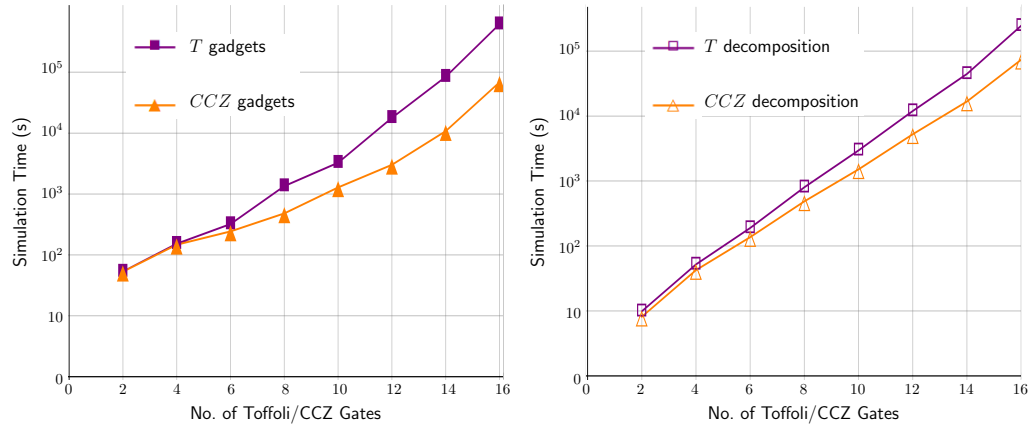
(a) Runtime of the hidden shift simulation as a function of the number of CCZ gates, using the random codes method to build decompositions, using Clifford+T synthesis and direct decomposition.

(b) Runtime of the hidden shift simulation as a function of the number of CCZ gates, using the sum-over-Cliffords method to build decompositions, comparing Clifford+T synthesis with CCZ gates.
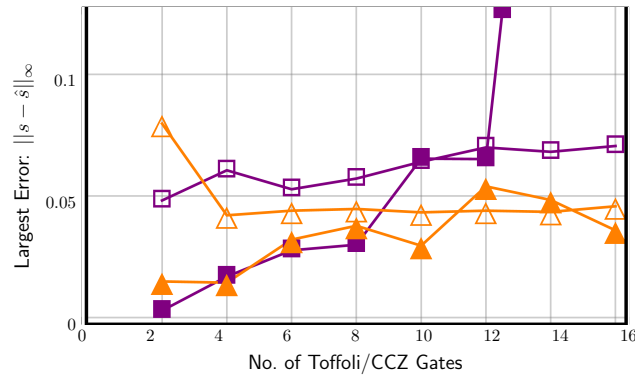
(c) The maximum observed approximation error in single-qubit probabilities over all bits in the hidden-shift string. The colour and markers correspond to the timing plots above. Not shown are two data-points in the T random-code methods, for 14 and 16 Toffoli gates, with large errors 0.304 and 0.512 respectively.

on NISQ devices. The main class of these algorithms are 'variational methods', hybrid quantum-classical algorithms with applications in optimization and quantum computational chemistry [97].

In general, variational methods use a simple processing scheme where the quantum computer is used to prepare an 'ansatz' state using a low-depth circuit. The gates in the circuit are typically parameterized. We then perform a series of measurements, and these outcomes are post-processed by a classical algorithm. This can be iterated, where the parameters of the ansatz state are updated by the classical algorithm, to converge to a heuristic solution [86, 97].

The Quantum Approximate Optimization Algorithm (QAOA) is an example of a variational method, applied to classical combinatorial optimization problems [98]. These kind of optimization problems are usually specified by a number of boolean clauses, and we are interested in optimizing a function 'satisfied clauses'

$$C(\vec{\mathbf{z}}) = \sum_{\alpha} C_{\alpha}(\vec{\mathbf{z}}),$$

where each sub-clause C_{α} acts on a subset of bits from the full n-bit string $\vec{\mathbf{z}}$, and evaluates to either $\{0, 1\}$ or ± 1 depending on the definition of the problem [98]. A clause is said to be 'satisfied' if it evaluates to 1. Examples of combinatorial optimization problems include MaxSat, where we are tasked with finding the string $\vec{\mathbf{z}}$ that satisfies the most clauses simultaneously.

Given a clause C_{α}, we can define an operator $\hat{C}_{\alpha}$ by replacing the bits z_{α_i} in the clause with Pauli Z operators, and in turn we can define $\hat{C} = \sum_{\alpha} \hat{C}_{\alpha}$ [98]. Different computational basis strings are eigenstates of this operator, such that

$$\hat{C} |\vec{\mathbf{z}}\rangle = C(\vec{\mathbf{z}}) |\vec{\mathbf{z}}\rangle.$$

The QAOA algorithm proceeds by preparing an ansatz state paramterised by $2p$ angles β_i and γ_i, for some fixed value of p. The system is initialized in the ground state $|g\rangle$ of the operator $\hat{C}$, which depends on the definition of the problem but is typically a trivial assignment such as $\left|0^{\otimes n}\right\rangle$ or $\left|+^{\otimes n}\right\rangle$ [98, 99].

We then apply p rounds of a pair of paramaterised rotation operators

$$U_C\left(\gamma_i\right) = \mathrm{e}^{-\mathrm{i}\gamma\hat{C}} \quad U_B\left(\beta_i\right) = \prod_i \mathrm{e}^{i\beta_i X(\vec{\mathbf{e}}_i)} \ .$$

For each paramaterised sate $\left|\psi_{\vec{\gamma},\vec{\beta}}\right\rangle$ has been prepared, we can determine the expectation value of the $\hat{C}$ operator

$$E_{\vec{\gamma},\vec{\beta}} = \left\langle\psi_{\vec{\gamma},\vec{\beta}}\right|\hat{C}\left|\psi_{\vec{\gamma},\vec{\beta}}\right\rangle.$$

Importantly, it can be shown that as $p \to \infty$, the maximum of this expectation value corresponds to the maximum of $C\left(\vec{\mathbf{z}}\right)$ [98]. The authors further show that even with $p = 1$, reasonable results that some classical strategies can be obtained [98, 99].

We consider the application of QAOA to a combinatorial optimization problem called MaxE3LIN2, where QAOA has been shown to outperform random classical guesses at $p = 1$ [99]. We choose this problem over MaxCut as it requires slightly fewer rotations, but nonetheless contains a significant number of non-Clifford gates. In particular, we consider randomly generated instances of MaxE3LIN2 with 50 variables and 66 clauses, requiring 50 qubits and 66 Pauli Z rotations.

The goal of MaxE3LIN2 is to maximize an objective-function

$$C\left(\vec{\mathbf{z}}\right) = \frac{1}{2}\sum_{1\leq u<v<w\leq n} d_{uvw}z_u z_v z_w$$

where each clause acts on 3 variables [99, 12], and the coefficients $d_{uvw} = \{0,\pm1\}$. The number of clauses is given by the number of non-zero coefficients. When generating the problems, restrict ourselves to instances with fixed degree 4, such that each qubit appears in at most 4 terms. We then prepare a state

$$\left|\psi_{\gamma,\beta}\right\rangle = U_B\left(\beta\right)U_C\left(\gamma\right)\left|+^{\otimes n}\right\rangle$$

with two parameters, using a single round of rotations [99].

Classical preprocessing methods exist for estimating $E_{\gamma,\beta}$, which can be used to speed-up the classical step of the variational algorithm. In particular, we use a method that allows the expectation variables of a sparse Hamiltonian with 'computationally tractable' states, states which can be efficiently specified in the computational basis [100]. This allows us to approximately compute

$$\langle \psi_\gamma | U_B(\beta)^\dagger \hat{C} U_B(\beta) | \psi_\gamma \rangle$$

with additive error ϵ in time $O(m^4 \epsilon^{-2})$ [12]. Figure **??** plots the estimates of $E_{\gamma,\beta}$ for a particular instance of MaxE3LIN2.

In their original paper, Farhi et al. fix $\beta = \pi/4$. This has the advantage that the rotation U_B becomes a Clifford operator

$$e^{-i\pi/4 X(\vec{\mathbf{e}}_i)} = H(\vec{\mathbf{e}}_i) S(\vec{\mathbf{e}}_i) H(\vec{\mathbf{e}}_i),$$

meaning all non-Clifford terms arise from the Z rotations. We can also see from Figure **??** that the line from $\beta = \pi/4$ passes through both a minima and a maxima of $C(\vec{\mathbf{z}})$. Thus, in our simulation, we also fix $\beta = \pi/4$. The cost function is symmetric about $\gamma = 0$, and so we sweep γ from 0 to π.

Each rotation $e^{i\gamma Z_u Z_v Z_w}$ has a sum-over-Cliffords expansion [12]

$$U_{C_{u,v,w}}(\gamma) = e^{-i\gamma d_{uvw} Z_u Z_v Z_w} = \begin{cases} \alpha I + \beta i CNOT_{u,v} CZ_{v,w} S_v^\dagger S_w^\dagger CNOT_{u,v} & d_{uvw} = -1 \\ \alpha I + \beta CNOT_{u,v} CZ_{v,w} S_v S_w CNOT_{u,v} & d_{uvw} = 1 \end{cases}$$

where the coefficients α and β are the phase terms associated with each branch

$$\begin{aligned} b_0 &= e^{i\gamma} - i & \alpha &= \frac{b_0}{|b_0|} \\ b_1 &= 1 - e^{i\gamma} & \beta &= \frac{b_1}{|b_1|} \end{aligned}.$$

For each value of γ, we build the corresponding stabilizer state decomposition with

$$\chi = \lceil \xi(\gamma) \epsilon^{-2} \rceil = \lceil (|b_0| + |b_1|)^{2m} \epsilon^{-2} \rceil$$

terms for m clauses. We then run the Metropolis method to take 40000 samples from the output distribution of the state $|\psi_\gamma\rangle$, and compute an estimate of the expectation value

$$E_{sim}(\gamma) \frac{1}{40000} \sum_{s=1}^{40000} C(z_s). \tag{4.9}$$

The simulations were run on the UCL Legion supercomputing cluster, running on Dell C6100 compute nodes, using a shared-memory parallelism model with 12 parallel threads and 24GB of RAM. We ran these methods with $\epsilon = 0.1$ and 0.15, and compare our estimates to the results from the heuristic method of [100]. Results are shown in Figure **??**.

Random Circuit Models

4.3   Discussion

4.3.1   Simulating NISQ Circuits

4.3.2   Simulating Random Circuits

4.3.3   Incorporating Noise

Chapter 5

General Conclusions

Bibliography

[1] D. Gottesman. The Heisenberg Representation of Quantum Computers (1998). `arXiv:quant-ph/9807006`.

[2] S. Aaronson and D. Gottesman. Improved simulation of stabilizer circuits. *Phys. Rev. A*, **70**, 052328 (2004). `arXiv:quant-ph/0406196`.

[3] M. Van den Nest. Classical simulation of quantum computation, the Gottesman-Knill theorem, and slightly beyond (2008). `arXiv:0811.0898`.

[4] J. R. Seddon and E. Campbell. Quantifying magic for multi-qubit operations (2019). `arXiv:1901.03322`.

[5] J. Dehaene and B. de Moor. Clifford group, stabilizer states, and linear and quadratic operations over GF(2). *Phys. Rev. A*, **68**, 042318 (2003). `arXiv:quant-ph/0304125`.

[6] S. Anders and H. J. Briegel. Fast simulation of stabilizer circuits using a graph-state representation. *Phys. Rev. A*, **73**, 022334 (2006). `arXiv:quant-ph/0504117`.

[7] H. J. García, I. L. Markov, and A. W. Cross. Efficient inner-product algorithm for stabilizer states. page arXiv:1210.6646 (2012). `arXiv:1210.6646`.

[8] S. Bravyi and D. Gosset. Improved Classical Simulation of Quantum Circuits Dominated by Clifford Gates. *Phys. Rev. Lett.*, **116**, 250501 (2016). `arXiv:1601.07601`.

[9] CHP. `https://www.scottaaronson.com/chp/`. Last Accessed: 2019-05-13.

[10] H. J. García and I. L. Markov. Simulation of Quantum Circuits via Stabilizer Frames. *IEEE Transactions on Computers*, **64**, 2323 (2017). `arXiv:1712.03554`.

[11] K. N. Patel, I. L. Markov, and J. P. Hayes. Efficient Synthesis of Linear Reversible Circuits (2003).

[12] S. Bravyi, D. Browne, P. Calpin *et al.* Simulation of quantum circuits by low-rank stabilizer decompositions (2018). `arXiv:1808.00128`.

[13] S. Bravyi, D. Gosset, and R. König. Quantum advantage with shallow circuits. *Science*, **362**, 308 (2018).

[14] E. T. Campbell and M. Howard. Unified framework for magic state distillation and multiqubit gate synthesis with reduced resource cost. *Phys. Rev. A*, **95**, 022316 (2017).

[15] C++ reference: Fundamental types. `https://en.cppreference.com/w/cpp/language/types`. Last Accessed: 2019-06-19.

[16] C++ reference: Bitwise operators. `https://en.cppreference.com/w/cpp/language/operator_arithmetic#Bitwise_logic_operators`. Last Accessed: 2019-06-19.

[17] Mathworks documentation: External language interfaces. `https://uk.mathworks.com/help/matlab/external-language-interfaces.html`. Last Accessed: 2019-06-20.

[18] D. Schlingemann. Stabilizer codes can be realized as graph codes (2001).

[19] M. Van den Nest, J. Dehaene, and B. De Moor. Efficient algorithm to recognize the local clifford equivalence of graph states. *Phys. Rev. A*, **70** (2004).

[20] Github.com: Graphsim. `https://github.com/Roger-luo/GraphSim`. Last Accessed: 2019-06-23.

[21] M. J. Flynn. Some Computer Organizations and Their Effectiveness. *IEEE Transactions on Computers*, **C-21**, 948 (1972).

[22] Intel streaming simd extensions technology. `https://www.intel.com/content/www/us/en/support/articles/000005779/processors.html`. Last Accessed: 2019-06-24.

[23] Lapack in matlab. `https://uk.mathworks.com/help/matlab/math/lapack-in-matlab.html`. Last Accessed: 2019-06-24.

[24] J. Dongarra, R. Pozo, and D. Walker. Lapack++: A design overview of object-oriented extensions for high performance linear algebra. , pages 162– 171 (1993).

[25] C. L. Lawson, R. J. Hanson, D. R. Kincaid *et al.* Basic linear algebra subprograms for fortran usage. *ACM Trans. Math. Softw.*, **5**, 308 (1979).

[26] S. Bravyi, G. Smith, and J. A. Smolin. Trading Classical and Quantum Computational Resources. *Phys. Rev. X*, **6** (2016).

[27] M. Yoganathan, R. Jozsa, and S. Strelchuk. Quantum advantage of unitary Clifford circuits with magic state inputs. *Proceedings of the Royal Society of London Series A*, **475** (2019).

[28] S. Bravyi and A. Kitaev. Universal quantum computation with ideal Clifford gates and noisy ancillas. *Phys. Rev. A*, **71** (2005).

[29] D. Gottesman and I. L. Chuang. Demonstrating the viability of universal quantum computation using teleportation and single-qubit operations. *Nature*, **402**, 390 (1999).

[30] N. J. Ross and P. Selinger. Exact and approximate synthesis of quantum circuits. `https://www.mathstat.dal.ca/~selinger/newsynth/`. Last Accessed: 2019-07-08.

[31] N. J. Ross and P. Selinger. Optimal ancilla-free Clifford+T approximation of z-rotations. page arXiv:1403.2975 (2014).

[32] M. Howard and E. Campbell. Application of a Resource Theory for Magic States to Fault-Tolerant Quantum Computing. *Phys. Rev. Lett.*, **118**, 090501 (2017).

[33] S. van der Walt, S. C. Colbert, and G. Varoquaux. The numpy array: A structure for efficient numerical computation. *Computing in Science Engineering*, **13**, 22 (2011).

[34] S. K. Lam, A. Pitrou, and S. Seibert. Numba: A llvm-based python jit compiler. In *Proceedings of the Second Workshop on the LLVM Compiler Infrastructure in HPC*, LLVM '15, pages 7:1–7:6. ACM, New York, NY, USA (2015).

[35] M. Lundberg and L. Svensson. The haar measure and the generation of random unitary matrices. In *Processing Workshop Proceedings, 2004 Sensor Array and Multichannel Signal*, pages 114–118 (2004).

[36] A. Knyazev and M. Argentati. Principal angles between subspaces in an a-based scalar product: Algorithms and perturbation estimates. *SIAM Journal on Scientific Computing*, **23**, 2008 (2002).

[37] A. W. Harrow. The Church of the Symmetric Subspace. *arXiv e-prints*, page arXiv:1308.6595 (2013).

[38] H. Zhu, R. Kueng, M. Grassl *et al.* The Clifford group fails gracefully to be a unitary 4-design. *arXiv e-prints*, page arXiv:1609.08172 (2016).

[39] M. Artin. *Algebra: 2nd Edition.* Pearson (2010).

[40] H. Pashayan, J. J. Wallman, and S. D. Bartlett. Estimating outcome probabilities of quantum circuits using quasiprobabilities. *Phys. Rev. Lett.*, **115**, 070501 (2015).

[41] S. Boyd and L. Vandenberghe. *Convex Optimization.* Cambridge University Press (2004).

[42] B. Regula. Convex geometry of quantum resource quantification. *Journal of Physics A Mathematical General*, **51**, 045303 (2018).

[43] D. Gottesman. *Stabilizer codes and quantum error correction*. Ph.D. thesis, California Institute of Technology (1997). arXiv:quant-ph/9705052.

[44] M. A. Nielsen and I. L. Chuang. *Quantum computation and quantum information*. Cambridge University Press (2000).

[45] C. Jones. Low-overhead constructions for the fault-tolerant Toffoli gate. *Phys. Rev. A*, **87**, 022328 (2013).

[46] L. E. Heyfron and E. T. Campbell. An efficient quantum compiler that reduces t count. *Quantum Science and Technology*, **4**, 015004 (2018).

[47] B. Natarajan. Sparse approximate solutions to linear systems. *SIAM Journal on Computing*, **24**, 227 (1995).

[48] D. Gross, S. Nezami, and M. Walter. Schur-Weyl Duality for the Clifford Group with Applications: Property Testing, a Robust Hudson Theorem, and de Finetti Representations. *arXiv e-prints*, page arXiv:1712.08628 (2017).

[49] M. Beverland, E. Campbell, M. Howard *et al.* Lower bounds on the non-Clifford resources for quantum computations. *arXiv e-prints*, page arXiv:1904.01124 (2019).

[50] A. M. Dalzell. *Lower bounds on the classical simulation of quantum circuits for quantum supremacy*. Bacherlor's, Massachusetts Institute of Technology (2017).

[51] B. Schumacher. Quantum coding. *Phys. Rev. A*, **51**, 2738 (1995).

[52] H. Pashayan, S. D. Bartlett, and D. Gross. From estimation of quantum probabilities to simulation of quantum circuits. *arXiv e-prints*, arXiv:1712.02806 (2017).

[53] I. L. Markov, A. Fatima, S. V. Isakov *et al.* Quantum Supremacy Is Both Closer and Farther than It Appears. page arXiv:1807.10749 (2018).

[54] B. Villalonga, S. Boixo, B. Nelson *et al.* A flexible high-performance simulator for the verification and benchmarking of quantum circuits implemented on real hardware (2018).

[55] A. Dahlberg and S. Wehner. SimulaQron - A simulator for developing quantum internet software. *arXiv e-prints*, page arXiv:1712.08032 (2017).

[56] W. G. T. Delft. Netsquid. Last Accessed: 2019-07-24.

[57] A. Dahlberg, M. Skrzypczyk, T. Coopmans *et al.* A Link Layer Protocol for Quantum Networks. *arXiv e-prints*, arXiv:1903.09778 (2019).

[58] T. Häner, D. S. Steiger, K. Svore *et al.* A software methodology for compiling quantum programs. *Quantum Science and Technology*, **3**, 020501 (2018).

[59] Welcome to the microsoft quantum development kit prview. `https://docs.microsoft.com/en-gb/quantum/`. Last Accessed: 2019-07-25.

[60] K. M. Svore, A. Geller, M. Troyer *et al.* Q#: Enabling scalable quantum computing and development with a high-level domain-specific language. *arXiv e-prints*, arXiv:1803.00652 (2018).

[61] D. S. Steiger, T. Häner, and M. Troyer. ProjectQ: An Open Source Software Framework for Quantum Computing. *arXiv e-prints*, arXiv:1612.08091 (2016).

[62] Ibmq: Quantum systems. `https://www.research.ibm.com/ibm-q/technology/devices/`. Last Accessed: 2019-07-25.

[63] G. Aleksandrowicz, T. Alexander, P. Barkoutsos *et al.* Qiskit: An open-source framework for quantum computing (2019).

[64] A. W. Cross, L. S. Bishop, J. A. Smolin *et al.* Open Quantum Assembly Language. *arXiv e-prints*, arXiv:1707.03429 (2017).

[65] Github.com: Google circ. `https://github.com/quantumlib/Cirq`. Last Accessed: 2019-07-25.

[66] Google ai blog: Announcing circ. `https://ai.googleblog.com/2018/07/announcing-cirq-open-source-framework.html`. Last Accessed: 2019-07-25.

[67] Rigetti computing: Forest sdk. `https://www.rigetti.com/forest`. Last Accessed: 2019-07-25.

[68] R. S. Smith, M. J. Curtis, and W. J. Zeng. A Practical Quantum Instruction Set Architecture. *arXiv e-prints*, arXiv:1608.03355 (2016).

[69] Rigetti computing: Qpu specifications. `https://www.rigetti.com/qpu`. Last Accessed: 2019-07-25.

[70] T. Häner, D. S. Steiger, M. Smelyanskiy *et al.* High performance emulation of quantum circuits. In *Proceedings of the International Conference for High Performance Computing, Networking, Storage and Analysis*, SC '16, pages 74:1–74:9. IEEE Press, Piscataway, NJ, USA (2016).

[71] Top500.org: Summit. `https://www.top500.org/system/179397`. Last Accessed: 2019-07-25.

[72] M. Smelyanskiy, N. P. D. Sawaya, and A. Aspuru-Guzik. qHiPSTER: The Quantum High Performance Software Testing Environment. *arXiv e-prints*, arXiv:1601.07195 (2016).

[73] N. Khammassi, I. Ashraf, X. Fu *et al.* Qx: A high-performance quantum computer simulation platform. In *Design, Automation Test in Europe Conference Exhibition (DATE), 2017*, pages 464–469 (2017).

[74] G. Aleksandrowicz, T. Alexander, P. Barkoutsos *et al.* `https://qiskit.org/aer`. Last Accessed: 2019-07-25.

[75] T. Jones, A. Brown, I. Bush *et al.* QuEST and High Performance Simulation of Quantum Computers. *arXiv e-prints*, arXiv:1802.08032 (2018).

[76] D. Gil. Discovering a new era of computing. `https://rebootingcomputing.ieee.org/rebooting-computing-week/industry-summit-2017` (2017). IEEE Industry Summit 2017.

[77] Google ai blog: A preview of bristlecone. `https://ai.googleblog.com/2018/03/a-preview-of-bristlecone-googles-new.html`. Last Accessed: 2019-07-26.

[78] D. Aharonov, M. Ben-Or, E. Eban *et al.* Interactive Proofs for Quantum Computations. *arXiv e-prints*, arXiv:1704.04487 (2017).

[79] U. Mahadev. Classical Verification of Quantum Computations. *arXiv e-prints*, arXiv:1804.01082 (2018).

[80] E. Pednault, J. A. Gunnels, G. Nannicini *et al.* Breaking the 49-Qubit Barrier in the Simulation of Quantum Circuits. *arXiv e-prints*, page arXiv:1710.05867 (2017).

[81] J. Chen, F. Zhang, C. Huang *et al.* Classical Simulation of Intermediate-Size Quantum Circuits. *arXiv e-prints*, page arXiv:1805.01450 (2018).

[82] Z.-Y. Chen, Q. Zhou, C. Xue *et al.* 64-Qubit Quantum Circuit Simulation. *arXiv e-prints*, arXiv:1802.06952 (2018).

[83] B. Villalonga, D. Lyakh, S. Boixo *et al.* Establishing the Quantum Supremacy Frontier with a 281 Pflop/s Simulation. *arXiv e-prints*, page arXiv:1905.00444 (2019).

[84] S. Boixo, S. V. Isakov, V. N. Smelyanskiy *et al.* Simulation of low-depth quantum circuits as complex undirected graphical models. *arXiv e-prints*, arXiv:1712.05384 (2017).

[85] I. L. Markov and Y. Shi. Simulating quantum computation by contracting tensor networks. *arXiv e-prints*, quant-ph/0511069 (2005).

[86] J. Preskill. Quantum Computing in the NISQ era and beyond. *arXiv e-prints*, page arXiv:1801.00862 (2018).

[87] E. Gamma, R. Helm, R. Johnson *et al. Design Patterns: Elements of Reusable Object-Oriented Software.* Addison Wesley (1994).

[88] C++ reference: Name requirements - function object. `https://en.cppreference.com/w/cpp/named_req/FunctionObject`. Last Accessed: 2019-07-31.

[89] C++ reference: Templates. `https://en.cppreference.com/w/cpp/language/templates`. Last Accessed: 2019-07-31.

[90] G. M. Amdahl. Validity of the single processor approach to achieving large scale computing capabilities. In *Proceedings of the April 18-20, 1967, Spring Joint Computer Conference*, AFIPS '67 (Spring), pages 483–485. ACM, New York, NY, USA (1967).

[91] C. Kessler and J. Keller. Models for parallel computing: Review and perspectives. *PARS-Mitteilungen, ISSN 0177-0454*, **24**, 13 (2007).

[92] OpenMP Architecture Review Board. Openmp 4.5 api c/c++ syntax reference guide. `https://www.openmp.org/wp-content/uploads/OpenMP-4.5-1115-CPP-web.pdf` (2015).

[93] Open mpi: Open source high performance computing. `https://www.open-mpi.org/`. Last Accessed: 2019-08-03.

[94] Message Passing Interface Forum. *MPI: A Message-Passing Interface Standard, Version 3.1.* High Performance Computing Center Stuttgart (2015).

[95] M. Mosca. Quantum Algorithms. *arXiv e-prints*, page arXiv:0808.0369 (2008).

[96] M. Roetteler. Quantum algorithms for highly non-linear Boolean functions. *arXiv e-prints*, page arXiv:0811.3208 (2008).

[97] N. Moll, P. Barkoutsos, L. S. Bishop *et al.* Quantum optimization using variational algorithms on near-term quantum devices. *Quantum Science and Technology*, **3**, 030503 (2018).

[98] E. Farhi, J. Goldstone, and S. Gutmann. A Quantum Approximate Optimization Algorithm. *arXiv e-prints*, arXiv:1411.4028 (2014).

[99] E. Farhi, J. Goldstone, and S. Gutmann. A Quantum Approximate Optimization Algorithm Applied to a Bounded Occurrence Constraint Problem. *arXiv e-prints*, arXiv:1412.6062 (2014).

[100] M. Van den Nest. Simulating quantum computers with probabilistic methods. *arXiv e-prints*, page arXiv:0911.1624 (2009).